1. Report No.	2. Government Accession No.	3.
FHWA/TX-92+1169-2		

4. Title and Subtitle	5. Report Date
MECHANISTIC ANALYSIS OF CONTINUOUSLY REINFORCED CONCRETE PAVEMENTS CONSIDERING MATERIAL CHARACTERISTICS, VARIABILITY, AND FATIGUE	March 1991
	6. Performing Organization Code

7. Author's)	8. Performing Organization Report No.
Mooncheol Won, Kenneth Hankins, and B. Frank McCullough	Research Report 1169-2

9. Performing Organization Name and Address	10. Work Unit No.
Center for Transportation Research The University of Texas at Austin Austin, Texas 78712-1075	
	11. Contract or Grant No.
	Research Study 3-8-88/1-1169
	13. Type of Report and Period Covered

12. Sponsoring Agency Name and Address	
Texas State Department of Highways and Public Transportation; Transportation Planning Division P. O. Box 5051 Austin, Texas 78763-5051	Interim
	14. Sponsoring Agency Code

15. Supplementary Notes
Study conducted in cooperation with the U. S. Department of Transportation, Federal Highway Administration Research Study Title: "Concrete Pavement Design Update"

16. Abstract

In this study, a mechanistic analysis was performed to evaluate structural responses of continuously reinforced concrete (CRC) pavements to various environmental and wheel loading conditions. For environmental loads, most of the volume change stresses are caused by a transfer of stress from the steel to concrete through bond slippage between concrete and steel. The current knowledge of bond stresses is used in the development of the volume change mechanism incorporated in this analysis. Wheel load stresses depend on many factors. In this study, an effort was made to identify the relationship between wheel load stresses and transverse crack spacings. One major characteristic of CRC pavement behavior is that there is variability in the performance. A simulation model is used to incorporate the material variabilities in the analysis. A mechanistic analysis of the CRC pavement system, including the stochastic nature of material variabilities, is presented herein. A distress prediction model is developed considering fatigue behavior of concrete.

The performance of CRC pavement is closely related to the variation in transverse crack spacings. There are many factors affecting transverse cracking in CRC pavement. Basically there are two types of loadings. One is environmental loading and the other is external wheel loading. Steel bars and subbase friction restrain concrete volume changes due to temperature and moisture changes. If the stresses developed by restrained volume changes exceed the tensile strength of the concrete, cracks develop to relieve the stresses. Stresses develop when a wheel load is applied, due to the bending action of the concrete slabs. In the interior condition, tensile stresses develop at the bottom of the slab. The combined effects of restrained volume change stresses and wheel load stresses induce more cracks. In the early stages of pavement life, environmental loading has a significant effect on pavement behavior. Initial cracks develop due to temperature and moisture variations. After the pavement is opened to traffic, external wheel loads play an important role in crack development. The significance of volume change mechanisms becomes small as crack spacings are stabilized. Relatively short crack spacings and decrease in bond stress due to cyclic loading contribute to the reduction in the role of volume change mechanisms determining pavement behavior. However, the effect of wheel loads on pavement behavior depends on the crack spacing distributions developed early by volume change mechanisms. Pavement distresses occur when fatigue failure reaches some of the slab segments. It is possible to evaluate the effect of two types of loads and to estimate the frequency of distresses.

The major failure mode in CRC pavement is the punchout. It is due to the fatigue failure of concrete. A mechanistic model to estimate pavement life in terms of frequency of punchouts is developed in this project. This approach is a sound one, because it correlates the factors causing failures with the actual distress occurrence. After it is refined and calibrated with field data, it is expected that this model can be used for the design and economic analysis of CRC pavement systems.

17. Key Words	18. Distribution Statement
continuously reinforced concrete (CRC) pavement, mechanistic model, CRCP-5, punchout prediction, transverse cracking, crack spacing, fatigue failure, distress prediction	No restrictions. This document is available to the public through the National Technical Information Service, Springfield, Virginia 22161.

19. Security Classif. (of this report)	20. Security Classif. (of this page)	21. No. of Pages	22. Price
Unclassified	Unclassified	116	

Form DOT F 1700.7 (8-69)

MECHANISTIC ANALYSIS OF CONTINUOUSLY REINFORCED CONCRETE PAVEMENTS CONSIDERING MATERIAL CHARACTERISTICS, VARIABILITY, AND FATIGUE

by

Mooncheol Won
Kenneth Hankins
B. Frank McCullough

Research Report Number 1169-2

NOT INTENDED FOR CONSTRUCTION,
PERMIT, OR BIDDING PURPOSES

B. Frank McCullough, P.E. (Texas No. 19914)
Research Supervisor

Kenneth Hankins, P.E. (Texas No. 20244)

PREFACE

In this study, a mechanistic analysis was performed to evaluate structural responses of continuously reinforced concrete (CRC) pavements for various environmental and wheel loading conditions. Since the major failure mode in CRC pavements is the punchout, a mechanistic model was developed to estimate a pavement's life according to the of frequency of punchouts. A complete review of the CRC pavements design theory, materials characteristics, and CRC pavement behavior are included in this report. A review of repetitive loading and fatigue concepts is also included.

The study considers materials characteristics and variability, particularly at early ages of the pavement, combining stresses caused by concrete volume changes and other environmental effects with external wheel load stresses that cause initial distress

manifestations such as transverse and longitudinal cracking of CRC pavements.

The mechanistic model presented in this report was incorporated in computer program CRCP-5. The working system of this program, as well as the input format, and a full description of the program's output, are reported herein. This program allows the user to estimate steel stresses, transverse crack widths, and the number of transverse cracks based on concrete properties at various ages. Using fatigue characteristics of the pavement concrete, the model can also be used to predict crack spacing and occurrence of punchouts at various stages of the CRC pavement's life.

Mooncheol Won
Kenneth Hankins
B. Frank McCullough

LIST OF REPORTS

Research Report 1169-1, "A Study of Drainage Coefficients for Concrete Pavements in Texas," by Venkatakrisna Shyam, Humberto Castedo, W. R. Hudson, and B. Frank McCullough, discusses the efforts to determine coefficients of drainage for concrete pavements with three subbase types and a range of rainfall conditions. May 1989.

Report No. 1169-2, "Mechanistic Analysis of Continuously Reinforced Concrete Pavements Considering Material Characteristics, Variability, and Fatigue,"

by Mooncheol Won, Kenneth Hankins, and B. Frank McCullough, presents a mechanistic model for estimating continuously reinforced concrete (CRC) pavement life in terms of frequency of punchouts. This model was incorporated in computer program CRCP-5, which is described in detail. The model uses the stochastic nature of the materials' properties and the fatigue behavior of pavement concrete for predicting the extent and time of occurrence of punchouts in CRC pavements. April 1990.

ABSTRACT

In this study, a mechanistic analysis to evaluate structural responses of continuously reinforced concrete (CRC) pavements to various environmental and wheel loading conditions was performed. For environmental loads, most of the volume change stresses are caused by a transfer of stress from the steel to the concrete through bond slippage between the concrete and the steel. Current knowledge of bond stresses was applied in the development of the

volume change mechanism incorporated in this analysis.

Wheel load stresses depend on many factors. In this study, an effort was made to identify the relationship between wheel load stresses and transverse crack spacings. One major characteristic of CRC pavement behavior is that there is variability in the performance. A simulation model is used to incorporate the material variabilities in the analysis.

A mechanistic analysis of the CRC pavement system, including the stochastic nature of material variabilities, is presented herein. A distress prediction model is developed considering fatigue behavior of concrete.

The performance of CRC pavement is closely related to the variation in transverse crack spacings. There are many factors affecting transverse cracking in CRC pavement. Basically, there are two types of loadings. One type is environmental loading and the other type is external wheel loading. Steel bars and subbase friction restrain concrete volume changes due to temperature and moisture changes. If the stresses developed by restrained volume changes exceed the tensile strength of the concrete, cracks develop to relieve the stresses. Stresses develop when a wheel load is applied, due to the bending action of the concrete slabs. In the interior condition, tensile stresses develop at the bottom of the slab. The combined effects of restrained volume change stresses and wheel load stresses induce more cracks. In the early stages of pavement life, environmental loading has a significant effect on pavement behavior. Initial cracks develop due to temperature and moisture variations. After the pavement is opened to traffic, external wheel loads play an important role in crack development. The significance of volume change mechanisms becomes small as crack spacings are stabilized. Relatively short crack spacings and decrease in bond stress due to cyclic loading contribute to the reduction in the role of volume change mechanisms determining pavement behavior. However, the effect of wheel loads on pavement behavior depends on the crack spacing distributions developed early by volume change mechanisms. Pavement distresses occur when fatigue failure reaches some of the slab segments. It is possible to evaluate the effect of two types of loads and to estimate the frequency of distresses.

The major failure of CRC pavement is the punchout. A punchout occurs when there is concrete fatigue failure. A mechanistic model that estimates pavement life by examining frequency of punchouts is developed in this project. This approach is a sound one, because it correlates the factors causing failures with the actual distress occurrence. After being refined and calibrated with field data, it is expected that this model may be used for the design and economic analysis of CRC pavement systems.

SUMMARY

A major distress in continuously reinforced concrete (CRC) pavements is punchouts. Punchouts occur when very narrow transverse cracks are connected by longitudinal cracks. These longitudinal cracks are generally associated with external wheel load applications, which in turn affect the fatigue life of the pavement. In this study, the structural response of CRC pavements was evaluated for various environmental and wheel loading conditions by means of a mechanistic analysis.

A methodology was developed to predict distress by examining the frequency of punchouts in CRC pavements. The methodology was incorporated into computer program CRCP-5. The equations in this program allow for the input of variabilities in material properties, which are analyzed by the Monte Carlo technique. The newly developed model has the capability of estimating transverse crack spacing distributions for various designs and environmental conditions. In addition, estimates of the number of punchouts for various numbers of wheel load applications throughout the pavement's life can be produced.

IMPLEMENTATION STATEMENT

The CRC pavement distress prediction model developed in this study can be used to estimate pavement life in terms of the number of the distresses. This model enables the user to evaluate the effect of each pavement variable on the life of the pavement.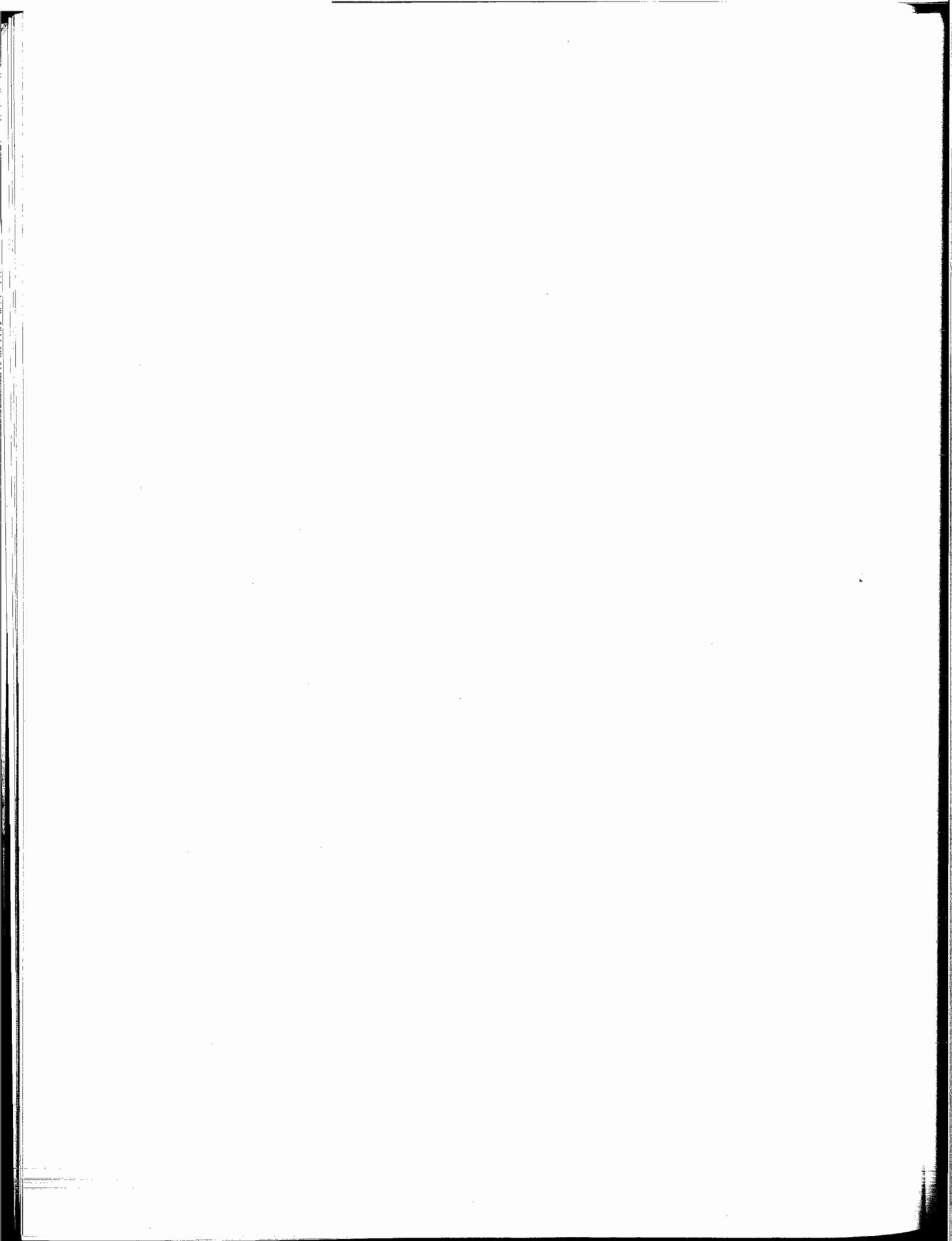 Therefore, this model can be used in a pavement design program. An economic analysis of the CRC pavement system can also be performed with this program. The model should be tested and calibrated against the field performance observations for CRC pavements.

TABLE OF CONTENTS

CHAPTER 1. INTRODUCTION

Continuously Reinforced Concrete (CRC) pavement is a relatively new type of pavement. In this chapter, the evolution of CRC pavements is examined. The performance of this pavement type and the factors affecting CRC pavement performance are also investigated. The objective of this study is presented, followed by the scope of the study.

BACKGROUND

Continuously Reinforced Concrete (CRC) pavement has continuous longitudinal reinforcing steel, without transverse joints other than construction joints. The earliest concrete pavements were poured without joints and were unreinforced. These pavements, during their service life, developed random cracks resulting from vehicular traffic, subgrade influence, or environmental effects. Eventually this uncontrolled cracking led to pavement distresses and failures. Joints were used as a means of controlling random cracks. The presence of joints ensures that cracks either do not develop at all or develop only in a controlled manner which is related to the location of the joints. Although the joints made an improvement, they were still the source of major pavement distresses, such as pumping and faulting.

The principle of continuous reinforcement in concrete pavements was introduced in order to avoid the need for transverse joints. The first CRC pavement was built by the U. S. Bureau of Public Roads in Maryland in the early 1920's. The second one was built in Indiana in 1939 (Ref 1). The performance of the Indiana project and other projects (built in Illinois, California, and New Jersey around 1949) led to an increased interest in this design. More than 13,000 equivalent two-lane miles of CRC pavement have been constructed since 1958 (Ref 2). With the increased usage of CRC pavements, vast amounts of information on this type of pavement have been accumulated, and design procedures have been improved. Most users of CRC pavements are reasonably satisfied with its performance. Usually the amount and the severity of the distress that has occurred has been within the normal bounds for pavements serving high volumes of heavy traffic. Advantages that have been attributed to CRC pavements include improved riding quality and

safety, a relatively long life, and a limited need for maintenance (Ref 3).

However, common types of distresses are found in most of the CRC pavements and are closely related to the deterioration of the pavement condition. Research has been conducted in this area to identify the relationship of distresses as well as other design and construction variables.

OBJECTIVES OF THE STUDY

There is a certain relationship between the occurrence of distresses in CRC pavements and the characteristics of transverse crack spacing distributions. Identifying this relationship and improving design and construction practices will minimize the occurrence of pavement distresses. Since repairing CRC pavement is more difficult and more expensive than repairing other pavements, these improvements will be beneficial.

The primary objectives of this study are as follows:

(1) to develop a mechanistic model capable of simulating field conditions for various design, environmental, and wheel-loading conditions (including material variabilities);
(2) to identify the relationship between the frequency of pavement distresses and other pavement behavior; and
(3) to develop a model which can predict the frequency of pavement distresses and can estimate pavement life for various design combinations so that an optimum design can be derived.

SCOPE OF THE STUDY

This study, in order to achieve the above objectives, resulted in the development of the computer program CRCP-5. A discussion of the existing design procedures and of needed research is presented in Chapter 2.

In Chapter 3, variables affecting CRC pavement behavior are examined. How each variable affects pavement behavior is thoroughly investigated.

The development of a mechanistic model to analyze CRC pavements is explained in Chapter 4. Current knowledge of bond stress characteristics is

included in the model. The methodology to include material variability in the mechanistic model is described in this chapter.

The method of attacking nonlinear problems is explained in Chapter 5.

The causes of a major pavement distress type are explored in Chapter 6. Fatigue failures of concrete are examined. An effort is made to identify a relationship between the occurrence of this distress type and other pavement behavior. The results of this effort were incorporated into computer program CRCP-5.

In Chapter 7, the computer program developed in this study, CRCP-5, is described. The working system of this program is explained. Input format is introduced, and a full description of the computer output is presented.

In Chapter 8, example problems are presented to demonstrate the capabilities of CRCP-5. Also presented are the effects of various factors on CRC pavement responses.

A summary of this study, conclusions, and recommendations are contained in Chapter 9.

CHAPTER 2. EXISTING DESIGN PROCEDURES AND NEEDED RESEARCH

In this chapter, the evolution of CRC pavement design procedures and current design procedures are reviewed. Current design and construction practices of CRC pavements provide, overall, satisfactory performance. However, there is room to improve current design procedures. Areas which have not been fully explored but which are essential to a better performance of CRC pavements are discussed.

CURRENT DESIGN PROCEDURES FOR CRC PAVEMENTS

The design of CRC pavements has evolved mostly from observations made on early experimental and normal construction projects and to a lesser extent from theoretical and laboratory studies. In these studies, many of the parameters that influence the design and the behavior of CRC pavements were tested, and this led to the current designs that were developed for use in particular states. Empirical methods have been used in several states. In the most current design procedures (Ref 2), a rational design method was developed for CRC pavements by modifying the performance equation for jointed concrete pavements developed in the AASHO Road Test. In this section, a review of each design variable and its evolution is made.

Slab Thickness

There are many factors to be considered in determining slab thickness. They include traffic, concrete strength and modulus of elasticity, modulus of subgrade reaction, and load transfer at cracks. Failures in CRC pavements are closely related to critical wheel load stress. Therefore, critical wheel load stresses must be examined when considering slab thickness. In CRC pavements, critical stresses occur near cracks, assuming that wheel loads are applied away from the pavement edge. Those critical wheel load stresses depend largely on slab thickness and load transfer. Steel reinforcement in CRC pavements does not increase the bending capacity of the slab. However, longitudinal steel reinforcement partly determines load transfer at cracks by holding cracks tight and by its shearing action. Thicker slabs significantly reduce deflections that are due to wheel load.

Reduced deflections alleviate loss of aggregate interlock at cracks. However, a relationship between slab thickness and load transfer has not yet been well established. It is not surprising to find that at the present time there is no single method of designing CRC pavement thickness that is universally accepted.

A common practice has been to determine the thickness required for a jointed pavement and then to use a lesser thickness for the CRC pavements. The 1972 "Interim Guide" (Ref 5) simply states that the thickness of CRC pavements "may be less than that obtained from the charts, with the amount of reduction in thickness being based on local experience or other studies." The logic behind this statement is that better load transfer is achieved in CRC pavements than in JRC pavements. The most current design procedure that determines slab thickness is the AASHTO Guide for the Design of Pavement Structures (Ref 2). The procedure in the Guide combines the empirical nature of the design-performance equation, originally developed in the AASHO Road Test, with mechanistic procedures.

Longitudinal Steel Reinforcement

Longitudinal steel reinforcement in CRC pavements induces transverse cracks and holds cracks tightly closed, thereby providing structural continuity of the slab at the cracks. Pavement responses depend not only on the amount of reinforcing steel but also bar size, location, and number of layers of the steel bars.

Percent Steel. Percentage of longitudinal steel was found to be the most significant factor affecting cracking in CRC pavement (Ref 3). In 1933, Vetter presented an analysis of the stresses occurring in a continuous reinforced concrete structure owing to variations in temperature and moisture content (Ref 4). Vetter's formula for minimum reinforcement is as follows:

$$p = \frac{f_t}{f_y - nf_t} \times 100 \qquad (2.1)$$

where

    p = steel percentage of longitudinal reinforcement,

f_t = concrete tensile strength (psi),

f_y = yield strength of steel (psi), and

n = the ratio of modulus of elasticity of steel to concrete.

The yield strength of steel in CRCP is usually 60,000 psi. If 4 million and 29 million psi are taken for modulus of elasticity of concrete and steel, respectively, and concrete tensile strength is assumed to be 420 psi at 28 days, Eq 2.1 yields 0.737 percent. Experience has shown that this value is greater than what is required. Part of the reason is that the subbase frictional resistance was not included in the analysis.

The 1972 AASHO Interim Guide for Design of Pavement Structures (Ref 5) recommends the following relationship:

$$p = (1.3 - 0.2\,F)\,\frac{f}{f_s} \times 100 \tag{2.2}$$

where

F = friction factor of subbase,

f = tensile strength of concrete (psi), and

f_s = allowable working stress in steel (psi).

In this formula, the percent steel reinforcement (p) is directly proportional to the concrete tensile strength.

In the 1986 AASHTO Guide for Design of Pavement Structures (Ref 2), a separate formula is recommended considering crack spacing, crack width, and steel stress at a crack:

$$\overline{X} = \frac{1.32\left(1+\dfrac{f_t}{1,000}\right)^{6.70} * \left(1+\dfrac{\alpha_s}{2a_c}\right)^{1.15} * (1+\phi)^{2.19}}{\left(1+\dfrac{\sigma_w}{1,000}\right)^{5.20} * (1+P)^{4.60} * (1+1,000Z)^{1.79}} \tag{2.3}$$

$$\Delta X = \frac{0.00932\left(1+\dfrac{f_t}{1,000}\right)^{6.53} * (1+\phi)^{2.20}}{\left(1+\dfrac{\sigma_w}{1,000}\right)^{4.91} * (1+P)^{4.55}} \tag{2.4}$$

$$\sigma_s = \frac{47300\left(1+\dfrac{DT_D}{100}\right)^{0.425} * \left(1+\dfrac{f_t}{1,000}\right)^{4.09}}{\left(1+\dfrac{\sigma_w}{1,000}\right)^{3.14} * (1+1,000Z)^{0.494} * (1+P)^{2.74}} \tag{2.5}$$

where

$\overline{X}$ = crack spacing (feet),

ΔX = crack width (inches),

σ_s = steel stress (psi),

f_t = concrete tensile strength (psi),

α_s = thermal coefficient of steel (inch/inch/°F),

a_c = thermal coefficient of concrete (inch/inch/°F),

ϕ = rebar diameter (inches),

σ_w = wheel load tensile stress (psi),

P = percent steel reinforcement,

Z = concrete shrinkage (inch/inch), and

DT_D = design temperature drop (°F).

The desired crack spacing range is selected, and Eq 2.3 is solved for percentage of steel. For crack width and steel stress, maximum allowable values are selected and Eqs 2.4 and 2.5 are solved. The design percentage of steel is selected which satisfies the three conditions. Conceptually, this process is explained in Figure 2.1. As percent steel increases, crack spacing decreases. Crack spacings between 3.5 and 8 feet are considered optimum values. Therefore, maximum and minimum steel percentages are determined. For crack width, 0.023 inch is the recommended value for maximum crack width (Ref 6). Steel stress must be below the yield stress to ensure tight crack width.

Most states have standardized the percentage of longitudinal steel. By far, the most commonly used amount of steel is 0.6 percent. A few northern states use 0.7 percent steel (Ref 1). At the present time, there is no strong movement toward the use of larger percentages of longitudinal steel in CRC pavements in order to improve CRCP performance. This could change when more is known about the influence of crack width on CRCP performance (Ref 1).

Size and Spacing of Steel. The size of the bar influences the bond stress between steel and concrete. Given the steel percentage, the use of smaller bars provides a larger steel surface area and increases stress transfer from the steel to the concrete, resulting in narrower crack spacings and tighter crack widths. McCullough and Ledbetter (Ref 7) suggest that the ratio of the bond area to concrete volume should not be less than 0.03 $inch^2/inch^3$, which is checked by the following formula:

$$Q = \frac{4p}{\phi} \tag{2.6}$$

where

Q = the ratio of bond area to concrete volume ($inch^2/inch^3$),

p = percent steel, and

ϕ = bar diameter (inch).

The spacing of steel should be large enough to permit easy placement and consolidation of concrete, yet not so large as to lose bond strength. The Continuously Reinforced Pavement Group (Ref 8)
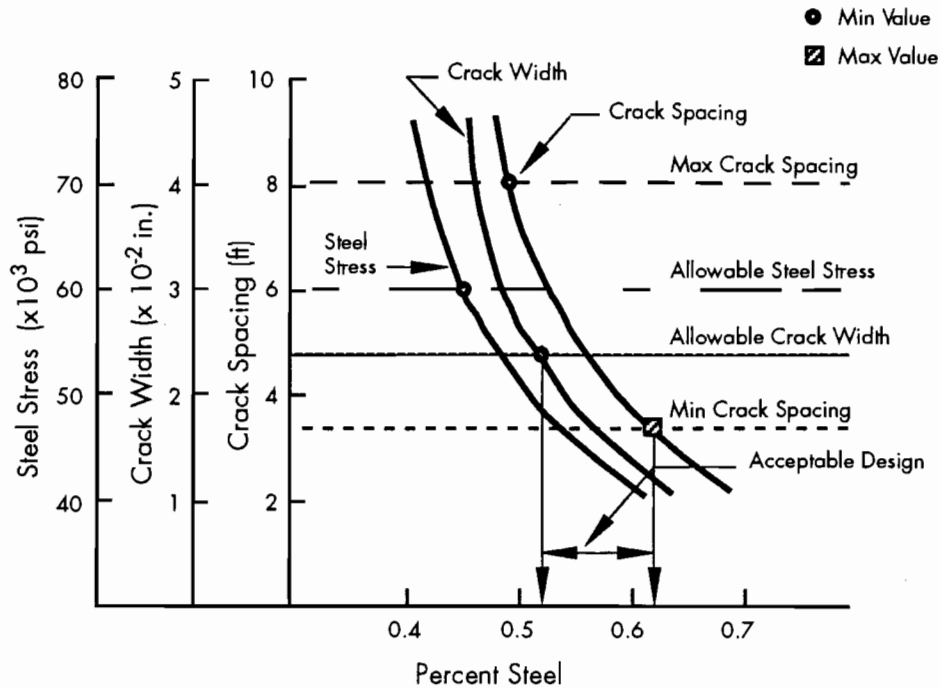
Figure 2.1. Conceptual illustration for selecting percent longitudinal steel

recommends that longitudinal spacing not be less than 4 inches nor more than 9 inches, to provide good load transfer and bond strength.

Location of the Steel. There has been some disagreement about the proper depth of the reinforcement. Field experience showed an average crack spacing of 1.7 feet with a centerline of 2.5 inches below the surface (8-inch slab) and an average crack spacing of 2.9 feet with the steel 3-11/16 inches below the surface (Ref 9). The concrete in CRC pavements experiences differential volume changes owing to temperature and moisture gradient. The volume changes at the top part of the slab are greater than those at the bottom part. If the steel is placed too close to the top, the restraint by the steel on concrete volume changes becomes greater and results in narrower crack spacings. On the other hand, if the steel is placed too close to the bottom, the primary objective of the longitudinal reinforcement, to hold cracks tightly closed, cannot be achieved.

Reference 10 recommends that the longitudinal steel be located vertically, so that there will be at least 2.5 inches of cover, and the resulting placement should not be more than 1 inch below mid-depth of the pavement. It states that a variation of ±1 inch in vertical and horizontal locations does not appear to adversely affect pavement performance; therefore, steel placement tolerances should not be set so tightly as to add to costs without significantly improving performance.

Number of Layers of the Steel. The majority of CRC pavements constructed so far have pavement thicknesses of 8 inches or at most 10 inches. One-layer reinforcement has been successful for pavements with those slab thicknesses. However, there is a trend toward the use of greater slab thicknesses. For the same steel percentage of longitudinal reinforcement, increasing slab thicknesses means using more steel bars. With one-layer reinforcement, it means closer spacing between longitudinal bars.

The Texas SDHPT developed Design Standard CRCP(B)-85 (Ref 11) which permits the use of two-layer reinforcement for pavements greater than 10 inches thick. Several projects now under construction are using two-layer reinforcement, and subsequent performance studies are needed to determine the adequacy of two-layer reinforcement.

The longitudinal reinforcements in CRC pavements consist of many lengths of deformed bars. Continuity of reinforcement in the longitudinal direction is provided by overlapping the ends of the steel to form a splice. The lapped splice transfers force from one bar to another through the surrounding concrete by means of the bond between the steel and the concrete. Most of the early problems occurred at locations involving splices at which very wide transverse cracks had developed (Ref 8). Investigations usually revealed that there was insufficient steel overlap distance at the splice to transfer steel stress from one bar to its extension, or that all longitudinal steel terminated in the same vertical plane.

Lepper and Kim found through laboratory experiments that a lap of 32 times the bar diameter was satisfactory (Ref 12). The laps are staggered or skewed in many ways. One method is that not more

than one-third of the bars be lapped at any transverse location. Some of the many other methods (Ref 10) include: not more than one-fourth of the bars in a 4-foot length of slab; skewing the splice location at 60 degrees to the longitudinal direction; not more than four bars in any cross-section and 6 feet between adjacent laps; and skewed across a single-lane width over a length of 20 feet. Some of these methods of lapping are shown in Figure 2.2.

Transverse Steel

Transverse reinforcement has been used for several purposes (Ref 13):

(1) to maintain the spacing of the longitudinal steel,
(2) to aid in supporting longitudinal steel at the desired depth,

(3) to serve as tie bars across longitudinal joints, and
(4) to hold chance longitudinal cracks tightly closed for proper load transfer.

With the development and improvement of mechanical methods for placing longitudinal reinforcement, the need for transverse reinforcement to achieve (1) and (2) has been almost eliminated. Tie bars can be used at longitudinal joints (3). Therefore, (4) is the only reason for transverse reinforcement. In the United States, several states do not require transverse reinforcement (Ref 13). The design of transverse reinforcement is based on "subgrade drag theory," shown below, as is the design of longitudinal reinforcement in JRC pavements:

Skewed Splice Locations
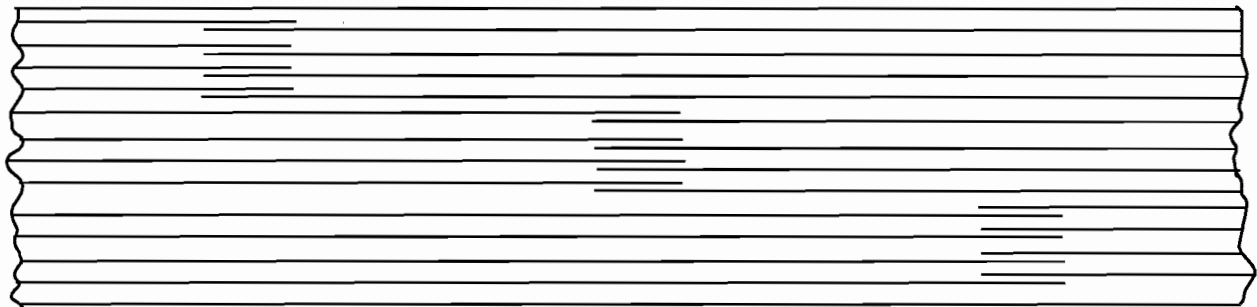
Not More than Four Bars at Any Cross-section
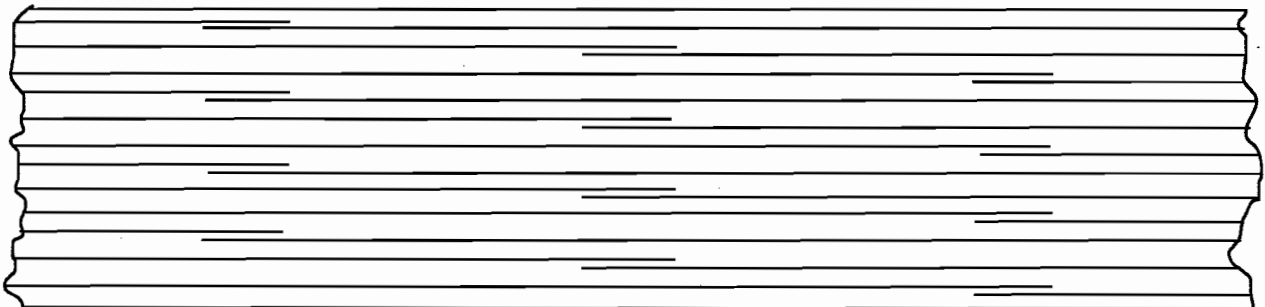
Not More than One-Third of the Bars at Any Transverse Location

Figure 2.2. Some of the many methods of lapping reinforcing bars (Ref 10)

6

$$p = \frac{WF}{2f_s} \times 100$$

where

p = required transverse steel percent,

W = width of the pavement (feet), and other variables are as defined in Eq 2.2.

The size and spacing of transverse steel do not appear to be as critical as the size and spacing of longitudinal steel. The Continuously Reinforced Pavement Group (Ref 8) recommends that transverse bars not be spaced farther apart than 60 inches.

Pavement Joints

Although CRC pavement is often termed "jointless pavement," certain types of joints are required to minimize possible damages. These are longitudinal, transverse construction, and terminal joints.

Longitudinal Joints. Where concrete placement is two or more lanes in width, as is usually the case, longitudinal joints are necessary to prevent longitudinal cracking. Concrete-volume-change stresses in the transverse direction increase with pavement width because of subbase friction and especially because of warping. Unlike transverse cracks, longitudinal cracks are not intended and are sources of pavement distress. Using a longitudinal weakened plane joint with tie bars has provided successful performance.

Transverse Construction Joints. Construction of CRC pavements is sometimes interrupted for various reasons. Since concrete properties change with time, whenever there is a delay in the paving operation for a considerable amount of time, transverse construction joints are needed. Deformed bars are added across the construction joint to increase the steel content by at least one-third and often to double the amount of regular reinforcement. Bar lengths usually range between 3 and 6 feet (Ref 1). McCullough (Ref 14) states that the steel across the joint should be increased to 1 percent.

Terminal Joints. "Pavement Growth" has been observed in concrete pavements (Ref 15). Pavement growth is the lengthening of the total pavement length because of the intrusion of incompressibles into joints or cracks and because of subsequent temperature increase. As a result of concrete pavement growth, internal forces are built up in the slab and an outward push is produced toward the free ends that closes the expansion joint at the bridge ends, ruptures the abutment walls, and applies an undesirable amount of pressure on the bridge or structure. There are two ways to treat this problem. One is to restrain this movement. The other is to accommodate the movement. Anchors are used to restrain the movement. Expansion systems are used to accommodate the movement.

(1) *Anchors.* If restraint is planned, a series of reinforced concrete lugs set transversely in the foundation material and rigidly connected to the CRC pavement slab are usually installed (Figure 2.3). The lugs are spaced at 15- to 40-foot intervals. The lugs, however, were found to be partially effective, and a few short reinforced concrete slabs were installed in conjunction with the anchor lugs. These short slabs are separated by dowelled expansion joints. The short slabs compensate for the movements the lugs cannot restrain.

(2) *Expansion Systems.* With expansion systems, all of the movement is allowed to occur. Several methods have been used. Among these, the wide-flange-beam terminal joint has been reported to work well and, in fact, is a more satisfactory design than other systems (Refs 9 and 16). As shown in Figure 2.4, this method consists of a concrete sleeper slab with a wide-flange beam section on it.

NEEDED RESEARCH

Current CRCP design and construction methods have provided overall satisfactory performance. Advantages such as improved riding quality and safety, relatively long life, and a limited need for maintenance have been attributed to well-designed and well-constructed CRC pavements. However, extensive field studies on the performance of CRC pavements in Texas have revealed that the performance varied even within a project where identical design construction techniques were employed (Ref 17). These studies imply that there are variables affecting CRCP performance that have been overlooked.

Repair of CRC pavements is very costly due to the heavy equipment and quantity of steel needed. Any measure to reduce failures in CRC pavements will save a significant amount of maintenance and user cost. In this section, variables that have not been considered in the current design procedures but have been found to have significant effect on the performance of CRC pavements are discussed. Research needed to incorporate those variables into the design of CRC pavements is also discussed.

Variability

Concrete in CRC pavements is subjected to two different types of loadings. One results from restrained volume changes, owing to environmental conditions (internal loading). The other is external wheel loading. Cracks develop whenever stresses exceed strength. In CRC pavements, transverse cracks have contradictory effects on two different types of loadings. Volume-change stresses are lessened by crack formations. On the other hand, transverse cracks increase wheel load stresses owing to the reduction in bending stiffness at the cracks. The former is a beneficial effect, while the latter is

7
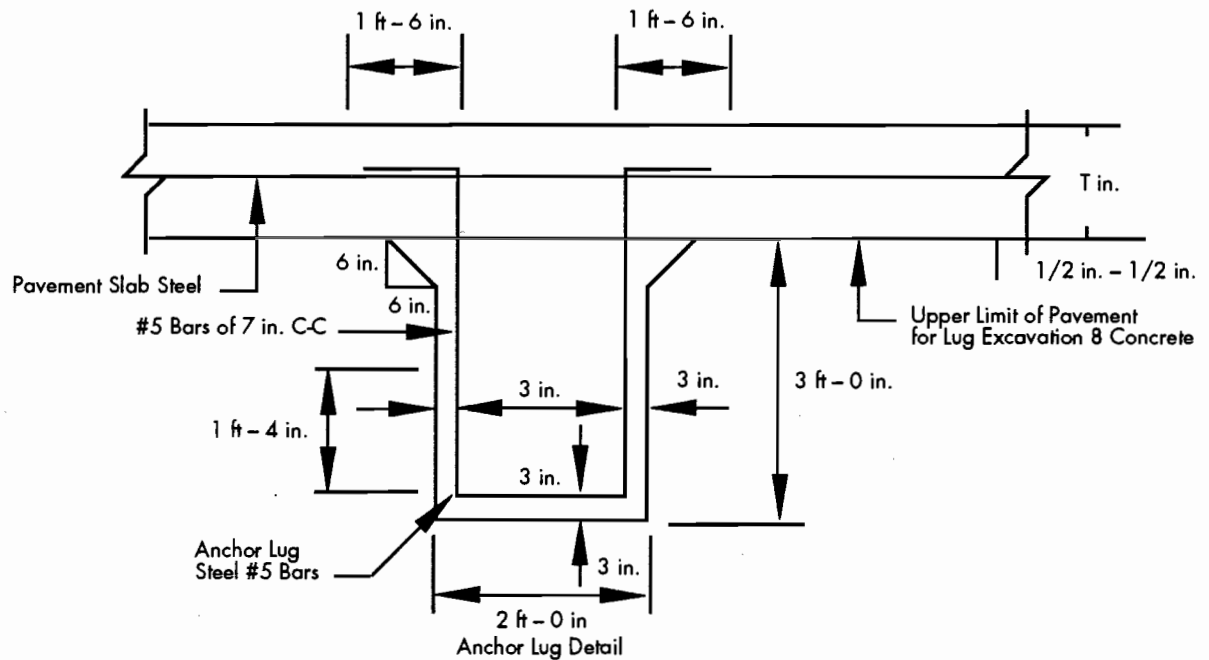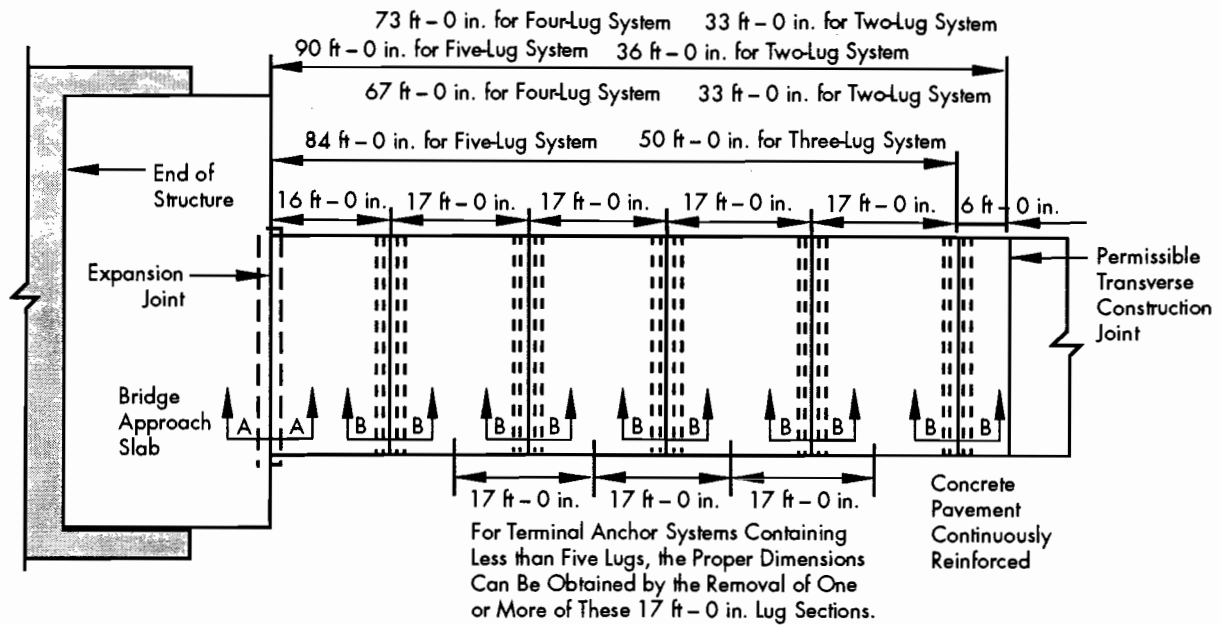
Figure 2.3. Typical terminal anchorage for use in CRC pavements (Ref 13)

an adverse effect inherent to transverse cracks. The increase in wheel load stresses because of transverse cracks depends on the ability of the cracks to transfer bending moments across the cracks. This subject is treated separately later in this chapter.

Volume-change stresses are greatest around the middle of a slab bounded by two adjacent transverse cracks, which is referred to as a slab segment in this study. Forming new cracks around the middle of a slab segment lessens volume-change stresses. However, forming new cracks close to existing cracks does not reduce volume change stresses much, but subjects the newly formed short slab segment to high wheel load stresses. Some CRCP sections have uniform crack-spacing distributions, while others do not. For the reasons given above, in order to increase the beneficial effect and decrease the adverse effect that transverse cracks cause, it is desirable to have
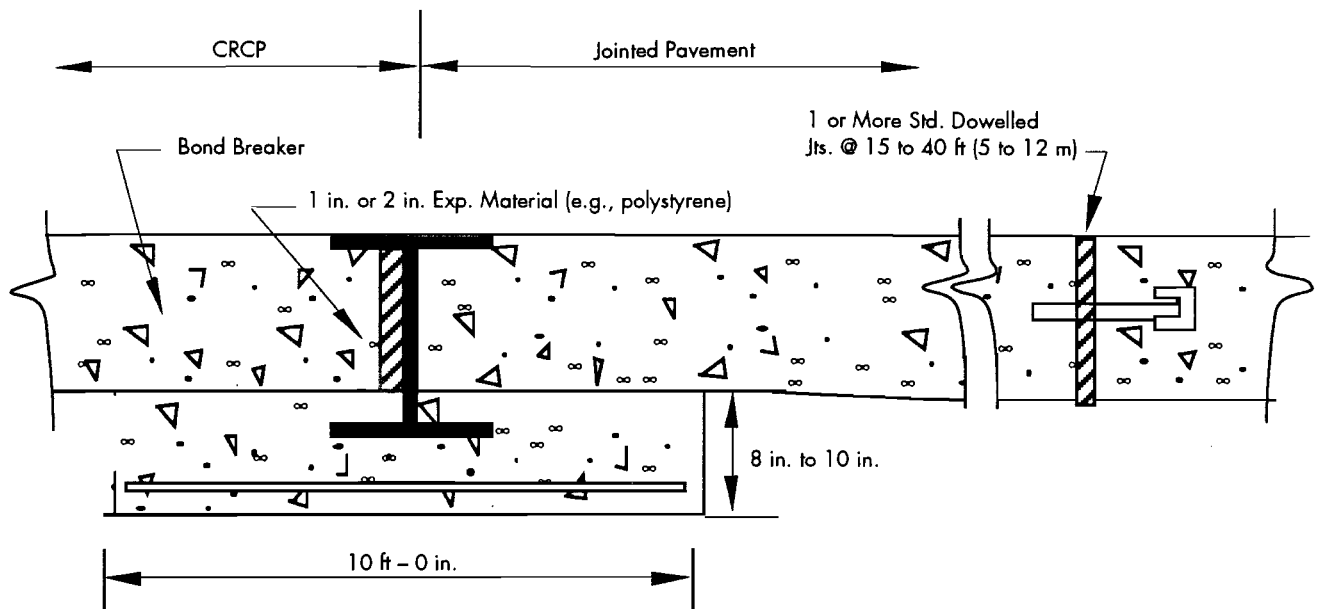
Figure 2.4. Wide-flange terminal joint (Ref 10)

uniform crack-spacing distribution with adequate intervals. The factors affecting the uniformity of crack-spacing distributions need to be investigated.

Aggregate Type

For given environmental conditions, concrete volume change stresses depend on modulus of elasticity, thermal properties, and drying shrinkage of concrete. Those concrete properties depend, to some extent, on the coarse aggregate type used. Concrete with larger values of the above properties has smaller crack spacings. Figure 2.5 shows the crack spacing distribution of pavements containing siliceous river gravel and limestone. The data were obtained from the rigid pavement data base at the Center for Transportation Research. The other conditions, except for coarse aggregate type, such as slab thickness and percent steel, were practically the same for
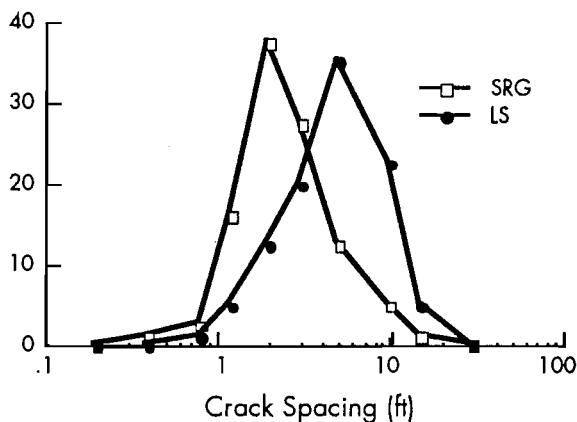
both sections. There is a significant difference in crack spacing distributions between sections containing siliceous river gravel and limestone aggregate. Concrete containing siliceous river gravel has larger values of thermal coefficient and modulus of elasticity than concrete containing limestone. High modulus and thermal coefficient values result in larger concrete stresses, and thus more cracking.

Unrestrained concrete volume changes, because of temperature variations, are directly proportional to the thermal coefficient of the concrete. Therefore, concrete stresses resulting from restraints on concrete volume changes are larger for concrete with higher thermal coefficients. A larger thermal coefficient for concrete containing siliceous river gravel explains part of the reason for the smaller crack spacing in CRC pavement with that aggregate type.

Volume-change stresses are less for slab segments with smaller crack spacings than for slab segments with larger crack spacings. However, slab segments with smaller crack spacings cause large wheel load stresses in the transverse direction, resulting in longitudinal cracking or punchouts. The mechanism of punchouts is discussed in Chapter 7.

Figure 2.6 presents the performances of two adjacent pavement sections which have almost identical conditions except for coarse aggregate type. The data were obtained from the rigid pavement data base at the Center for Transportation Research. Two things are observed. First, the number of failures increases with pavement age. Second, coarse aggregate type plays an important role. The difference in the performance of two sections is attributed to the coarse aggregate types, because all of the other conditions including traffic were practically the same in both sections.

Figure 2.5. Crack spacing distributions of concrete containing siliceous river gravel (SRG) and limestone coarse aggregate (LS)

9

Figure 2.6.   Number of failures and age relationship for SRG and LS concretes

For CRC pavement design, most states do not consider coarse aggregate type a design variable. The underlying assumption that ignores coarse aggregate type is that strength is the only variable to be considered and that the other concrete properties can be ignored. The assumption ignores the concrete properties which cause stress and cracks to develop. The results of the assumption are shown in Figure 2.6. The Texas SDHPT recognized this mistake and developed a CRCP design standard which incorporates the effect of coarse aggregate type (Ref 18). The design is expected to provide equal performance for pavements containing any coarse aggregates.

Structural Continuity at Cracks

Cracks themselves do not necessarily indicate the deterioration of pavements. However, CRC pavement distresses are invariably associated with cracks. Cracks are linked with pavement distresses because transverse crack spacings and crack widths determine how slabs react to wheel loads. Wheel load stresses depend on crack spacings in that wheel load stresses in the transverse and the longitudinal directions are determined by transverse crack spacings. The relationship between transverse crack spacings and wheel load stresses is conceptually illustrated in Figure 2.7. In Figure 2.7(a), three wheel loading conditions are presented. When wheel loads are applied close to a pavement edge with no shoulder, more tensile stresses develop at the top of the slab than develop whe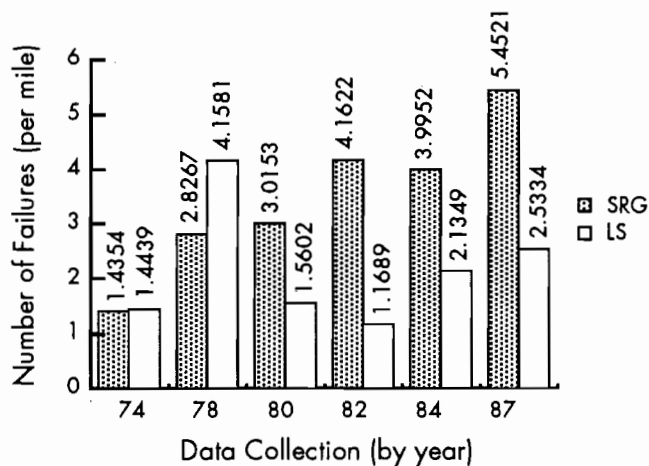n wheel loads are applied at the interior section of pavement. At transverse cracks, aggregate interlock and longitudinal steel bars transfer load across the cracks. Therefore, stresses when the load is applied close to the cracks are smaller than when it is at the edge. However, wheel load stresses at cracks, relative to those at the edge or interior, are

dependent on how much bending moment is transferred across those cracks.

Figure 2.7(b) illustrates wheel load stresses which have developed around cracks, when wheel loads are applied close to the cracks, as a function of crack spacing. When crack spacing is less than x_i', the slab segment behaves like a transverse beam, and the effect of crack spacings on wheel load stresses in both transverse and longitudinal directions is significant. Slab segments with spacings greater than x_i' behave as longitudinal beams, and wheel load stresses in the transverse direction are kept low. Wheel load stresses in longitudinal directions remain fairly constant up to the crack spacing of x_i''. Crack width is closely related to crack spacing because crack width is the sum of the concrete strains of two halves of the slab segments at each side of the crack. Larger crack spacing means larger contraction of concrete due to drying shrinkage and temperature drop. For crack spacings larger than x_i'', there is a loss of aggregate interlock due to large crack width. Load is transferred to the next slab through longitudinal bars only. Tensile stresses will develop at the top of the slab when wheel load is applied near cracks. Those stresses will be greater than those at the interior but less than those at the edge. Slab segments with spacings between x_i' and x_i'' are the desirable crack spacing ranges. Load transfer in terms of crack spacings is illustrated in Figure 2.7(c). For crack spacings between x_i' and x_i'', full load transfer is achieved. Loss of load transfer occurs when crack spacings are greater than x_i'', due to large crack widths. When crack spacing is very small, bond slip occurs throughout the slab. Repeated load applications deteriorate the bond between the concrete and steel because slab segments with narrow crack spacings experience more movement due to wheel loads than slab segments with large crack spacings. The restraint of longitudinal steel on concrete volume changes is not as effective when compared with the restraint where fully bonded zone exists. Therefore, concrete stress due to environ-mental loading is kept low and, considering small crack spacing, relatively large crack widths result. These large crack widths lead to the loss of aggregate interlock at the cracks. The crack spacing at which bond development length is equal to half of the crack spacing is represented as x_i in Figure 2.7(c). For slab segments with spacings between x_i and x_i', tighter crack widths, compared with those of crack spacings less than x_i, are maintained and almost full load transfer is achieved. The increase in wheel load stresses in transverse directions for slabs with spacings of x_i through x_i' [Figure 2.7(b)] is due to the decrease in the transverse beam action of slab segment. The crack spacing above which loss of

aggregate interlock occurs (x_i'') depends, in part, on the thermal coefficient of concrete. Concrete slabs with a high thermal coefficient lead to larger crack widths for the same crack spacing and temperature drop than concrete with a low thermal coefficient. Therefore, x_i'' is a function of the thermal coefficient of the concrete used as shown in Figure 2.7(c).

(a) Three wheel loading conditions

(b) Crack spacing vs wheel load stresses

(c) Crack spacing vs load transfer
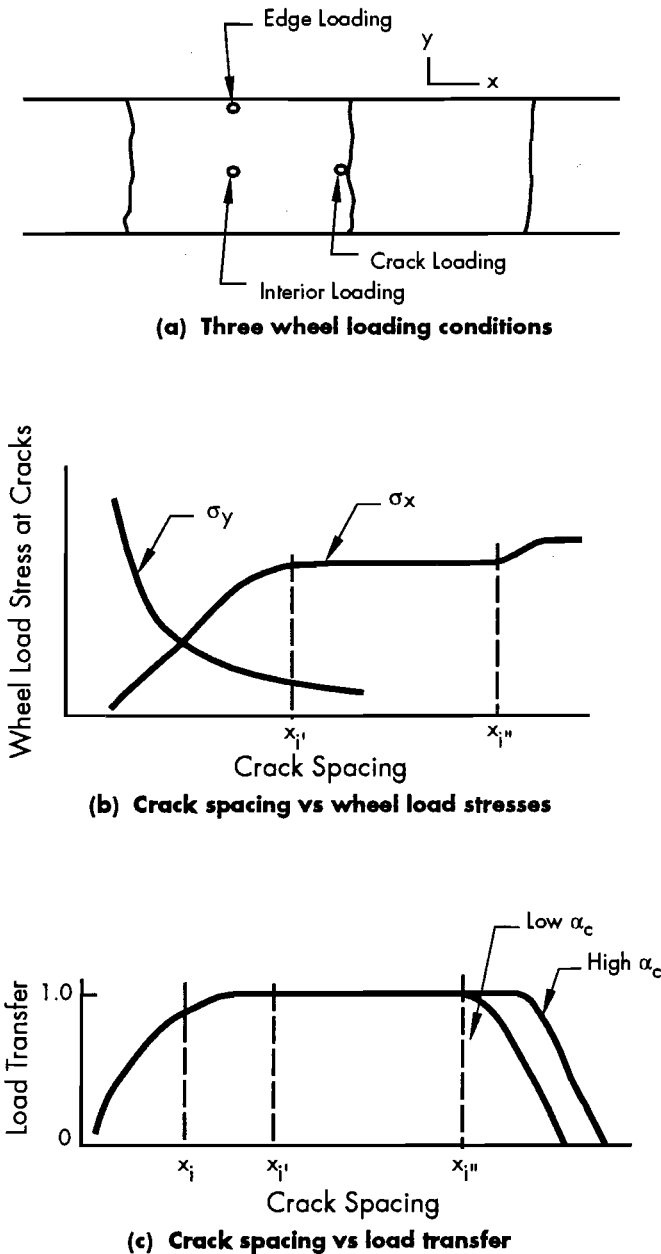
Figure 2.7. **Relationship between transverse crack spacings, wheel load stresses in both directions, and load transfer**

The effect of crack width on wheel load stress depends on the bending moment transferred at the crack. The ability of the transverse cracks to transfer bending moment across the cracks can be expressed in terms of bending stiffness at a crack. If full bending moment is transferred, bending stiffness at a crack will be the same as that in uncracked sections. On the other hand, bending stiffness would be zero if no bending moment were transferred at a crack. The transference of bending moment depends on crack width; therefore, the reduction in bending stiffness is related to crack width. Conceptually, the relationship is illustrated in Figure 2.8(a). If load transfer is 100 percent, the slab will behave as a continuous beam, and the reduction in bending stiffness will be zero. On the other hand, if the load transfer is zero, the reduction in bending stiffness would be 100 percent. In Figure 2.8(b), a relationship between wheel load stresses and bending stiffness at a crack is illustrated. If a full load transfer is achieved, an interior condition exists and wheel load stress is constant, regardless of the location of the wheel load applied, assuming it is away from the pavement edge. When there is a reduction in bending stiffness, wheel load stresses at cracks in longitudinal directions decrease. As the wheel load moves away from the crack, wheel load stresses become maximum when wheel load is applied at some distance from the crack. As the wheel load is moved further away from the crack, the effect of the reduction in bending stiffness at cracks becomes negligible, and wheel load stress approaches that of the interior condition. At the AASHO Road Test, there was a close correlation between performance of the pavement and critical wheel load stresses (Ref 21). It is important to evaluate wheel load stresses for various conditions at cracks. There are various methods to evaluate structural continuity of cracks. "Structural continuity" is used to express the ability of the cracks to transfer bending moment across themselves. Therefore, structural continuity is another expression for bending stiffness of the cracks. A quantitative relationship between structural continuity and bending stiffness needs to be explored.

There are several methods to evaluate the ability of cracks or joints to transfer wheel load from one side of the cracks or joints to the other. Teller and Sutherland proposed a method to evaluate the load transfer as follows (Ref 19):

$$LT(\%) = \frac{2d'_j}{d_i + d'_j} \times 100 \qquad (2.7)$$

where

LT = the load transfer, percent,

d_i = the deflection at the loaded slab, and

d'_j = the deflection at the unloaded slab.

If the load transfer is perfect, deflections at the loaded and unloaded slabs will be the same and the load transfer will be 100 percent. If, however, there were no load transfer, only the loaded slab will deflect and the load transfer will be zero.
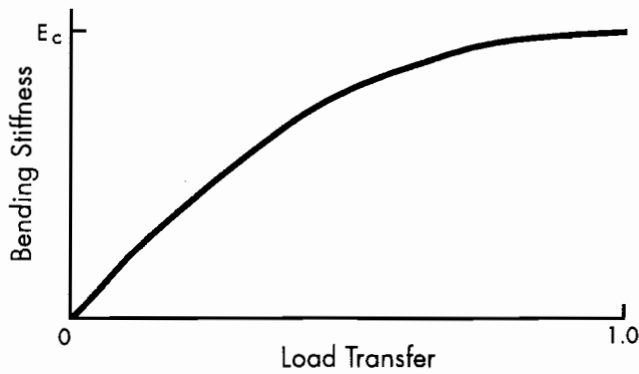
(a) **Relationship between load transfer and bending stiffness**
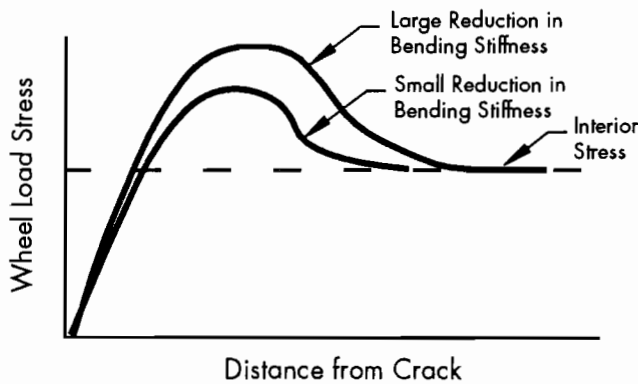
(b) **Variations in wheel load stresses for various values in reduction of bending stiffness at cracks**

Figure 2.8.   Relationship between load transfer, reduction in bending stiffness, and wheel load stresses

Ricci et al (Ref 20) proposed a method to evaluate load transfer using the Falling Weight Deflectometer. Deflection ratio is defined as the ratio of S_3 to S_2 (Figure 2.9). Upstream deflection ratio (UDR) and downstream deflection ratio (DDR) are obtained by applying load on each side of the joint. Load transfer is defined as the average of the two deflection ratios:

$$LT = \frac{UDR + DDR}{2} \tag{2.8}$$

This definition is based on the assumption that the deflection basin is symmetric with respect to the loading point. The value from this formula is the average ratio of the deflection in the unloaded side to the deflection in the loaded side. If actual load transfer is perfect, S_2 and S_3 will be the same. UDR and DDR will be 1 respectively, and load transfer (LT) = 1. On the other hand, if there is no actual load transfer, UDR and DDR will be 0; thus LT = 0.

One definition of load transfer is

$$LT = 1 - \frac{\delta_i - \delta_j}{\delta_i} = 2 - \frac{\delta_j}{\delta_i} \tag{2.9}$$

where δ_i and δ_j are deflections in the interior away from the crack and at the crack, respectively. If perfect load transfer exists at cracks, deflections at cracks and the interior will be the same and load transfer will be one. On the other hand, if the deflection at a crack is three times as large as that in the interior, a load transfer value of –1 will be obtained. Therefore, in this method the boundary condition is not always satisfied.

The first two methods are concerned with the relative deflections across a crack. The same deflections can occur across a crack due to longitudinal

Deflection Basin and Joint Location at Upstream Position

Deflection Basin and Joint Location at Downstream Position
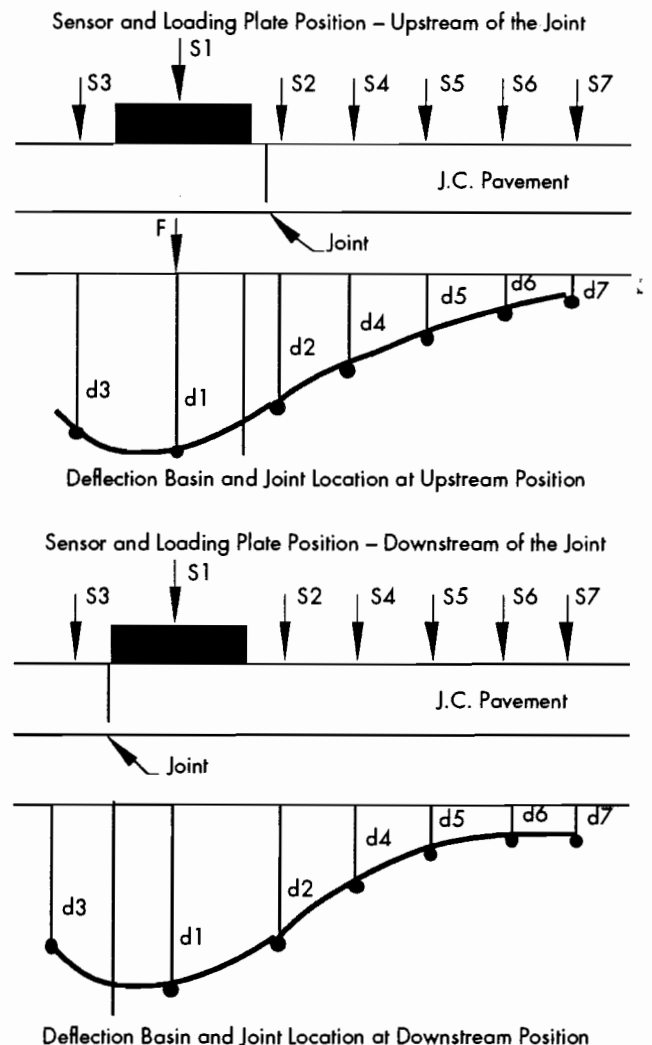
Figure 2.9.   One method for evaluating load transfer at joints (Ref 20)

steel bars without aggregate interlock. Even when bending stiffness at a crack is zero, as long as the deflections across the crack are the same, perfect load transfer is assumed. This approach is not adequate, because a unique relationship would not exist between bending stiffness and load transfer values obtained from these formulas. The third method considers the relative deflections in the interior and at a crack. However, deflection at a crack must be twice that in the interior to satisfy the boundary condition that load transfer is zero when no load is transferred at a crack.

A formula proposed in this study for the measure of structural continuity at a crack along with the discussions made above concerns the deflections in the interior and at a crack relative to that at the edge without a tied shoulder:

$$LT(\%) = 100 - \frac{\delta_j - \delta_i}{\delta_e - \delta_i} \times 100 \qquad (2.10)$$

where δ_i and δ_j are the same as in Eq 2.7, and δ_e is the edge deflection without a tied shoulder.

If there is no load transfer at a crack, the deflections at a crack and edge will be the same and load transfer will be zero percent. If perfect load transfer exists, deflection at a crack will be the same as that in the interior and load transfer would be 100 percent. This method satisfies boundary conditions and expresses structural conditions of a crack in terms of edge and interior conditions. Therefore, it is believed that this method is the most rational one among the four in evaluating structural conditions of a crack.

Development of a quantitative relationship between load transfer values from Eq 2.8 and bending stiffnesses and "J" values in the performance equation in the AASHTO Guide (Ref 2) will improve CRC pavement designs.

SUMMARY

CRC pavement designs have evolved through field experience and to a lesser extent theoretical studies. Current design and construction techniques provide overall satisfactory performance. However, more research is needed to minimize distresses in CRC pavements because repair is costly.

Cracks are closely related to pavement distresses. More study needs to be directed to investigating various characteristics of pavements related to cracks. A formula to be used in evaluating structural continuity at a crack is proposed. This formula is recommended for identifying structural continuity of cracks and developing useful relationships with other variables associated with cracks.

Coarse aggregate type plays an important role in CRC pavement behavior because material properties determining CRC pavement behavior to environmental conditions, such as thermal coefficient and tensile strength, largely depend on the coarse aggregate type. Field performance studies reveal that the performances of CRC pavements vary, depending on the coarse aggregate type used. Variations in material properties arising from using different coarse aggregates have been investigated at the Center for Transportation Research and the results are being considered for use in CRC pavement design standards.

Responses of CRC pavements to wheel loads are influenced by transverse crack spacings. Crack spacings between 3.5 and 8 feet are ideal. Variability in transverse crack spacings is closely related to material variability. Slabs with very small or very large crack spacings lead to pavement distress. It is best to have most cracks within the crack spacing range mentioned above. In this study, the effect of material variability on the performance of CRC pavements is investigated through a mechanistic analysis of the pavement system.

CHAPTER 3. CRC PAVEMENT BEHAVIOR

Pavement behavior is defined as the immediate response of the pavement to load. Pavement distress is the limiting response or damage in the pavement (Ref 21). Since the primary objective of the pavement is to provide smooth riding quality and adequate safety for the pavement users, investigation of pavement behavior is essential to achieving the primary goal of the pavement. CRCP behavior depends on many factors. Given the design conditions, such as slab thickness and stiffness of the subbase, CRCP behavior is largely a function of wheel load, transverse crack spacing, and crack width. Crack width is closely related to transverse crack spacing. Therefore, for given wheel loads, CRCP behavior can be considered to depend primarily on transverse crack spacing. Since the pavement distress is the limiting response or damage in the pavement, a relationship between distress and transverse crack spacing can be found.

In CRCP, concrete tensile stresses resulting from temperature changes and drying shrinkage are relieved by the forming of transverse cracks. The addition of wheel load stresses compounds the problem of cracking, i.e., by causing additional cracking. These transverse cracks, if spaced at adequate intervals, are not detrimental to pavement performance. In fact, uniformly spaced cracks, with adequate intervals, are the ideal conditions that CRC pavement designers are after. Most of the failures in CRC pavements are closely related to erratic transverse cracks or transverse cracks that are too small or too large.

In this chapter, the nature of transverse cracking and the factors affecting transverse cracking are discussed. The nature of the factors affecting transverse cracking and their relationships with transverse cracks are investigated. Finally, the relationship between the transverse crack spacing distribution and the pavement performance is discussed.

NATURE OF CRACKING IN CRC PAVEMENT

There are two different mechanisms in the formation of transverse cracks in CRC pavements. One is the development of the transverse cracks owing to restrained volume changes. The other is the bending action of the slab due to external wheel loads. The first mechanism is dominant at the early ages of the CRC pavements. After the pavement is open to traffic, the two mechanisms act together to induce more cracks. However, the second mechanism depends on the results of the first mechanism in that the stress induced by wheel loads partly depends on the crack spacing and crack width. Figure 3.1 presents the change of mean crack spacing over a long period of time (Ref 3). Mean crack spacing decreases rapidly in the first year (A through C). The decrease is due to
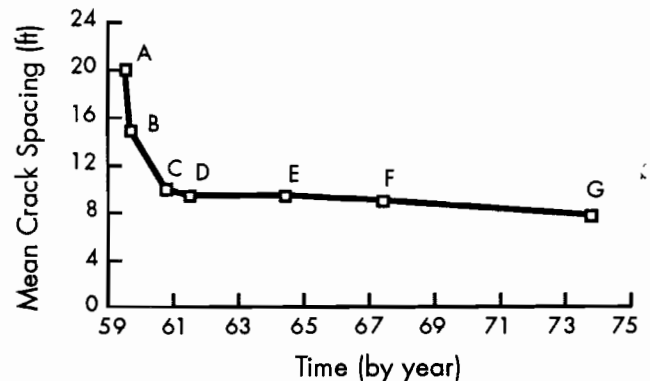
Figure 3.1. Change of mean crack spacings with age (Ref 3)

the combined effects of environmental and wheel loads. There is a small decrease in mean crack spacing for the following year. For virtually the next three years, there are no more cracks (C through E). Between five and eight years after construction (E through F), a slight decrease in mean crack spacing is observed. Since concrete strength increases with age, even though the amount at later ages is negligible compared with the amount at early ages, the additional cracks that developed during those three years are not considered to be due to environmental conditions. Instead, the additional cracks are believed to be developed due to fatigue. Additional cracks that developed for the next six and one-half years are also due to fatigue. The mechanism of the additional cracking after five years of construction is applied to longitudinal cracking as well as to transverse cracking. Any slab whose wheel load stress in

the transverse direction is greater than the stress which caused the additional transverse fatigue cracking will experience longitudinal cracking by exactly the same mechanism. Longitudinal cracks, when they connect two adjacent transverse cracks, lead to punchouts. A detailed discussion of the mechanism of punchouts is deferred until Chapter 7. In this section, the first restrained volume mechanism is discussed, followed by a discussion of the bending action mechanism.

Restrained Volume Change Mechanism

Concrete experiences volume changes due to temperature and moisture changes. If no restraint is applied to the volume changes, no stress and no cracking will result. Figure 3.2(a) shows a typical CRC pavement section between two adjacent transverse cracks. Generally, deformed longitudinal steel bars used in CRC pavements and an adequate lap between longitudinal bars prevent pullout of the bars. Therefore, it is considered that the longitudinal steel bar is fixed at transverse cracks. When there is a temperature drop and/or drying shrinkage, concrete contracts while longitudinal steel will not move in a longitudinal direction.

Since two materials in contact are trying to move in at different magnitudes, interfacial shear stress (so-called bond stress) develops at the interface between the steel bar surface and the concrete. The magnitude of the bond stress depends not only on the concrete contraction, but also on the chemical and mechanical shape of the longitudinal bar surface. If there is no bond between the steel and concrete and no subbase friction, concrete stress will not develop. Concrete contracts due to temperature drop; however, since the concrete in an unrestrained case is free to move, no stress develops in the concrete. In reality, a strong bond exists between the bar surface and the concrete, which is shown in Figure 3.2(b), and, thus, concrete volume changes are restrained.

Subbase frictional resistance is proportional, up to a certain point, to the magnitude of the concrete displacement. The direction of the frictional resistance is opposite to that of concrete displacement. Therefore, when the concrete contracts, subbase friction and the steel reinforcement resist the concrete displacement, thereby increasing concrete tensile stresses. The distribution of subbase frictional resistance is shown in Figure 3.2(c). The resistance to the concrete contraction through bond and subbase friction causes the concrete tensile stress to build up and the concrete displacement to be reduced. Figure 3.2(d) illustrates the concrete and steel stress distribution along the pavement slab. If the developed concrete stress exceeds the tensile strength, a crack will form. Thus, a balanced condition exists when the concrete tensile stresses do not exceed the tensile strength and when the crack pattern stabilizes.

Bending Slab Mechanism

When the external wheel load is applied to the pavement slab, the slab deflects; tensile stresses develop at the bottom of the slab, and compressive stresses at the top portion of the slab, shown in Figure 3.3(b). The objective of the longitudinal steel reinforcement is not to carry tensile stresses at the bottom of the slab when wheel loads are applied. Longitudinal bars are placed at about mid-depth of the slab, which is very close to the neutral axis. Therefore, longitudinal steel reinforcement does not carry tensile stresses at the bottom of the slab due to wheel loads. Since the concrete is very weak in tension in comparison to compression, cracks, due to wheel load, develop at the bottom of the slab first. These cracks, combined with the environmental conditions, spread through the top.

Combined Effects

The effects of two cracking mechanisms vary with age. In their early ages, crack spacings are relatively large and the rate of drying shrinkage is high. The volume change mechanism is significant during this period because there are large volume changes attributable to drying shrinkage and because of more restraint on volume changes from subbase friction. Maximum volume change stresses occur at the middle of the slab segment [Figure 3.3(a)]. The change in crack spacings from A to B in Figure 3.1 is due to the volume change mechanism.

After the pavement is open to traffic, the two mechanisms act together. Concrete stresses from both mechanisms are superimposed in Figure 3.3(c). The change in crack spacings from B to C and from C to D is due to the combined effects. Once cracks develop due to the combined effects, crack spacings become stabilized. Concrete usually undergoes cyclic volume changes once a day. These cyclic volume changes deteriorate the bond between the steel and the concrete. By the time crack spacings become stabilized, crack spacings are not as large as they were and stress transfer from the steel to concrete is not as effective as it had been because of bond deterioration. The volume change mechanism does not play a significant role. The bending mechanism becomes dominant.

The concrete then exhibits fatigue behavior. Even when wheel load stresses are below the modulus of rupture, cracks develop if the loads are repeatedly applied. Further cracks that develop after crack spacings become stabilized are due to the fatigue behavior of concrete. Fatigue cracks develop not only in transverse directions but in longitudinal

15
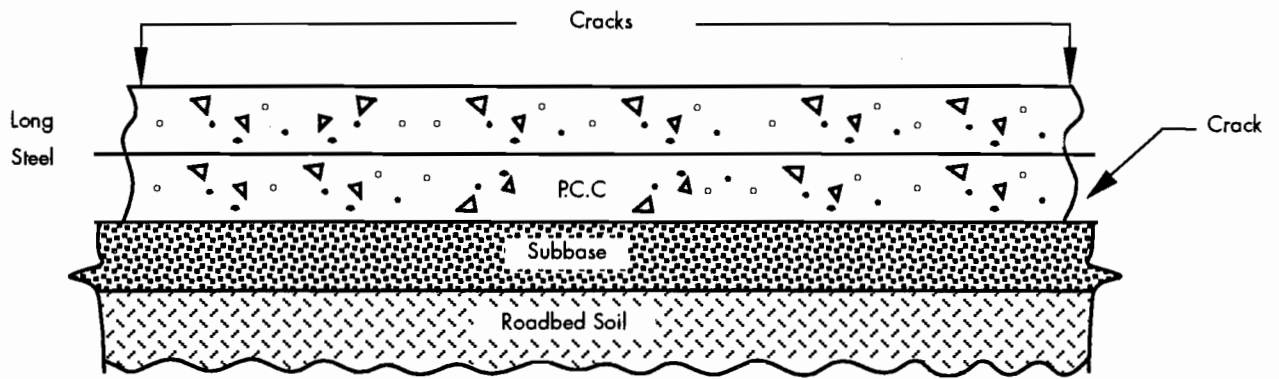
(a) Typical CRC pavement elements
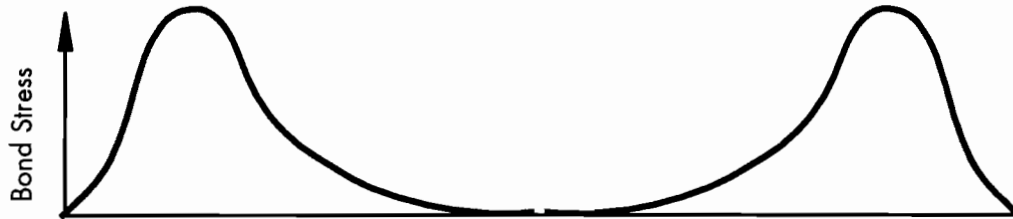
(b) Bond stress distribution between concrete and steel
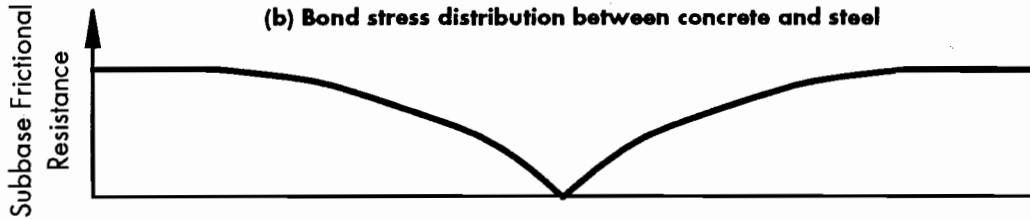
(c) Subbase frictional stress distribution
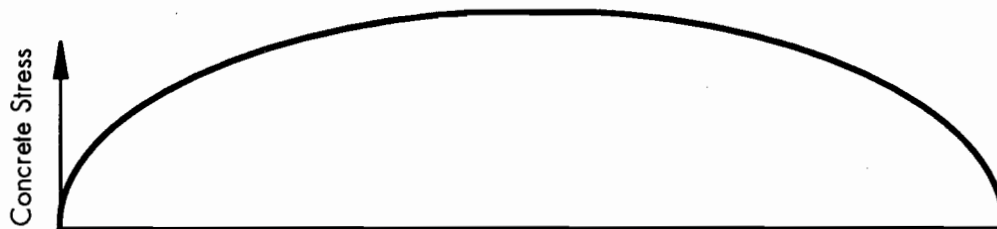
(d) Concrete and steel distributions

Figure 3.2. CRC pavement elements and distributions of various stresses

directions also. Development of fatigue cracks in transverse directions results in the decrease in mean crack spacings. The change in crack spacings from E to F and from F to G in Figure 3.1 is due to fatigue cracking. Fatigue cracks in longitudinal directions lead to punchouts. Punchouts can also develop from
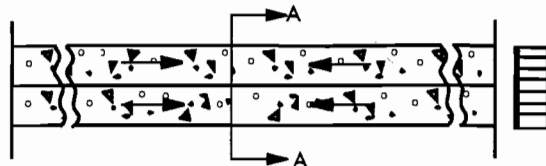
(a) Concrete restrained volume change stresses at A-A
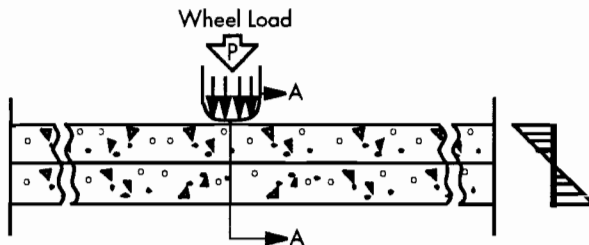
(b) Concrete stresses due to bending mechanism at A-A
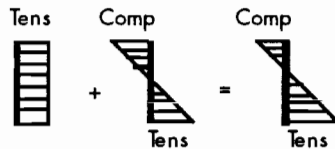
(c) Combined concrete stresses due to restrained volume changes and bending mechanism at A-A

Figure 3.3. Restrained volume change and bending stresses and their combined effect

uncontrolled longitidinal cracks that form at the early ages. This subject is discussed in more detail in Chapter 6.

FACTORS AFFECTING TRANSVERSE CRACKING IN CRC PAVEMENT

Many factors contribute to the formation of transverse cracking; these factors are summarized in Table 3.1. Cracks develop when the tensile stress exceeds the tensile strength of the concrete; thus, the tensile strength of the concrete is an important factor. Since the restrained concrete volume changes induce transverse cracking, thermal expansion of concrete and drying shrinkage of the concrete are important factors. The degree to which the concrete volume changes are restrained determines the concrete stress level. Thus, the ratio of the cross-sectional area of the steel to concrete, the surface deformation characteristics and the size of the longitudinal bars, and the subbase frictional characteristics influence the cracking of the concrete slab. Among the environmental conditions, concrete setting temperature, temperature change, and relative humidity at early ages have a significant effect on cracking. The wheel load stress depends on the slab thickness, the magnitude of the wheel load, and the stiffness of each layer, among other factors.

Concrete Properties

The structural responses in CRC pavements are the outcome of the interactions among material properties, environmental conditions, and traffic loading. Identifying and evaluating the significance of material properties in relation to CRC pavement behavior comprise one of the most important steps in improving designs.

Concrete Tensile Strength. There are two modes by which concrete fails: sliding and separation (Ref 22). A failure in compression occurs through sliding, whereas a failure in tension, without exception, follows the separation mode. In this report, attention was given to concrete failure in tension, because cracking in CRC pavements is due to excessive tensile stress. The problem is complex since there are many variables affecting concrete tensile strength.

Table 3.1.   Factors that influence crack spacing

I. System Stiffness
   A. Thickness of concrete
   B. Concrete modulus of elasticity
   C. Underlying support
   D. Bond
   E. Steel amount and depth

II. Restraints to Length Changes
   A. Internal restraints
      1. Steel: amount, surface area, deformations, connection to transverse steel, strength, coefficient of expansion, creep characteristics.
      2. Concrete: thickness, strength, modulus of elasticity, shrinkage, creep.
   B. External restraints
      1. Friction on base
      2. Bond to adjacent lane
      3. Distance from end
      4. Encroachment of adjacent pavement

III. Construction
   A. Laps
   B. Consolidation
   C. Construction joints
   D. Environmental conditions
      1. Temperature
      2. Precipitation

IV. Time
   A. Changing concrete properties
   B. Environmental conditions
      1. Temperature variations
      2. Precipitation
   C. Changing bond conditions
   D. Corrosion
      1. Deicing chemicals
   E. Traffic
   F. Base Erosion

17

The water/cement ratio is considered to be one of the most significant factors affecting concrete strength. The reason the water/cement ratio significantly affects the tensile strength of the concrete is that the water/cement ratio determines the porosity of the hardened cement paste at any stage of hydration. The pores lead to high stress concentrations in the material under load, so that a very high stress is reached in very small volumes of the concrete, with a consequent microscopic fracture. A tensile strength as high as 9,250 psi was obtained by reducing porosity by about 1 percent by the application of high pressure (50,000 psi) with a simultaneous high temperature (480°F) to cement paste (Ref 23). These and other tests show a direct relationship between concrete tensile strength and porosity, although the exact form of this relationship has not been established (Ref 24).

The properties of the coarse aggregate influence the concrete tensile strength. Jones and Kaplan conducted research to identify the effect of the bond strength between cement paste and the coarse aggregate surface on various concrete strengths using aggregate coated with polystyrene (Ref 25). They found that, whereas the compressive strength was not affected by the reduction in bond strength between the cement paste and the aggregate surface, there was a significant reduction in tensile strength. That indicates that tensile strength is controlled mainly by the strength of the bond at the cement-paste-aggregate interface. This result is also supported by the studies of Erntroy and Shacklock (Ref 26), who found that even though there was a relationship between compressive strength and indirect tensile strength, the relationship varied, depending on the coarse aggregate type used (Figure 3.4). For the
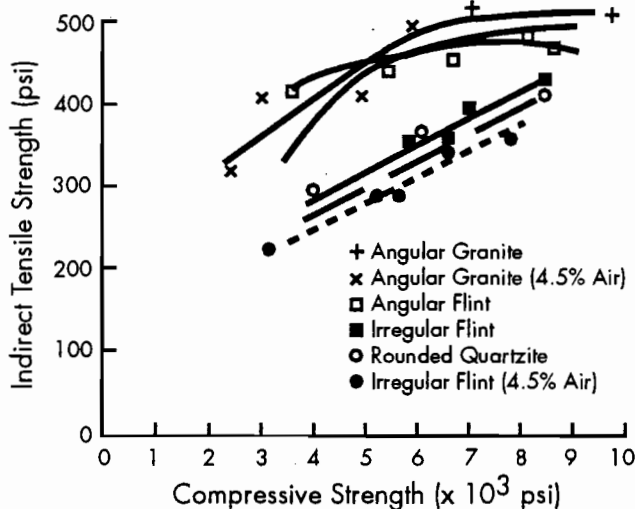
same compressive strength, concrete containing angular granite had as high as 1.2 times the tensile strength of the concrete containing rounded quartzite for a wide range of compressive strength. Coarse aggregates play an important role in some concrete properties, such as tensile strength, thermal coefficient, and modulus of elasticity. Those properties have a significant effect on CRC pavement performance. In order to evaluate the variations in concrete properties which arise from using different aggregates, and to develop CRC pavement designs which could make up for the differences in concrete properties, Research Project 3-8-86-422 was initiated. It consists of laboratory tests of concrete made with coarse aggregates collected from various parts of Texas and of a mechanistic analysis. The laboratory tests and the mechanistic analysis are geared to study the effect of variations in concrete properties on CRC pavement behavior and to develop CRCP designs which could provide equal performances regardless of coarse aggregate type used. A total of eight coarse aggregates were used. Figure 3.5 presents concrete tensile strength values obtained in this
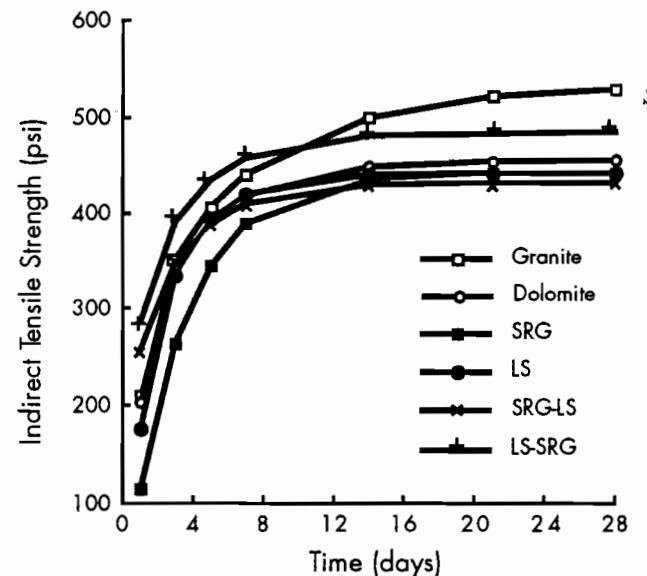
Figure 3.5. Tensile strengths as affected by coarse aggregate types

project. Differences are observed in tensile strength among concrete made with different aggregates. Granite gave the largest tensile strength values while siliceous river gravel and the blend of siliceous gravel and limestone produced the lowest tensile strength.

The effect of aggregate content on the concrete tensile strength is not significant, even though there is a general trend in which, as the volume of aggregate (as a percentage of the total volume) increases from 0 to 40, a gradual decrease in tensile strength

Figure 3.4. Compressive strength and indirect tensile strength relationship for various coarse aggregates (Ref 26)

occurs. However, there is an increase in tensile strength between 40 and 80 percent (Figure 3.6). The reasons for this effect are not clear (Ref 24).
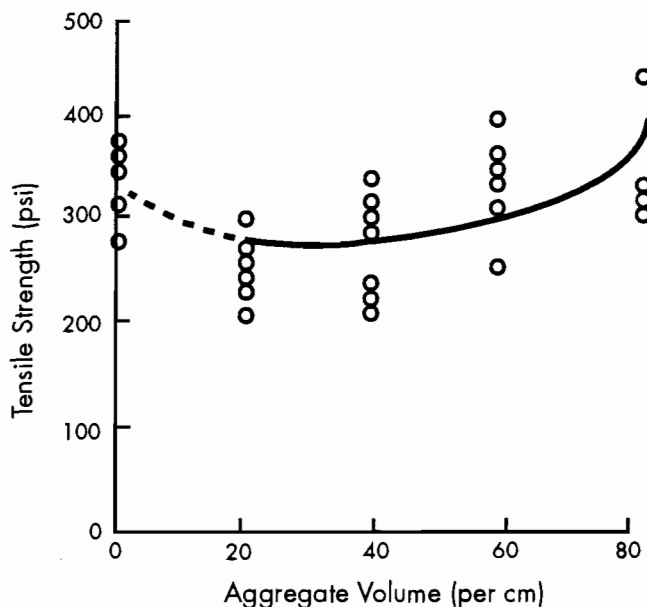
Figure 3.6. **Relationship between direct tensile strength and volume of aggregate at a constant water/cement ratio of 0.5 (Ref 24)**

Thermal Coefficient. The two main constituents of the concrete, cement paste and aggregate, have dissimilar thermal coefficients, with the coefficient for concrete being a resultant of the two values. Since about three-quarters of the concrete volume is aggregate, the biggest factor influencing the coefficient of thermal expansion appears to be the type of aggregate. Figure 3.7 shows the influence of the thermal
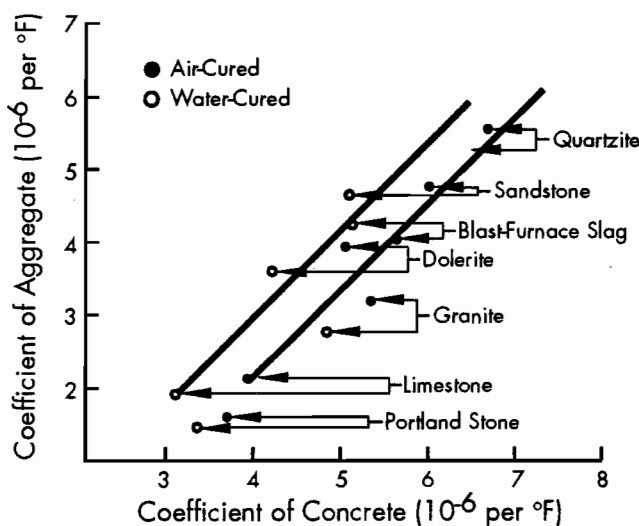
Figure 3.7. **Influence of the linear coefficient of thermal expansion of aggregate on the coefficient of thermal expansion of concrete (Ref 24)**

coefficient of the aggregate on that of concrete. There is an almost linear relationship between the thermal coefficients of the aggregate and the concrete. In thermal coefficient values measured in Project 422, there was a large difference among concretes containing various coarse aggregates (Table 3.2). Table 3.2 reveals an interesting point, which is that the thermal coefficient of concrete decreases as the content of siliceous river gravel decreases. In the same study, coarse aggregates from

Table 3.2. **Thermal Coefficient Values Obtained in Project 422**

Aggregate	Thermal Coefficient $(x10^{-6}$ per °F)
SRG	8.18
SRG - LS	6.15
Dolomite	5.90
Granite	5.74
LS - SRG	5.44
LS/LS-SRG	4.84

*Blend of 50 percent LS and 50 percent LS - SRG.

several sources contained both siliceous river gravel and limestone. In order to differentiate coarse aggregates containing various siliceous river gravel contents, terminologies such as siliceous-limestone and limestone-siliceous were used. Siliceous-limestone is used for coarse aggregates when more than 50 percent of coarse aggregates were siliceous river gravel, while limestone-siliceous is used for coarse aggregates when more than 50 percent were limestone. The highest value of thermal coefficient was obtained for concrete containing siliceous river gravel. Concrete containing siliceous-limestone aggregates gave slightly less value than that of concrete with siliceous river gravel. The thermal coefficient of concrete containing limestone-siliceous was much lower than that of siliceous-limestone. The lowest thermal coefficient was obtained when the blend of 50 percent limestone and 50 percent siliceous-limestone was used. Thermal coefficient values of concretes containing dolomite and granite were between those of siliceous-limestone and limestone-siliceous. The results of the thermal coefficient study in Project 422 indicate that the thermal coefficient of concrete is a function of siliceous river gravel content: the higher its content, the higher the thermal coefficient of the concrete. A study by Browne (Ref 27) shows that the effect of silica content in the aggregate on the thermal coefficient is significant: the higher the silica content, the higher the thermal coefficient of the concrete (Table 3.3). In Project 422, chemical analysis was made of various coarse aggregates, and a

Table 3.3. Coefficient of thermal expansion of aggregates and concrete (Ref 27)

| Rock Group | Normal Silica Content by Weight, Percent | Thermal Expansion ($\times 10^{-6}$ per °F) | | | |
| | | Rock | | Concrete | |
		Range	Average	Range	Average
Chert	94	4.1 - 7.2	6.6	6.3 - 6.8	7.3
Quartzite	94	3.9 - 7.3	5.7	6.5 - 8.1	6.7
Quartz	94	-	-	5.0 - 7.3	-
Sandstone	84	2.4 - 6.7	5.2	5.1 - 7.4	6.3
Marble	Negligible	1.2 - 8.9	4.6	2.4 - 4.1	5.9
Sil. limestone	45	2.0 - 5.4	4.6	4.5 - 6.1	5.9
Granite	66	1.0 - 6.6	3.8	4.5 - 5.7	5.3
Dolerite	50	2.5 - 4.7	3.8	-	5.3
Basalt	51	2.2 - 5.4	3.6	4.4 - 5.8	5.2
Limestone	Negligible	1.0 - 6.5	3.1	2.4 - 5.7	4.8
Glacial gravel	5-95	-	-	5.0 - 7.6	-
Lightwgt. agg.	-	-	-	2.8 - 6.1	4.4

positive relationship was found between the thermal coefficient of concrete and the silica content of coarse aggregates, (Figure 3.8). The effect of mix proportions shown in Table 3.4 indicates that mix proportions have little effect. It also shows that air-cured concrete has a larger thermal coefficient than wet-cured concrete, which is shown in Figure 3.7.
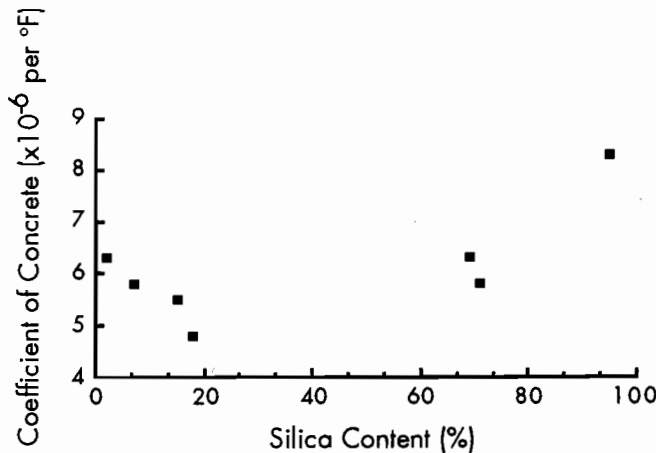
Figure 3.8. Relation between silica content and thermal coefficient of concrete

The effect of mix proportions and of aggregate types is shown in Figure 3.9. Figure 3.9 indicates that the thermal coefficient of the concrete is exclusively a function of the aggregate type used and, therefore, almost independent of the mix proportions.

Drying Shrinkage. Drying shrinkage plays an important role in the early cracking in CRC pavement. The theories offered in the literature to explain concrete shrinkage are numerous. And yet, none of them succeeds in explaining the effect of all factors. However, all theories advanced until now agree on one point: the main roll in the concrete shrinkage phenomena is played by water. According to Powers and Brownyard (Ref 28), water in cement paste is of three types: (1) non-evaporable water, (2) gel water, and (3) capillary water. The non-evaporable water has entered into chemical combination with the cement and can be removed only by the application of considerable heat. The gel, in addition to being composed of colloidal matter, comprises an appreciable proportion of pores, and these and the capillary pores are initially filled with water. It is the presence of these two types of water which largely determines drying shrinkage. The effect of water/cement ratio on drying shrinkage is shown in Figure 3.10. For the same richness of mix, shrinkage increases in fairly direct proportion to the water/cement ratio. The data in Figure 3.10 also show that at constant water/cement ratio the shrinkage increases considerably with the richness of the mix because of the larger amount of cement paste, which causes shrinkage.

While water/cement ratio is the single most important variable in drying shrinkage, an important influence is exerted by aggregate. The shrinkage of concrete is less than that of neat cement, owing to the restraining influence of the aggregate, and may be one-fifth to one-tenth, or even less, of that of neat cement (Ref 29). The aggregate is surrounded by cement paste, which, in shrinking, places the aggregate under compression and itself becomes subjected to tensile forces. From this reasoning, it would be expected that aggregate with a high modulus of elasticity would give a concrete with less shrinkage than an aggregate with a low modulus of elasticity would, and this is found to be the case, as shown in Figure 3.11 and Table 3.5 (Ref 30). Carlson (Ref 31) made some concrete using rubber as an aggregate. This contracted almost as much as the corresponding neat cement paste and about eight

	Thermal Expansion ($\times 10^{-6}$ per °F)							
			Concrete of Mix Proportions					
	Aggregate		Air Storage			Wet Storage		
Type of Aggregate	Dry	Wet	1:4 1/2	1:6	1:7 1/2	1:4 1/2	1.:6	1:7 1/2
Gravel	-	-	7.6	7.3	7.4	6.9	6.8	6.8
Granite	3.2	3.0	5.4	5.3	5.3	4.7	4.8	4.5
Quartzite	6.5	6.1	8.1	7.1	7.1	6.5	6.8	6.6
Dolerite	4.3	4.1	5.8	5.3	5.1	4.2	4.7	4.3
Sandstone	5.6	5.5	6.9	6.5	6.1	5.7	5.6	5.8
Limestone	2.5	2.2	4.3	4.1	3.4	3.5	3.4	3.2
Portland stone	2.4	2.1	4.2	4.1	3.8	3.8	3.1	3.5
Blast-furnace slag	4.4	4.4	6.2	5.9	5.7	5.3	5.1	4.8
Foamed slag	-	-	7.2	5.7	5.6	5.2	5.1	5.9

times as much as ordinary concrete. The size and grading of aggregate *per se* do not influence the
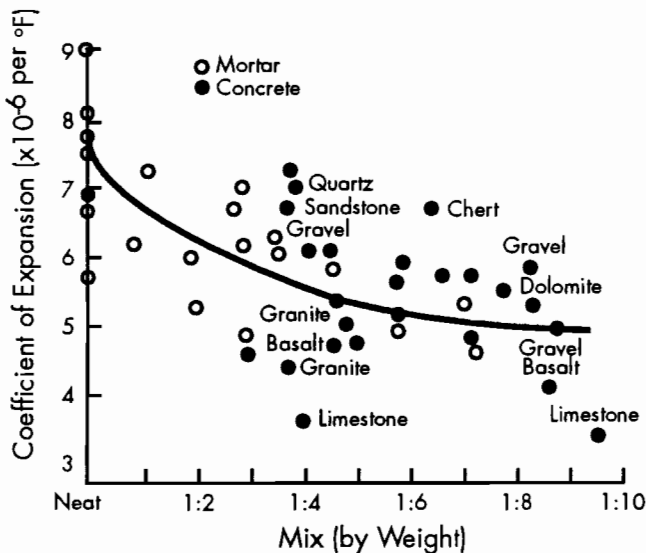
Figure 3.9. Thermal coefficients of neat cements, mortar, and concretes (Ref 49)

magnitude of shrinkage, but a larger aggregate permits the use of a leaner mix and hence results in a lower shrinkage. The relative humidity of the air surrounding the concrete greatly affects the magnitude of drying shrinkage, as shown in Figure 3.12. Shrinkage in 50 percent relative humidity is practically 1.5 times that at 70 percent of relative humidity. The changes in drying shrinkage with age are illustrated in Figures 3.11 and 3.12. According to Troxell et al (Ref 30), 66 to 88 percent of the 20-year shrinkage occurs in one year.

Steel Properties

Steel is used in CRC pavements for its high yield and tensile strengths. Steel does not experience drying shrinkage and, therefore, does not undergo as much volume change as concrete as a result of temperature and moisture variations. High yield and tensile strengths and less volume change of steel make it possible to keep continuity of CRC pavements. There are several design variables related to steel bars which have a significant effect on the behavior of CRC pavements. They include percent longitudinal steel, bar size, and vertical location of longitudinal steel.
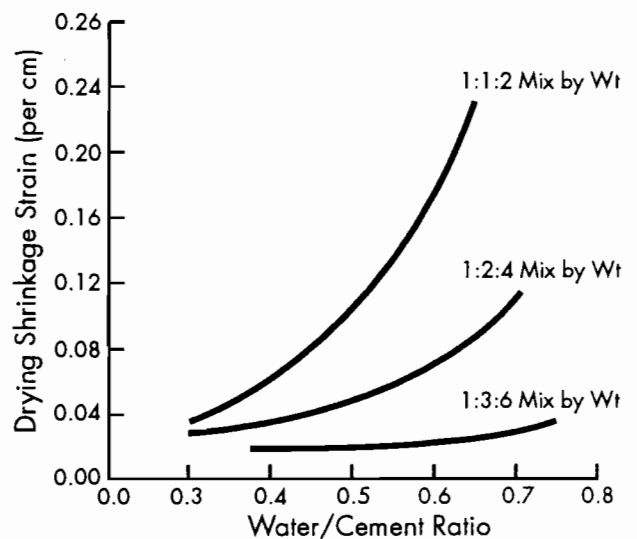
Figure 3.10. Effect of water/cement ratio on drying shrinkage (Ref 29)

21
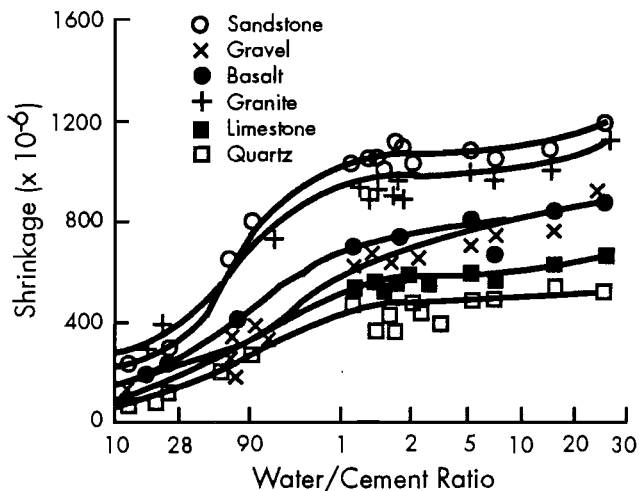
Figure 3.11. Shrinkage of concretes with fixed mix proportions but made with different aggregates (Ref 24)
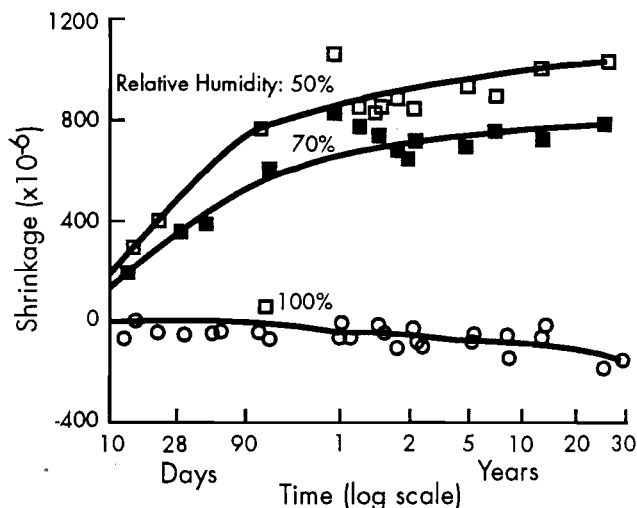
Figure 3.12. Relationship between shrinkage and time for concretes stored at different relative humidities (Ref 24)

Table 3.5.   Relationship Between Drying Shrinkage and Elastic Modulus (Ref 27)

Aggregate Type	Elastic Modulus $\times 10^6$ (psi)	Absorption Percent by volume	Drying Shrinkage at 1 year $\times 10^6$
Basalt	13.42	3.3	300
Rounded quartz	12.08	4.7	180
Crushed quartz	3.32	6.6	330
Marble	6.51	8.0	250
Granite	6.08	5.5	290
Mixed river gravel	5.51	3.2	280
Calcareous sandstone	2.76	9.7	1,020
Ferruginous sandstone	1.35	13.6	630

Longitudinal Reinforcing Steel. In CRC pavement, the restraint on concrete volume changes largely comes from the longitudinal reinforcing steel. The amount of the longitudinal reinforcing steel significantly influences the transverse cracking development: as the amount increases, so does the restraint, resulting in more cracks. The effect of the amount of the longitudinal steel, as observed in the field, is shown in Figure 3.13. The effect is not significant when the percentage of the longitudinal steel is greater then one percent. However, at a range of less than 1 percent, the effect is significant. The percentage of longitudinal reinforcement also affects the tightness of the transverse cracks, which, in turn, influences aggregate interlock and the load transfer at a crack. Field observations, in addition to theoretical design concepts, verify the fact that crack width in CRC pavements decreases with increase in percentage of longitudinal reinforcement (Refs 3 and 32).

Bar Size and Bond Area. Bar size has an influence in cracking development in that the restraint of

the longitudinal steel depends on the bar size. A great portion of concrete stress in CRC pavements comes from the steel stress at a crack through stress transfer. The stress transfer from the longitudinal steel to the concrete depends on the steel surface area and the surface deformation shape of the longitudinal steel. For the same percent of longitudinal steel, a smaller-size bar provides a larger steel surface area, which in turn increases the stress transfer from the steel to the concrete. Figure 3.14 presents the results of the condition survey conducted by the Center for Transportation Research. The effect of bar size on crack spacing is vividly shown. In 1962, McCullough and Ledbetter found that crack spacing was inversely proportional to the ratio of the bond area to concrete volume, as shown in Figure 3.15 (Ref 7). To investigate this concept, the Texas SDHPT built experimental CRCP test sections in Houston in 1964. On that particular study, the ratio of the bond area to concrete volume was held constant while the longitudinal steel percentage varied from 0.3 to 0.5.
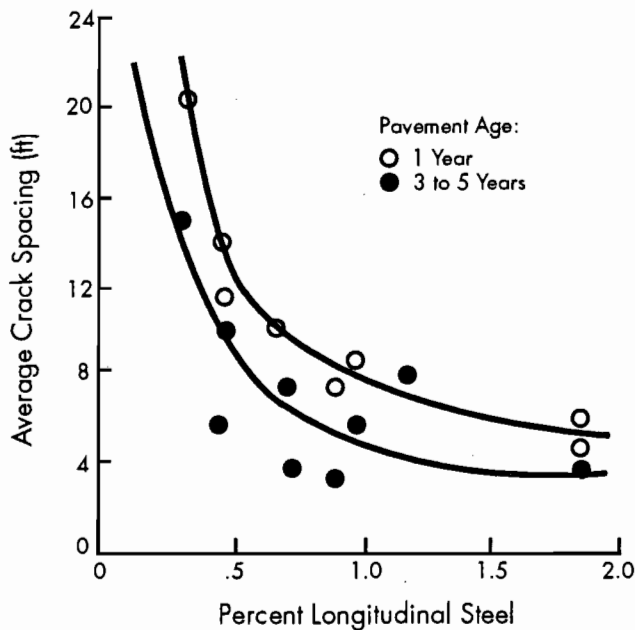
Figure 3.13. Effect of percent steel on crack spacing (Ref 32)

After 20 years, the crack spacings for all percentages of steel were practically the same (Ref 33). This finding suggests the strong relationship between the ratio of the bond area to the concrete volume. Although most states do not consider bond area in designing longitudinal reinforcement, the 1972 AASHO Interim Guide suggests that the ratio of the bond area to concrete volume be greater than 0.003 inch^2/inch^3.

Vertical Location of Longitudinal Steel. A review of the literature reveals that the vertical location of the longitudinal steel has a significant effect on the transverse crack spacing. The concrete in CRC pavements undergoes differential volume changes due to
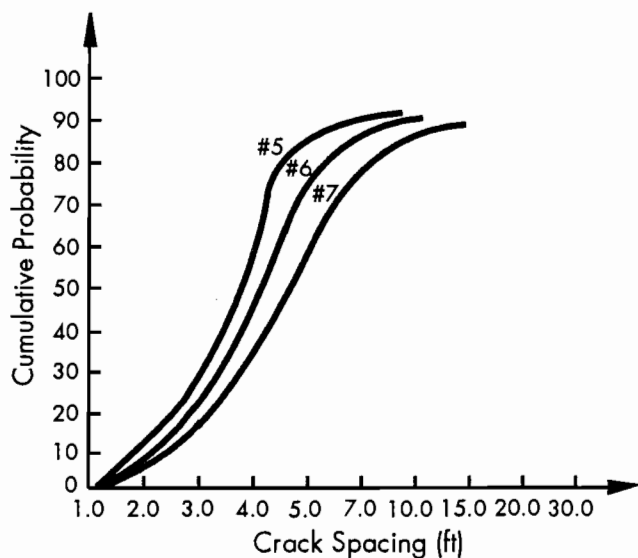
Figure 3.14. Effect of bar size on crack spacing

the temperature and the moisture gradients through the depth. The volume changes at the top part of the slab are greater than those at the bottom, because temperature and moisture changes at the top part are greater than those at the bottom. If the steel is placed close to the top, the steel's restraint to concrete volume changes becomes significant, and results in more cracks. A field study of CRC pavements in South Dakota shows an average crack spacing of 1.7 feet with the centerline of the steel 2.5 inches below the surface, and an average spacing of 2.9 feet with steel 3.68 inches below the surface.

Pavement Structure

In CRC pavements, the stiffness of each layer varies. The top PCC layer has the highest stiffness, and the subbase layer has less stiffness than the top layer, with roadbed soil having the lowest stiffness. It is well known that structural responses of CRC pavements are influenced by the relative stiffness of each layer. In addition to the relative stiffness of each layer, the physical configuration of the pavement system influences the responses of the CRC pavements to wheel loads.
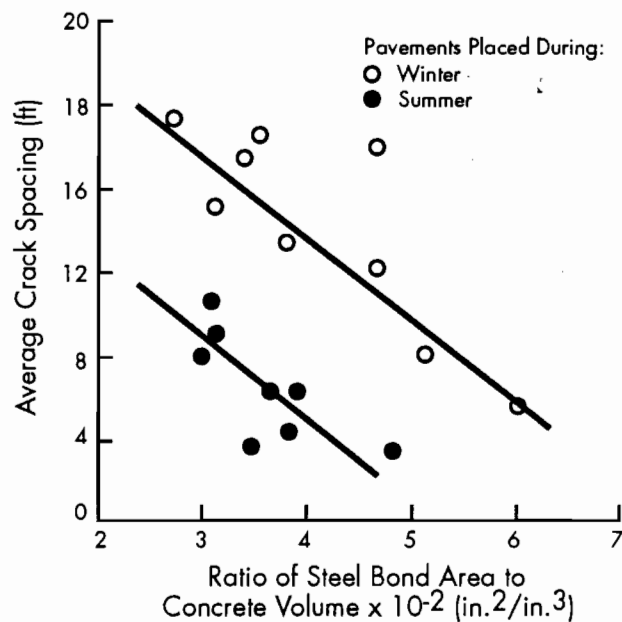
Figure 3.15. Relationship between steel bond area and crack spacing (Ref 7)

PCC Layer. Slab thickness is an important variable in that wheel load stress depends largely on slab thickness. An increase in slab thickness reduces wheel load stress. Thicker slabs result in larger crack spacing. The effect of slab thickness on wheel load stress is explained later in this section. Increasing slab thickness improves CRC pavement performance due to the reduction in deflections, as shown in Figure 3.16. Using a 15-inch-thick slab reduces deflections by 50 percent, in comparison to a 9-inch-thick
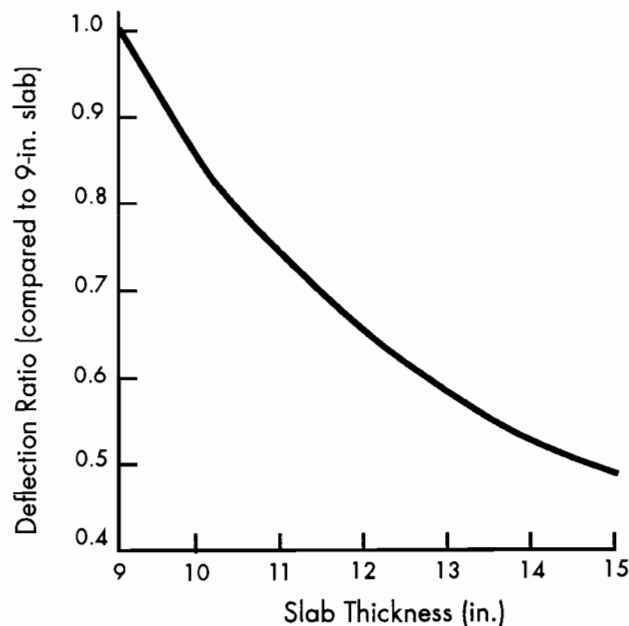
Figure 3.16. Deflection vs. slab thickness based on Westergaard's corner formula

slab. Reduced deflections prevent loss of aggregate interlock at cracks. Good aggregate interlock helps the continuity of pavement slabs and slows the deterioration of the pavement condition. This, in turn, reduces wheel load stress.

Subbase Layer. The effect of subbase friction on the cracking of concrete pavements has long been recognized, and numerous studies have been conducted. Recently, stabilized materials have been extensively used in concrete pavement as subbase material. Research was initiated at the Center for Transportation Research, The University of Texas at Austin, to get a more comprehensive understanding of the nature of the subbase friction. The results show that the characteristics of subbase friction are significantly different, depending on the subbase materials used (Table 3.6) (Ref 34). Failure planes were within the subbase layer, not at the interface between the concrete slab and the subbase layer, except when a thin ACP layer was used for the subbase. The adhesion between the PCC slab and the subbase was stronger than the shearing capacity of

Table 3.6. Results of Push-off Tests (Ref 34)

Subbase Type	Peak Frictional Resistance (psi)	Horizontal Movement at Sliding (in.)	Slab Depth (in.)
Flexible	3.0, 3.4	0.024, 0.020	4, 8
Asphalt-stabilized	1.6, 2.2	0.030, 0.038	3.5, 7
Cement-stabilized	15.4 +	0.001 +	3.5
Lime-treated clay	1.6, 1.7	0.011, 0.012	3.5, 7
Untreated clay	0.6, 1.1	0.030, 0.052	3.5, 7

the subbase materials. Thus, frictional characteristics were functions of the shear strength of subbase materials. When the subbase layer was thin ACP, failure occurred between the ACP subbase layer and the roadbed soil.

In JRC pavement, the subbase friction plays an important role in crack development because the slab length is large enough to cause significant frictional resistance. In CRC pavements, except for the cement-stabilized subbase, which has much higher peak frictional resistance, the effect of the subbase friction is confined to early ages, when the crack spacing is very large. Therefore, the subbase friction has an effect on the cracking development; however, once cracking has stabilized, the effect of the subbase friction is negligible because of the relatively short crack spacings.

Environmental Conditions

Behavior of CRC pavements at an early age is largely determined by environmental conditions. Later, structural responses of CRC pavements to wheel loads depend partly on the transverse crack spacings which have occurred because of the environmental conditions at early ages. Then more cracks develop due to the combined effect of the prevailing environmental conditions and wheel load applications. Therefore, it is important to evaluate the effect of environmental variables on CRC pavement behavior.

Setting Temperature of Concrete. The setting temperature of concrete is a reference point from which stresses at different temperatures are determined. The effect of the setting temperature on the crack spacing is shown in Figure 3.17. For a given temperature, larger concrete stresses develop in concrete pavement placed at a higher temperature than at a lower temperature. Therefore, CRC pavement placed at a higher temperature has smaller crack spacings than pavement placed at a lower temperature.

Time of Concrete Placement. Maximum concrete stress resulting from environmental conditions occurs in the winter when the temperature is lowest. Therefore, before maximum stress develops, concrete placed in the fall has less time to develop sufficient concrete strength than it would if it were placed in the spring. Concrete pavement placed in the fall is considered to have a smaller crack spacing than concrete pavement placed in the spring.

The time of day that concrete is placed also has an effect on CRC pavement behavior. Concrete placed in the morning has a lower setting temperature than concrete placed in the afternoon. In addition to the temperature effect, concrete placed in the morning has a longer time to develop strength before the low temperature occurs by the next morning than concrete placed in the afternoon. The effect is

Figure 3.17. Effect of setting temperature on crack spacing (Ref 50)

that concrete placed in the morning has larger crack spacings than concrete placed in the afternoon.

Temperature Drop. Before the pavement is open to traffic, all the cracks are due to environmental changes. In Project 422, it was found that the thermal coefficient of concrete did not change with age. Therefore, it is believed that, except when the concrete is "green," the thermal coefficient remains constant. This leads to the conclusion that the concrete strain due to temperature changes is directly proportional to the temperature difference from the setting temperature. If the temperature drops by 20 degrees in the morning on the day following concrete placement and the thermal coefficient of concrete is 6×10^{-6} inch/inch/°F, concrete strain due to temperature drop is 1.2×10^{-4} inch/inch, which amounts to 15 percent of ultimate drying shrinkage of 8×10^{-4} inch/inch. Therefore, temperature drop plays a very important role in the development of cracks in CRC pavements at very early ages. Figure 3.18 presents a relationship between the number of new cracks and the temperature drops obtained on CRCP sections on Dan Ryan Expressway in Cook County (Chicago), Illinois. Generally, there is a strong correlation between temperature drop and the number of new cracks. On day one, no cracks were observed although there was a 9-degree drop in temperature. A minimum temperature 10 degrees higher than the setting temperature occurred on day two and no new cracks developed. On day three, there was a 2-degree drop in temperature and six new cracks developed. The new cracks that developed on day three are believed to have been caused mostly by drying shrinkage. On day four, 33 new cracks were observed, when the temperature drop was 13 degrees. An 11-degree temperature drop occurred on day five and nine new cracks developed. The study illustrates the significant effect of temperature change

on the development of cracks in the early ages. It also demonstrates the importance of the thermal coefficient of concrete in cracking, because thermal strain is directly proportional to the thermal coefficient of concrete.

Wheel Load

CRC pavement behavior from wheel load applications depends on the geometric configuration of pavement slabs, i.e., slab thickness and transverse crack spacings, among other factors. Transverse crack spacings are the outcome of environmental and wheel loadings. Deterioration of pavement condition is observed with an increasing number of wheel load applications. Therefore, it is obvious that wheel load is responsible for the pavement deterioration. However, the rate of deterioration varies along the pavement beneath. This variation implies that there is an interaction between wheel load applications and other variables.
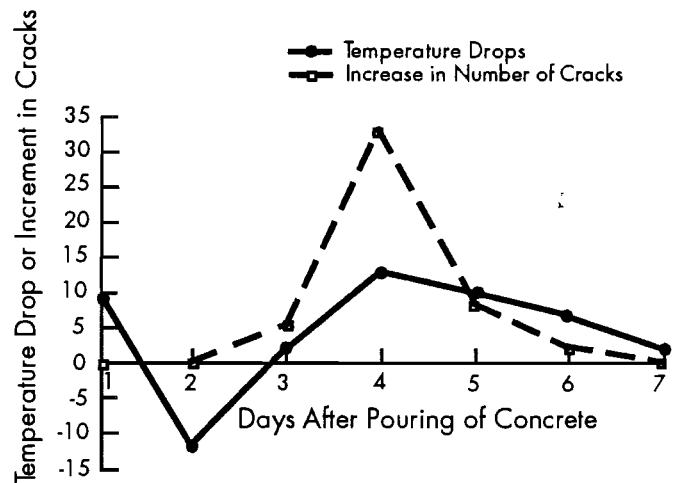
Figure 3.18. Effect of temperature drop on the development of new cracks

Wheel Load Stress. The identification of the relationship between wheel load stress and those variables having a bearing on it has been the subject of numerous researchers. Westergaard pioneered this subject in 1926 (Ref 35). He noticed that the wheel load stress differs according to the loading positions. Three loading positions—interior, corner, and edge—were selected and formulas for those positions were developed. In CRC pavements, stresses vary depending on the location of wheel loads. As discussed in Chapter 2, the condition of cracks also has a significant effect on wheel load stresses.

SUMMARY

The two most important materials comprising CRC pavements are concrete and steel. While steel

provides continuity of pavement, it also causes cracks by restraining concrete volume changes. In addition, cracks can be caused by the bending action from wheel loads. Those cracks become structural weak points, and the deterioration of the pavement condition is closely related to the combination of wheel loads and cracks.

Many factors cause cracks in CRC pavement. Concrete material properties have a significant effect on cracking due to environmental loading. The sub-base friction, amount of steel and bond area per unit of concrete volume determine the degree of restraint on concrete volume changes. Wheel load stress largely depends on slab thickness and location of wheel loads. Using thicker slabs reduces wheel load stress as well as deflections.

CHAPTER 4. THEORETICAL ANALYSIS AND MODEL DEVELOPMENT

In 1974, McCullough et al developed a computer program for the mechanistic analysis of CRC pavements for highways in NCHRP Research Project 1-15 (Ref 3). The computer program, CRCP, has proved to be a viable and valuable tool in the design of CRC pavements. Several studies found that the predictions from computer program CRCP agree well with field findings (Refs 3 and 36). In the model development, material properties were assumed homogeneous, and, therefore, the analysis was deterministic. However, there is a variability in material properties, and, therefore, the CRCP behavior is stochastic in nature, as shown in Figure 2.5. In this study, a method for including the material variability was developed, and the method is presented in this report.

In this chapter, the mechanistic analysis of CRC pavements is described, and the models developed considering material variabilities are presented. Concrete, like other engineering materials, experiences volume changes due to temperature changes. In CRCP, the restraint on concrete volume change by the longitudinal reinforcing steel causes the concrete to crack. Once a crack develops, the concrete stress is relieved, but the tension in the steel can increase considerably. The high level of steel stress at a crack is transferred to the concrete through bond as we move to the middle of a slab. The concrete stress developed through this mechanism accounts for most of the concrete stress. Therefore, it is important to evaluate accurately the stress transfer from the longitudinal steel to the surrounding concrete in order to get reasonable results. Thus, although bond stress is part of the mechanistic analysis, it is discussed in detail. The second section in the chapter deals with the relationship between bond stress and bond slip and its application to the analysis of the CRC pavement system.

The analysis of CRCP is a complex task, mainly because a number of variables are related through nonlinear equations. In order to include the stochastic nature of material properties in the analysis, a Monte Carlo technique was adopted in this study and it is reported in the third section of the chapter. Monte Carlo analysis is a powerful engineering tool which enables one to perform a statistical analysis of the uncertainty in structural engineering problems.

Thus, the Monte Carlo technique and how it is used in the analysis of CRCP is also explained in this chapter.

PREVIOUS DEVELOPMENT OF CRCP MODELS

Mechanistic analysis of pavement systems provides engineers with the tools for rational pavement design. Development of reasonable mechanistic models and accurate evaluation of material properties are the most important prerequisites for the analysis.

The initial mechanistic analysis of a CRC pavement system was made as a part of NCHRP Research Project 1-15 (Ref 3). The incorporation of the results of the mechanistic analysis into a computer program led to development of computer program CRCP-1. Extensive field study conducted to verify the validity of the program indicated that the predictions from CRCP-1 agreed with field observations. The effect of wheel load stresses was superimposed on the CRC pavement behavior due to environmental loading and resulted in the development of CRCP-2. Condition surveys on CRC pavement sections in Texas proved that the predictions from CRCP-2 were reasonable. In the development of previous mechanistic models, the following two assumptions, among others, were made: (1) there are no variabilities in material properties, and (2) bond stress is constant where bond slip occurs between the concrete and steel. Assuming no variabilities resulted in a deterministic analysis, and solutions were also deterministic. However, variabilities exist in material properties and in CRC pavement behavior. Bond stress is not constant but varies with bond slip and location. Most of the concrete stress due to environmental loading is caused by the restraint from longitudinal steel on concrete volume changes. Therefore, bond stress is a major mechanism by which concrete stress develops.

MECHANISTIC ANALYSIS OF CRCP

In order to analyze CRC pavement more realistically, the two assumptions made in the development of existing models were revised. Variabilities in the material properties are considered and a realistic bond stress distribution function was assumed. Differences in analyzing CRC pavements between

initial studies and the current study arising from revised assumptions are explained in detail wherever appropriate.

CRCP Geometric Model

The response of CRC pavements is the outcome of the interactions of the several materials, i.e., concrete, steel, and subbase, under environmental conditions and external wheel loads. The analysis in this study consists of the application of basic mechanistic principles to CRC pavements. The state of stress at the interface between the steel surface and the concrete is an important variable, and an effort was made to take advantage of the current knowledge of this variable.

In CRC pavements the longitudinal reinforcing steel is continuous throughout the length except at abutting structures, such as bridges. Figure 4.1(a) illustrates a full length of CRC pavement. Near the free ends of the pavement, some form of terminal treatment is provided. This minimizes the slab movement due to the discontinuity of longitudinal steel and low values of accumulated frictional resistance between the concrete slab and subbase. Therefore, CRC pavement sections away from the free ends are considered fully restrained. A geometric model developed by McCullough et al (Ref 3), which models CRC pavement sections, was adopted in this study and is shown in Figure 4.1(b).

Assumptions

In the analysis of CRC pavements, the following assumptions were made.

(1) Concrete and steel properties are linearly elastic.
(2) Temperature variations and drying shrinkage are uniformly distributed throughout the slab depth, and thus a uni-axial structural model was adopted.
(3) The characteristics of friction between the concrete slab and the subbase are elastic.
(4) The effect of creep and warping is neglected.

Derivation of Governing Equations

The basic unit of the CRC pavement is a slab segment bounded by two adjacent transverse cracks and longitudinal joints. A geometric model shown in Figure 4.1 represents the basic unit. Governing equations are derived using this model along with an assumption that all units are consistent, e.g., psi, inch^2, lb, °F, etc.

Equilibrium. The equilibrium condition is examined with the freebody diagram shown in Figure 4.2. At cracks, concrete stress is zero. The steel force developed at cracks and subbase frictional resistance are in equilibrium with the forces in the concrete and the steel at any point in the slab. Therefore, $\Sigma F_x = 0$ yields
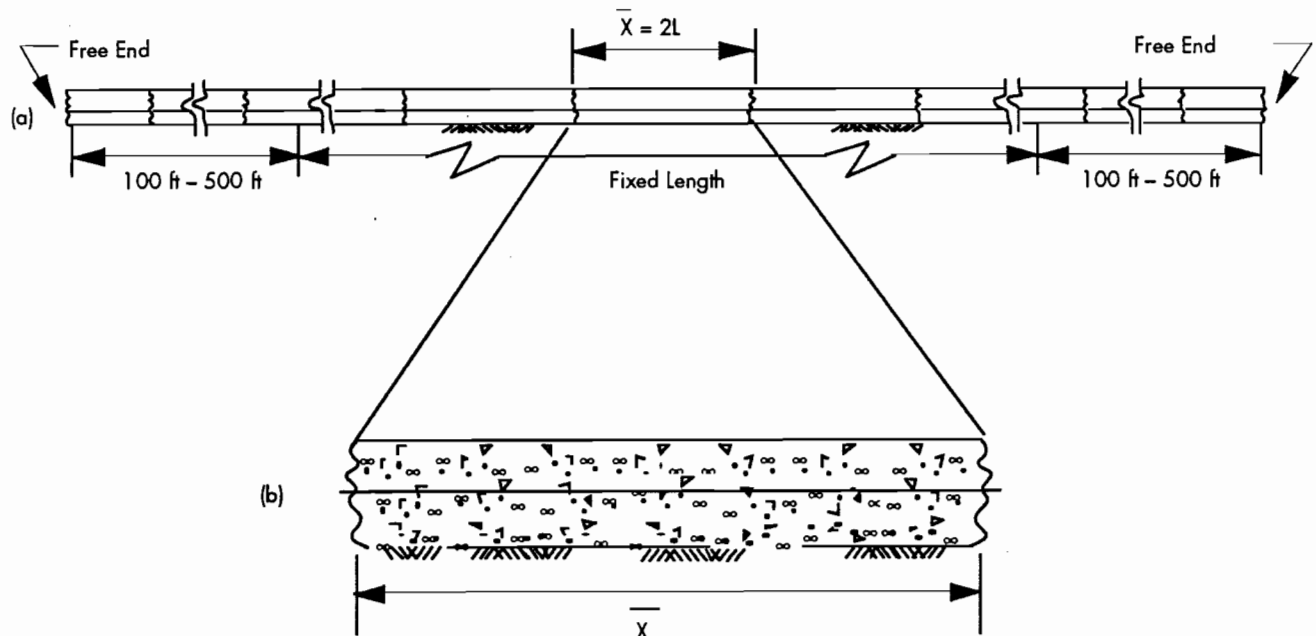
Figure 4.1. Full length of a CRC pavement section and a geometric model

28
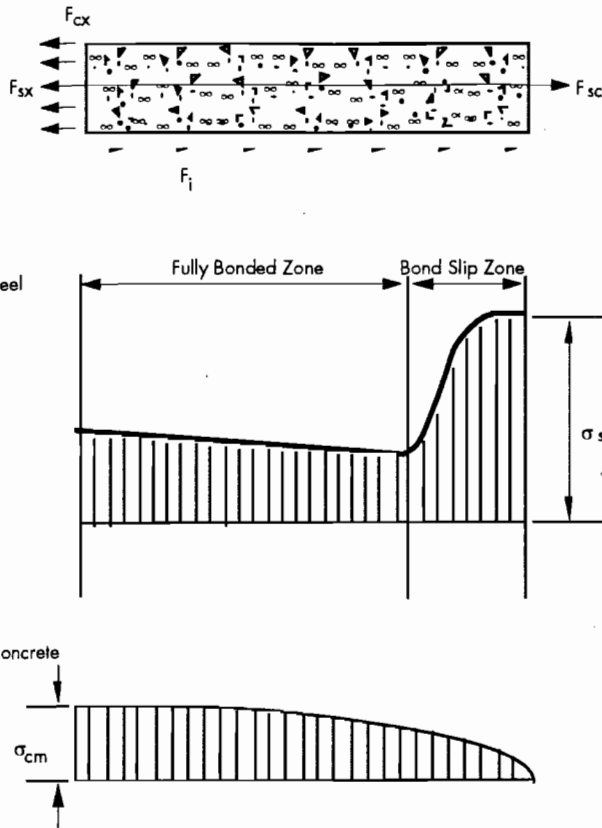
Figure 4.2. Freebody of CRCP segment and stress distributions in the concrete and steel

$$F_{sx} + F_{cx} = F_{sc} + \int_x^L F_i \, dt \qquad (4.1)$$

where

- F_{sc} = force in the steel at a crack,
- F_i = friction force per unit length along the slab,
- F_{sx} = force in the steel at location x, and
- F_{cx} = force in the concrete at location x.

Equation 4.1 can be written in terms of stress,

$$A_s\sigma_{sx} + A_c\sigma_{cx} = A_s\sigma_{sc} + \int_x^L F_i \, dt \qquad (4.2)$$

where

- σ_{sx} = stress in the steel at location x,
- σ_{cx} = stress in the concrete at location x,
- σ_{sc} = stress in the steel at a crack,
- A_s = cross-sectional area of longitudinal steel, and
- A_c = cross-sectional area of concrete.

For a unit width slab, Eq 4.2 can be written as

$$\sigma_{sx} + \frac{\sigma_{cx}}{p_s} - \sigma_{sc} - \frac{\int_x^L F_i \, dt}{p_s D} = 0 \qquad (4.3)$$

where

- D = thickness of the concrete slab, and
- p_s = ratio of cross-sectional area of steel to concrete = A_s/A_c.

Compatibility. At the middle of the geometric model, concrete and steel displacements are zero. At cracks, steel displacement is zero, but the concrete moves towards the middle of the geometric model. Therefore, the geometric model is divided by two regions; one where concrete and steel displacements are the same, and the other where there is a difference. In this study, the former is defined as a fully bonded zone, and the latter as a bond development zone. Full compatibility should hold in the fully bonded zone.

There are three components in concrete strain; strain owing to temperature variation, strain owing to drying shrinkage, and strain owing to stress. Steel strain is composed of strain due to temperature variation and strain owing to stress:

$$\frac{du_{sx}}{dx} = -\alpha_s\Delta T + \frac{\sigma_{sx}}{E_s} \qquad (4.4)$$

and

$$\frac{du_{cx}}{dx} = -\alpha_c\Delta T - \varepsilon_{sh} + \frac{\sigma_{cx}}{E_c} \qquad (4.5)$$

where

- u_{sx} = displacement of the steel at location x,
- u_{cx} = displacement of the concrete at location x,
- α_s = thermal coefficient of expansion of the steel,
- α_c = thermal coefficient of expansion of the concrete,
- ε_{sh} = drying shrinkage of the concrete,
- DT = temperature change, positive if temperature decreases,
- E_s = modulus of elasticity of the steel, and
- E_c = modulus of elasticity of the concrete.

Steel and concrete displacements are computed by integrating Eqs 4.4 and 4.5 and by using boundary conditions, that is, the steel and concrete displacements are zero at the middle of the geometric model:

$$u_{sx} = -\alpha_s\Delta T x + \frac{1}{E_s}\int_x^L \sigma_{sx} \, dt \qquad (4.6)$$

29

$$u_{cx} = -(\alpha_c \Delta T + \varepsilon_{sh}) + \frac{1}{E_c} \int_x^L \sigma_{cx}\, dt \qquad (4.7)$$

In the fully bonded zone, displacements of the concrete and the steel are the same. Therefore, first derivatives of the displacement (or strain) are the same. Equating Eqs 4.4 and 4.5 yields

$$\sigma_{cx} = \frac{\sigma_{sx}}{n} + E_c[(\alpha_c - \alpha_s)\Delta + \varepsilon_{sh}] \qquad (4.8)$$

where

$$n = \frac{E_s}{E_c}.$$

Equation 4.8 defines the relationship between the steel and the concrete stresses in the fully bonded zone. In the bond development zone, compatibility does not hold, because there is a relative movement between the concrete and the steel. The relationship defining force and defining displacement between the concrete and the steel is very complex and is discussed in detail later in this chapter.

Concrete and Steel Stress Distribution. At cracks, concrete stress is zero and steel is in considerable tension due to the drying shrinkage of concrete and/or temperature drop. The steel stress at cracks is transferred to the concrete. The mechanism of the stress transfer from the steel to the concrete is well explained in Ref 37. As is shown later, when there is no subbase friction, stress transfer from the steel to the concrete must accompany the relative movement between the concrete and the steel. In other words, where there is no relative movement between the concrete and the steel (fully bonded zone), there is no stress transfer between the concrete and the steel. Consider the equilibrium of the steel and concrete in a freebody (Figure 4.3).

For steel

$$F_{sx} = F_{sx} + dF_{sx} - f_b(x)\pi\phi\, dx,$$

where ϕ = diameter of steel.

Since

$$dF_{sx} = A_s\, d\sigma_{sx} = \frac{\pi\phi^2}{4}\, d\sigma_{sx},$$

then

$$\frac{d\sigma_{sx}}{dx} = \frac{4f_b(x)}{\phi} \qquad (4.9)$$

For concrete

$$F_{cx} = F_{cx} + dF_{cx} + f_b(x)\pi\phi\, dx + F_i\, dx \Leftrightarrow dF_{cx} = A_c\, ds_{cx}$$

$$\frac{d\sigma_{cx}}{dx} = -\frac{f_b(x)\pi\phi}{A_c} - \frac{F_i}{A_c}$$

where $dF_{cx} = A_c d\sigma_{cx}$.
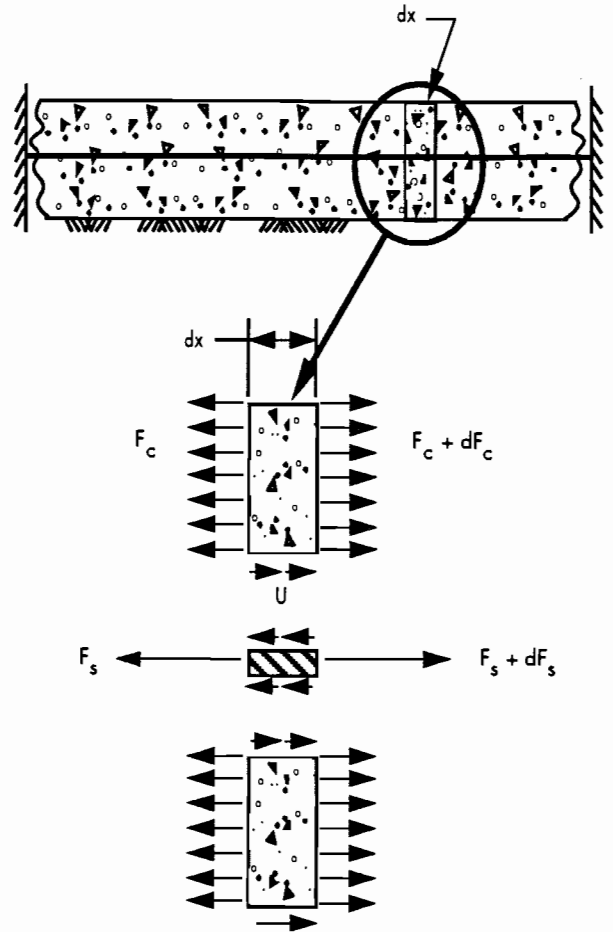
Figure 4.3. Freebody diagram of CRCP elements

Since

$$\frac{\pi\phi}{A_c} = \frac{4\pi\phi\frac{\phi}{4}}{A_c\phi} = \frac{4p_s}{\phi}$$

and

$A_c = D$ for a unit width of the slab,

then

$$\frac{d\sigma_{cx}}{dx} = -\frac{4f_b(x)p_s}{\phi} - \frac{F_i}{D} \qquad (4.10)$$

where

$f_b(x)$ = bond stress at location x.

Equation 4.9 indicates that the rate of change of the steel stress depends on the bond stress and bar size. Equation 4.10 illustrates that the bond stress, longitudinal steel percentage, bar size, subbase friction, and slab thickness affect the rate of change of the concrete stress. Equations 4.9 and 4.10 hold for the fully bonded zone as well as the bond development zone.

Stress Distribution in the Fully Bonded Zone. The rates of steel and concrete stress changes are given in Eqs 4.9 and 4.10, respectively. In the fully bonded

zone, a relationship exists between the rate of concrete and steel stress changes and other variables. By differentiating both sides of Eq 4.3 with respect to x, we get

$$F_{sx} + F_{cx} = F_{sc} + \int_x^L F_i \, dt \iff$$

$$p_s \frac{d\sigma_{sx}}{dx} + \frac{d\sigma_{cx}}{dx} = -\frac{F_i}{D} \qquad (4.11)$$

Since environmental conditions and material properties except strength are assumed independent of space, differentiating Eq 4.8 with respective to x yields

$$\frac{d\sigma_{cx}}{dx} = \frac{1}{n}\frac{d\sigma_{sx}}{dx} \qquad (4.12)$$

Substituting Eqs 4.12 into 4.11 gives

$$\frac{d\sigma_{sx}}{dx} = \frac{-F_i}{D\left(p_s + \frac{1}{n}\right)} \qquad (4.13)$$

From Eqs 4.12 and 4.13, we find

$$\frac{d\sigma_{cx}}{dx} = \frac{-F_i}{nD\left(p_s + \frac{1}{n}\right)} \qquad (4.14)$$

These governing equations are summarized as follows:

$$\sigma_{sx} + \frac{\sigma_{cx}}{p_s} - \sigma_{sc} - \frac{\int_x^L F_i \, dt}{p_s D} = 0 \qquad (4.3)$$

$$\sigma_{cx} = \frac{\sigma_{sx}}{n} + E_c[(\alpha_c - \alpha_s)\Delta + \varepsilon_{sh}] \qquad (4.8)$$

$$\frac{d\sigma_{sx}}{dx} = \frac{4f_b(x)}{\phi} \qquad (4.9)$$

$$\frac{d\sigma_{cx}}{dx} = -\frac{4f_b(x)p_s}{\phi} - \frac{F_i}{D} \qquad (4.10)$$

$$\frac{d\sigma_{sx}}{dx} = \frac{-F_i}{D\left(p_s + \frac{1}{n}\right)} \qquad (4.13)$$

$$\frac{d\sigma_{cx}}{dx} = \frac{-F_i}{nD\left(p_s + \frac{1}{n}\right)} \qquad (4.14)$$

By combining the equilibrium and compatibility conditions (Eqs 4.3 and 4.8), concrete stress is eliminated, and the equation can be expressed in terms of steel stresses.

$$\sigma_{sc} = \left(1 + \frac{1}{np_s}\right)\sigma_{sx} + \frac{E_c}{p_s}[(\alpha_c - \alpha_s)\Delta + \varepsilon_{sh}] - \frac{\int_x^L F_i \, dt}{p_s D}$$

or

$$\sigma_{sc} = C_1\sigma_{sx} + C_2 - C_3 \qquad (4.15)$$

where

$$C_1 = 1 + \frac{1}{np}$$

$$C_2 = \frac{E_c}{p_s}[(\alpha_c - \alpha_s)\Delta T + \varepsilon_{sh}], \text{ and}$$

$$C_3 = \frac{\int_x^L F_i \, dt}{p_s D}.$$

Equation 4.15 provides a relationship between the steel stress at cracks and the steel stress at any point in the fully bonded zone. The rate of steel stress change is given in Eq 4.9 for the bond development zone and in Eq 4.13 for the fully bonded zone. Another relationship is required to solve the above systems of equations. It is a steel boundary condition.

Steel Boundary Condition

In order to utilize the steel boundary condition for solving the system of equations, it is necessary to find locations where steel displacements are zero for various environmental loadings. In the development of previous models, it was assumed that steel displacements are zero at cracks and at the middle of the geometric model. The assumption was reasonable because crack spacings were uniform. However, in reality, crack spacings are not uniform unless material properties are homogeneous. When the crack spacings are not uniform, steel displacements at cracks are not necessarily zero, for reasons given later in this section. In the following discussions, a relationship between crack spacings and steel stresses at cracks is examined and and appropriate steel boundary condition is established.

Steel Stress and Transverse Crack Spacing. In CRC pavements, steel stresses at cracks are almost identical, regardless of transverse crack spacings. If the effect of subbase friction is ignored, steel stresses at cracks must be the same for all the slab segments in order for the equilibrium to hold. Even when the subbase friction is considered, as long as the point of

zero concrete displacement exists close to the middle of the slab segments, the effect of subbase friction on the variation of steel stresses at cracks can be ignored. Figure 4.4 presents typical subbase friction characteristics. Sliding occurs at a slab movement of
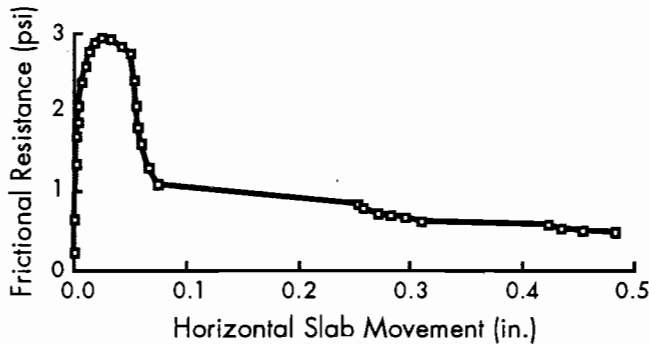
Figure 4.4. Typical slab movement vs. friction resistance (Ref 34)

about 0.03 inch with maximum frictional stress of 3.0 psi. In CRC pavements, slab movement at cracks are well below the value of movement at sliding. For example, for concrete having a thermal coefficient of 6 x 10^{-6} inch/inch/°F, possible maximum movement when there is no restraint on concrete volume changes is 0.01 inch, if the daily temperature drop is 30 degrees and crack spacing is 10 feet (60 inch x 30°F x 6 x 10^{-6} inch/inch/°F = 0.0108 inch). Actually, there is a restraint on concrete volume changes, and tensile stresses develop in the concrete. The tensile stresses reduce concrete displacement. Therefore, less than 1 psi of frictional resistance will develop at cracks for a slab segment with 10-foot spacing, if there is a 30-degree temperature drop. Figure 3.2(c) presents the distribution of frictional resistances along the slab segment. If frictional resistance is assumed to be linearly proportional to concrete displacements of up to 0.03 inch, the distribution of frictional resistance has the same shape as that of concrete displacements. From Figure 3.2(c), it is found that as long as the point of zero concrete displacement is at the middle of the slab segment, steel stresses at both cracks of the slab segment are the same, because the frictional resistances in both directions cancel each other out. Even when the point of zero concrete displacement is not at the middle of the slab segment, the difference between frictional resistances in both directions will be very small as long as the location of zero concrete displacements is near the middle of the slab segments. In this study, and from this reasoning, steel stresses at cracks are the same. This assumption is not compatible with the assumption that steel displacements are zero at cracks. If steel displacements are zero at

cracks, steel stresses at cracks will be different, depending on crack spacings. If crack spacings are large, concrete contraction owing to temperature drop and drying shrinkage will be large, resulting in high steel stresses at cracks. On the other hand, if the crack spacings are very narrow, low steel stresses will result at cracks. However, a unique steel stress exists at a crack regardless of slab segment lengths. Therefore, the fact that steel stress at a crack is almost the same regardless of the crack spacings contradicts the assumption of zero steel displacements at cracks. In other words, when the crack spacings are not uniform, steel displacements are not necessarily zero at cracks. Instead, steel experiences displacements at cracks so that the steel stresses will be the same at every crack.

Steel Boundary Condition. The steel boundary condition is necessary to solve the system of equations developed above. In order to utilize the steel boundary condition, it is necessary to find the location of zero steel displacements. Since it is assumed that steel stresses at cracks are the same, steel displacements at cracks are not necessarily zero.

The fact that steel displacements are not necessarily zero at cracks makes it impossible to find the locations of zero steel displacements. Therefore, a different approach is considered. Consider the area under the steel stress curve for half of a slab segment whose length is X_1 (Figure 4.5). Let L_1 be a half of X_1. L_1 is divided into two regions. One is the fully bonded zone with a length of a, and the other is the bond development zone with a length of b. Let A_1 be the area under the steel stress curve in the fully bonded zone and A_2 be the area in the bond
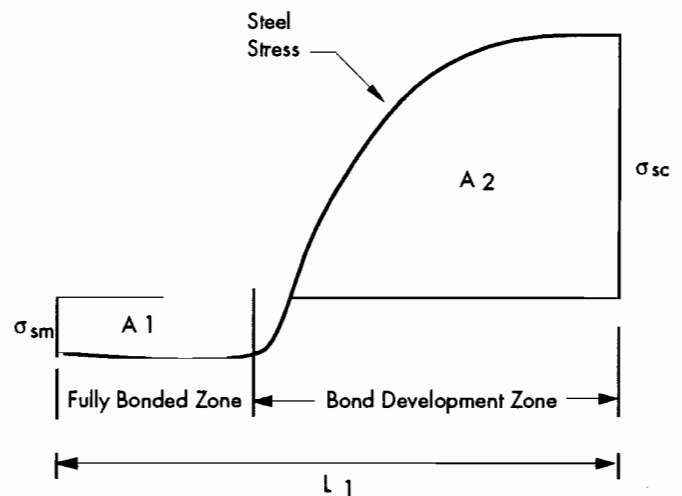
Figure 4.5. Steel stress distributions in the fully bonded zone and bond development zone

32

development zone. In a fully bonded zone, steel stress is determined by using Eq 4.13:

$$\frac{d\sigma_{sx}}{dx} = \frac{-F_i}{D\left(p_s + \frac{1}{n}\right)} \Leftrightarrow \int_0^x d\sigma_{sx} = \int_0^x \frac{-F_i}{D\left(p_s + \frac{1}{n}\right)} dt \Leftrightarrow$$

$$\sigma_{sx} - \sigma_{sm} = \int_0^x \frac{-F_i}{D\left(p_s + \frac{1}{n}\right)} dt \Leftrightarrow$$

$$\sigma_{sx} = \sigma_{sm} + \int_0^x \frac{-F_i}{D\left(p_s + \frac{1}{n}\right)} dt \quad (0 < x < a) \quad (4.16)$$

where σ_{sm} is the steel stress at the middle of a slab segment.

Since subbase frictional stresses are practically zero in the fully bonded zone, the second term in Eq 4.16 can be ignored in the calculation of the area under the steel stress curve. Therefore,

$$A_1 = \int_0^a \sigma_{sm} dx = a \cdot \sigma_{sm} \quad (4.17)$$

Steel stress in the bond development zone is determined from Eq 4.9:

$$\frac{d\sigma_{sx}}{dx} = \frac{4f_b(x)}{\phi} \Leftrightarrow \int_a^x d\sigma_{sx} = \int_a^x \frac{4f_b(t)}{\phi} dt \Leftrightarrow$$

$$\sigma_{sx} - \sigma_{sa} = \int_a^x \frac{4f_b(t)}{\phi} dt \Leftrightarrow$$

$$\sigma_{sx} = \sigma_{sa} + \int_a^x \frac{4f_b(t)}{\phi} dt \quad (4.18)$$

where σ_{sa} is the steel stress where bond slippage begins. From Eq 4.16, σ_{sa} is obtained by substituting a for x.

$$\therefore \sigma_{sa} = \sigma_{sm} + \int_0^a \frac{-F_i}{D\left(p_s + \frac{1}{n}\right)} dx \quad (a < x < 1)$$

$$\therefore \sigma_{sx} = \sigma_{sm} - \int_0^a \frac{-F_i}{D\left(p_s + \frac{1}{n}\right)} dx + \int_a^x \frac{4f_b(t)}{\phi} dt \quad (4.19)$$

Since subbase frictional stresses are negligible in the fully bonded zone, the second term is dropped. A_2 is obtained by integrating σ_{sx} from a to L_1

$$A_2 = \int_a^{L_1} \sigma_{sm} dx + \int_a^{L_1}\int_a^x \frac{4f_b(t)}{\phi} dt\, dx \quad (a < x < 1) \quad (4.20)$$

Therefore,

$$A_1 + A_2 = \int_0^a \sigma_{sm} dx + \int_a^{L_1} \sigma_{sm} dx + \int_a^{L_1}\int_a^x \frac{4f_b(t)}{\phi} dt\, dx =$$

$$\sigma_{sm} L_1 + \int_a^{L_1}\int_a^x \frac{4f_b(t)}{\phi} dt\, dx \quad (4.21)$$

since

$$\sigma_{sc} = C_1\sigma_{sm} + C_2 - C_3, \quad \sigma_{sm} = \frac{\sigma_{sc} - C_2 + C_3}{C_1}.$$

Therefore, Eq 4.21 is expressed in terms of σ_{sc}:

$$A_1 + A_2 = \frac{\sigma_{sc} - C_2 + C_3}{C_1} L_1$$

$$+ \int_a^{L_1}\int_a^x \frac{4f_b(t)}{\phi} dt\, dx \quad (4.22)$$

The value of C_3 is negligible compared with σ_{sc} or C_2, because, for example, $C_3 = (60 \cdot 0.5)/(10 \times 0.006) = 500$ psi. The value of σ_{sc} is normally more than 30,000 psi and C_2 is 153,333 psi when the values in the previous example are used with a shrinkage value of 0.0002 and a modulus of elasticity of 4,000,000 psi. Therefore, the area under the steel stress curve is

$$A_1 + A_2 = \frac{\sigma_{sc} - C_2}{C_1} L_1 + \int_a^{L_1}\int_a^x \frac{4f_b(t)}{\phi} dt\, dx \quad (4.23)$$

Then, the area under steel stress curve for a slab segment length of X_1 becomes

$$\frac{\sigma_{sc} - C_2}{C_1} X_1 + \int_a^{L_1}\int_a^x \frac{8f_b(t)}{\phi} dt\, dx \quad (4.24)$$

where $L_1 = X_1 / 2$.

The bond stress distribution function ($f_b(t)$) is assumed to depend on steel stress at a crack and bond development length, not on crack spacing. This assumption is reasonable if subbase friction is ignored

in the fully bonded zone. In this study, steel stress at a crack and bond development length are assumed to be constant regardless of slab segment lengths, which is discussed in detail later in this chapter. Therefore, the second term in Eq 4.23 is constant for every slab segment. Note that C_1 and C_2 are functions of material properties and design variables but not of slab segment lengths. Therefore, the area under steel stress distribution for n slabs becomes

$$\frac{\sigma_{sc} - C_2}{C_1} \sum_{i=1}^{n} X_i + n \int_{a_i}^{L_i} \int_{a_i}^{x} \frac{8 f_b(t)}{\phi} \, dt \, dx \qquad (4.25)$$

where $L_i = X_i/2$ and $a_i = L_i - b$.

Now, let us consider a family of slab segments with uniform spacing $\overline{X}$. The same formulas are applied to these slabs. Since the crack spacings are uniform, steel displacements are zero at cracks, owing to the symmetry, and the steel boundary condition is applied between any cracks. Therefore, the steel boundary condition for these n slabs is

$$\frac{\sigma_{sc} - C_2}{C_1} \, n \, \overline{X} + n \int_c^{\frac{\overline{X}}{2}} \int_c^x \frac{8 f_b(t)}{\phi} \, dt \, dx$$

$$= E_s \alpha_s \Delta T \, n \, \overline{X} \qquad (4.26)$$

where $c = \overline{X}/2 - b$.

If the mean crack spacings are the same for two distributions, then $\sum X_i = n \overline{X}$. If it is assumed that steel stresses at cracks are the same regardless of crack spacing distributions, as long as the mean crack spacings are the same, then Eq 4.25 is equivalent to the left side of Eq 4.26. Equating Eq 4.25 with the right-hand side of Eq 4.26 yields

$$\frac{\sigma_{sc} - C_2}{C_1} \sum_{i=1}^{n} X_i + n \int_{a_i}^{L_i} \int_{a_i}^{x} \frac{8 f_b(t)}{\phi} \, dt \, dx$$

$$= E_s \alpha_s \Delta T n \, \overline{X} \qquad (4.27)$$

Dividing both sides of Eq 4.27 by n gives

$$\frac{\sigma_{sc} - C_2}{C_1} \frac{\sum_{i=1}^{n} X_i}{n} + \int_{a_i}^{L_i} \int_{a_i}^{x} \frac{8 f_b(t)}{\phi} \, dt \, dx$$

$$= E_s \alpha_s \Delta T \overline{X} \qquad (4.28)$$

$\sum_{i=1}^{n} X_i \Big/ n$ is the mean crack spacing. Equation 4.28 shows that even when the crack spacings are not uniform (therefore steel displacements may not be zero at cracks), the steel boundary condition can be applied to a slab segment of mean crack spacing. Therefore, the steel boundary condition is applied to a slab segment with mean crack spacing:

$$\int_0^X \sigma_{sx} \, dt = E_s \alpha_s \Delta T \overline{X} \qquad (4.29)$$

The steel boundary condition (Eq 4.29) and Eq 4.15, together with Eqs 4.9 and 4.13, are used to find the steel stress distribution. However, the major problem is that the bond stress distribution ($f_b(x)$) and the bond development length are not known. In order to solve the above system of equations, bond stress distribution and bond development length must be known. In the previous analysis (Ref 3), bond stress was assumed to be a function of concrete strength. Therefore, at a given time, bond stresses were constant and bond development length was determined from the steel boundary condition. In this study, the bond stress-bond-slip relationship is considered. Therefore, it is necessary to examine the characteristics of bond stress and the relationship between bond stress and bond slip at the interface of the concrete and the steel.

THE RELATIONSHIP BETWEEN BOND STRESS AND BOND SLIP

In order to solve the system of equations developed in the previous section, the relationship between bond stress and bond slip needs to be identified. In this section, major findings on this subject are presented. Various methods for solving the system of equations are discussed, and the most appropriate one is selected.

Nature of Bond Stress

Bond is the shearing stress between a steel surface and the surrounding concrete. Bond is made up of three components (Ref 39): (1) chemical adhesion, (2) friction, and (3) mechanical interaction between concrete and steel. Bond of plain bars depends primarily on the first two elements, although there is some mechanical interlocking due to the roughness of the bar surface. Deformed bars, however, depend primarily on mechanical interlocking for superior bond properties.

In this section, the subbase friction is ignored to simplify the discussions. It can be shown that no bond stress develops where there is no relative movement between the concrete and the longitudinal steel. Let us consider a freebody cut between a crack

and anywhere in the fully bonded zone (Figure 4.2). Equilibrium Eq 4.1, together with Eqs 4.4 and 4.5, is expressed in terms of displacements:

$$(E_s \frac{du_{sx}}{dx} + E_s \alpha_s \Delta T) A_s +$$

$$\left(E_c \frac{du_{cx}}{dx} + E_c \alpha_c \Delta T + E_c \varepsilon_{sh} \right) A_c = \sigma_{sc} A_s \Leftrightarrow$$

$$E_s A_s \frac{du_{sx}}{dx} + E_c A_c \frac{du_{cx}}{dx} =$$

$$\sigma_{sc} A_s - (E_s A_s \alpha_s \Delta T + E_c \alpha_c \Delta T A_c + E_c \varepsilon_{sh} A_c) \quad (4.30)$$

Since the displacements of the concrete and steel are the same in the fully bonded zone,

$$u_{sx} = u_{cx} ,$$

and, therefore,

$$\frac{du_{sx}}{dx} = \frac{du_{cx}}{dx} ,$$

Eq 4.30 can be rewritten as

$$\frac{du_{sx}}{dx} = \frac{\sigma_{sc} A_s - \{E_s A_s \alpha_s \Delta T + E_c A_c (\alpha_c \Delta T + \varepsilon_{sh})\}}{E_c A_c + E_s A_s} \quad (4.31)$$

Bond stress develops when there is a change in steel stress along the bar, as shown in Eq 4.9. Equation 4.31 shows that, for given geometric and environmental conditions, steel strain is constant in the fully bonded zone. Therefore, steel stress is constant in the fully bonded zone, and no bond stress develops. Equation 4.31 implies that the stress transfer occurs with relative movement between the concrete and the steel. The relationship between the relative movement and the concrete and the steel (bond slip) and bond stress should be examined. Extensive research has been conducted to identify the relationship between bond slip and bond stress, and has provided vast data.

Literature Review

In 1941, Watstein (Ref 40) presented the results of the investigation to determine the distribution of bond stress using six types of steel bars embedded in 6 x 18-inch concrete pull-out specimens. In one series of specimens, steel strains were measured at the quarter points along the embedded bars using 2-inch Tuckerman optical strain gauges. Bond stress at the quarter points was calculated from the steel strain measurements. Therefore, it was possible to produce bond stress distribution along the steel bar. However, the results were not compatible with current knowledge of bond stress distribution in that the maximum bond stress always occurred at the loaded end.

Watstein (Ref 41) published a paper on the bond stress distribution, which is a continuation of the work mentioned above. In the study, the same 2-inch Tuckerman optical strain gauges were used to measure steel strains at the quarter points. The values of bond slip were computed from the observed tensile strains in the steel and from estimated compressive strains in the concrete. Bond stresses were calculated using the same method of the previous study. The relationship between bond stress and slip was obtained. The relationship was not the same at different points, but varied from point to point.

Clark (Ref 42) reported the results of tests conducted to find information on the effects of bar size and type of deformation on the bars and of the strength of the concrete on the bond. Slip of the bar was measured at the loaded and free ends only. Therefore, the study does not provide information on the local bond stress-slip relationship. However, he found that bond stress increased as the end slip increased.

Nilson (Ref 43) conducted research in an attempt to develop experimental means for establishing bond stress-slip relationship. Steel strain distribution was measured through the steel bar using a technique developed by Mains (Ref 44). For the concrete, internal strain gauges were used to find the concrete strain distribution. Thus, he was able to get bond slip for the entire length of the specimen. Bond stress was calculated from the slope of the steel strain curve. It was found that the location of the elemental interface area was an important variable, so separate curves were established at different distances from the end face of the specimen (Figure 4.6). In the figure, c is the distance from the loaded end. For the same bond slip, bond stress varies as much as 100 percent, depending on the location.
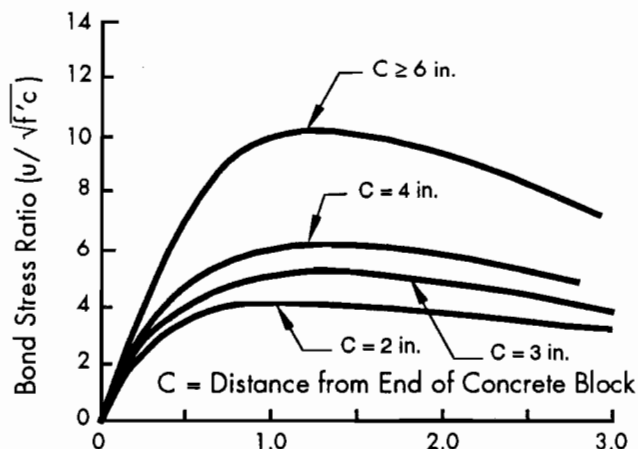
Figure 4.6. Bond stress – bond slip relationship for various locations (Ref 43)

Bond Stress Distribution Function (BSDF)

Since the relationship between bond stress and slip is not unique, the analysis based on a unique bond stress vs slip relationship cannot be correct. There are two approaches to solving this problem. One is to define a bond stress vs slip relationship at each nodal point, and to solve the system of equations numerically. The other is to assume the bond stress distribution along the steel bar, and to solve the system of equations.

The first approach requires the definition of as many bond stress vs slip relationships as the number of nodal points in the geometric model. There has not been sufficient information on this subject. On the other hand, a realistic bond stress distribution function is all that is needed in the second approach. Several researchers have applied this method to solve the problem (Refs 45, 51, 52, and 53). In this study, the second approach was selected to solve the system of equations.

Several bond stress distribution functions are suggested. They are be examined in order to find which one represents the bond stress distribution in CRC pavements most accurately. Mylrea (Ref 46) found that bond stress varied with the bar subjected to an increasing pull, which is shown in Figure 4.7. The steel bar was a plain bar. It shows that the bond slip zone progresses with increasing tensile force at the end of the steel bar. It also indicates that the location of the maximum bond stress moves from the loaded end toward the unloaded end, and that
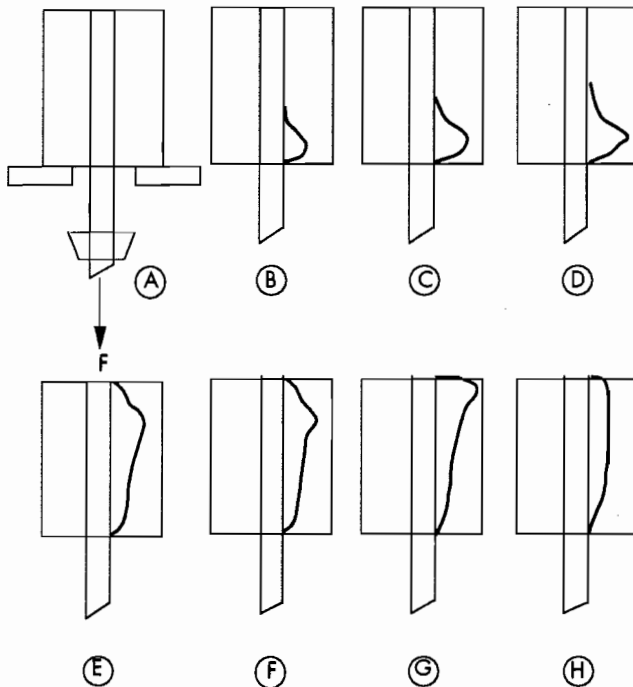
eventually the bond stress is almost the same throughout the bar.

Perry and Thompson (Ref 47) conducted a study to investigate the correlation between the bond stress distributions in pull-out specimens, at bar cutoff points in reinforced concrete beams and in reinforced concrete beams at a crack in constant moment zones. Figure 4.8 shows the results of the pull-out tests. The maximum bond stress increased and the point of the maximum bond stress shifted toward the unloaded end as the pull-out force increased.
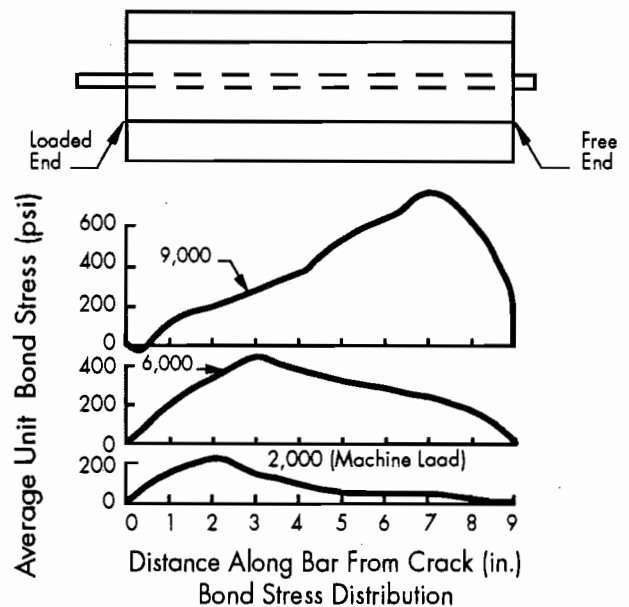
Figure 4.8.   Progression of bond stress in pull-out test (Ref 47)

The reinforcing bar was a deformed bar. This and Mylrea's findings indicate that, for the pull-out test, the location of the maximum bond stress moves from the loaded end to the unloaded end regardless of the type of bar (plain or deformed) used. The bond stress distribution in reinforced concrete beams in the constant moment zone is shown in Figure 4.9. It illustrates that the maximum bond stress occurs almost at the same location for various steel forces at a crack. It also indicates that the shape of bond stress distribution along the steel bar remains similar regardless of the various steel forces applied at a crack. The findings of Milrea and of Perry and Thompson clearly indicate that the shape of bond stress distribution varies, depending on the test methods. It is necessary to examine what causes the difference and which one represents the bond stress distribution in CRC pavements more accurately.

In a pull-out test (Figure 4.7A), the concrete is in compression when the pulling force is applied to the steel. There is no force applied to the steel at the unloaded end. It is quite possible that the bond slip

Figure 4.7.   Progression of bond stress with increasing pull-out force (Ref 46)
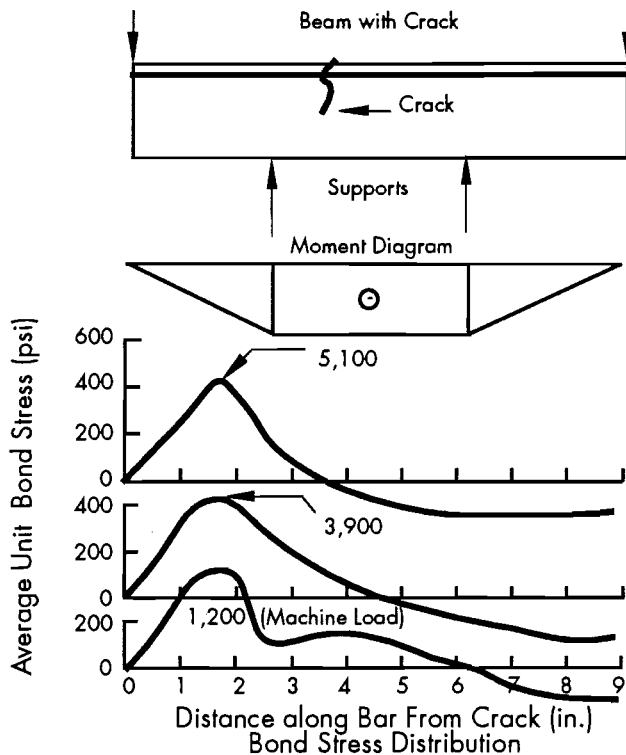
Figure 4.9. Progression of bond stress in a beam test (Ref 48)

occurs over the entire steel length, which is indicated in Figure 4.7H. This may be the reason the location of the maximum bond stress progresses toward the free end as the pulling force increases. In some of the pull-out tests, pull-out failure was experienced (Ref 48). This is very different from the situation in CRC pavements. On the other hand, in a beam test (Figure 4.9), the concrete is in tension, and cracks occur before pull-out failure takes place. Therefore, the beam test more realistically represents CRC pavements.

Somayaji and Shah (Ref 51) proposed an analytical model to predict the cracking response and the tension-stiffening effect in a reinforced concrete member subjected to uniaxial tension. Instead of assuming relationships between bond stress and bond slip for various locations, an exponential bond stress distribution function was assumed. The shape of the bond stress distribution from the exponential function is symmetrical with respect to the middle of the bond development length, with maximum bond stress taking place at the center of symmetry. Jiang et al (Ref 52) suggested a parabolic bond stress distribution function. The maximum bond stress occurs at the middle of the bond development length; paralleled in the bond stress distribution function suggested by Somayaji and Shah.

Yang and Chen (Ref 53) proposed a more realistic bond stress distribution function based on the test results:

$$f_b(x) = Kw(x) + (Cx^2 + D) + E\cos\left(\frac{px}{2b}\right) \quad (4.32)$$

where

K = bond stiffness which is the bond stress per unit slip,

w(x) = bond slip,

b = bond development length, and

C, D, E = constants to be determined with boundary conditions.

The above function forces the location of the maximum bond stress to move from the center of the bond development length toward the loaded end (Figure 4.10). The shape of the bond distribution from the above function agrees with the actual data, which is shown in Figure 4.9. Therefore, the above function was selected for this study.
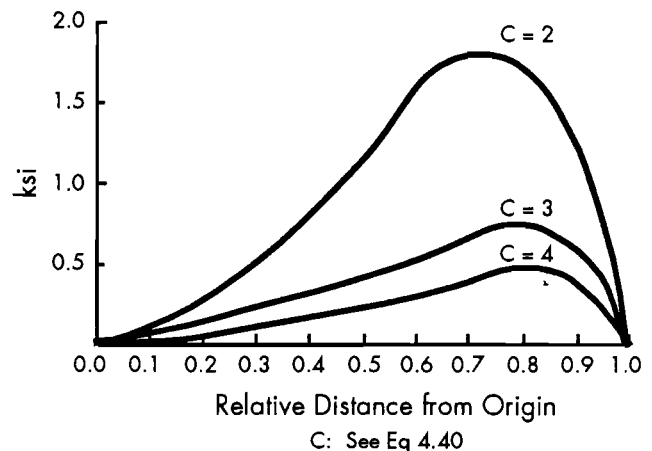
Figure 4.10. Bond stress distributions proposed by Yang and Chan (Ref 53)

SOLUTION OF GOVERNING EQUATIONS

Once a bond stress distribution function is assumed, the governing equations can be solved. However, the constants in Eq 4.32 must be determined. It is assumed that the displacements of the concrete and the steel are the same at the middle of a slab segment. In other words, there is a full bond between concrete and the steel at the middle of a slab segment. The next question is: where does the relative movement between the steel and the concrete, or bond slip, begin? Does the bond slip begin right next to the middle point of the geometric model? Or does a finite length of fully bonded zone exist? In this study, initially, it is assumed that a finite length of fully bonded zone exists, and the system of equations is solved. The coordinate system adopted in this study is shown in Figure 4.11. The length of half the geometric model, L, is divided into two regions: (1) a fully bonded zone of length a, and (2) a bond development zone of length b. In order

37
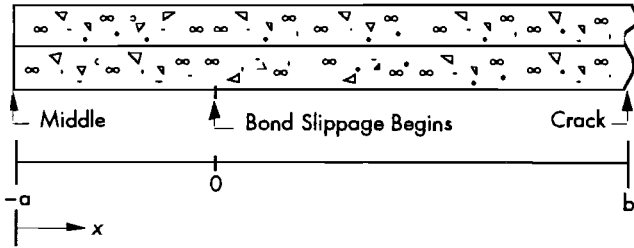
Figure 4.11. Coordinate system used in this study

to simplify the calculations, the location where the bond slip begins is selected as the origin. Therefore, the middle of the geometric model has a coordinate of $x = -a$, and the coordinate of a crack face is $x = b$.

Bond slip at any point is a cumulative difference in the displacements of the concrete and the steel from the middle of the geometric model or from the point where relative movement starts to the point concerned.

Therefore

$$w(x) = \int_0^x \left(\frac{du_{st}}{dt} - \frac{du_{ct}}{dt} \right) dt \qquad (4.33)$$

Differentiating Eq 4.33 once and twice with respect to x gives

$$w'(x) = \frac{du_{st}}{dt} - \frac{du_{ct}}{dt} \qquad (4.34)$$

and

$$w''(x) = \frac{d^2 u_{st}}{dt^2} - \frac{d^2 u_{ct}}{dt^2} \qquad (4.35)$$

Differentiating the equilibrium Eq 4.2 with respect to x yields

$$E_s A_s \frac{d^2 u_{sx}}{dx^2} + E_c A_c \frac{d^2 u_{cx}}{dx^2} = -F_i \Leftrightarrow$$

$$\frac{d^2 u_{cx}}{dx^2} = -n\,p_s \frac{d^2 u_{sx}}{dx^2} - \frac{F_i}{E_c A_c} \qquad (4.36)$$

Substituting Eq 4.36 into 4.35 gives

$$w''(x) = (1 + np_s) \frac{d^2 u_{sx}}{dx^2} + \frac{F_i}{E_c D} \qquad (4.37)$$

From Eqs 4.4 and 4.9,

$$\frac{d^2 u_{sx}}{dx^2} = \frac{1}{E_s} \frac{d\sigma_{sx}}{dx} = \frac{1}{E_s} \frac{4 f_b(x)}{\phi}$$

and

$$w''(x) = \frac{4(1+np_s)}{\phi E_s} f_b(x) + \frac{F_i}{E_c D}$$

$$= \alpha f_b(x) + \frac{F_i}{E_c D} \qquad (4.38)$$

where

$$\alpha = \frac{4(1+np_s)}{\phi E_s}$$

Substituting Eq 4.38 into Eq 4.32 yields

$$w''(x) - \alpha K w(x) =$$

$$\alpha(Cx^2 + D) + \alpha E \cos\left(\frac{\pi x}{2b}\right) + \frac{F_i}{E_c D} \qquad (4.39)$$

This is a second order non-homogeneous differential equation. It is assumed that subbase friction (F_i) is linearly distributed, with the value zero at the middle of the geometric model and maximum values at a crack. The details of solving Eq 4.39 are presented in Appendix A, and the general solution is

$$w(x) = A \exp\left(\frac{cx}{b}\right) + B \exp\left(\frac{-cx}{b}\right) -$$

$$\left[\frac{1}{K} Cx^2 + \frac{2C}{\alpha K} + D \right] - \frac{\alpha E}{\alpha K + \frac{\pi^2}{4b^2}} \cos\left(\frac{\pi x}{2b}\right)$$

$$- \frac{\beta}{\alpha K} (x + a) \qquad (4.40)$$

where

$$c = \sqrt{aK}\, b$$

$$\beta = \frac{\Theta}{E_c D}$$

Θ = slope of the subbase frictional stress distribution (Figure 4.12).
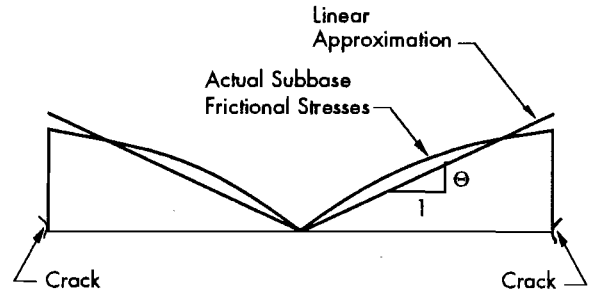
Figure 4.12. Subbase frictional stresses and linear approximation

Constants A, B, C, D, and E are found from boundary conditions. The boundary conditions are given below.

Since $u_{cx} = u_{sx}$ in the fully bonded zone, at the end of the fully bonded zone ($x = 0$)

(1) $w(x) = 0$ (no slip),

(2) $w'(x) = 0$ (compatibility),

(3) $w''(x) = 0$ (no bond stress),

At a crack ($x = b$)

(4) $w'(x) = \dfrac{\sigma_{sc}}{E_s} + \{(\alpha_c - \alpha_s)\Delta T + \varepsilon_{sh}\}$
(no concrete stress), and

(5) $w''(x) = \dfrac{F_i}{E_c D}$ (no bond stress).

With these boundary conditions, constants A, B, C, D, and E were found: they are shown in Appendix B. By substituting the constants into Eq 4.40, $w(x)$ is obtained.

(See Eq 4.41, below.)

Substituting Eq 4.41 into Eq 4.32 yields

(See Eq 4.42, below.)

where 2A is given by

(See Eq 4.43, below.)

Equation 4.42 shows that the bond stress distribution function depends on the steel stress at a crack and the bond development length. If steel stress at a crack and the bond development length are known, the bond stress distribution function (Eq 4.42) is defined. Then, the governing equations derived in the previous section can be solved. Therefore, two relationships, which correlate the steel stress at a crack and the bond development length, are needed to get those values. One is the steel boundary condition (Eq 4.29).

From Eq 4.9,

$$\int_x^b d\sigma_{sx} = \frac{4}{\phi}\int_x^b f_b(t)\, dt \iff$$

$$\sigma_{sx} = \sigma_{sc} - \frac{4}{\phi}\int_x^b f_b(t)\, dt \tag{4.44}$$

From the steel boundary condition (Eq 4.29),

$$\int_{-a}^b \sigma_{sx}\, dx = \int_{-a}^b \sigma_{sc}\, dx - \frac{4}{\phi}\int_{-a}^b\int_x^b f_b(t)\, dt\, dx$$

$$= E_s\alpha_s\Delta TL \iff$$

$$-\frac{4}{\phi}\int_{-a}^b\int_x^b f_b(t)\, dt\, dx = \sigma_{sc}L - E_s\alpha_s\Delta TL \tag{4.45}$$

where b = crack location, -a = middle location.

Equation 4.45 defines a relationship between the steel stress at a crack and the bond development length. Any values of steel stress at a crack and of bond development length satisfying Eq 4.45 satisfy the steel boundary condition. Figure 4.13 shows the relationship derived from the steel boundary condition. The higher the steel stress at a crack, the

$$w(x) = 2A\cosh\left(\frac{cx}{b}\right) - \frac{\beta b}{\alpha Kc}\exp\left(\frac{-cx}{b}\right) - \frac{c^2 x^2}{2b^2}\left(2A\cosh(c) - \frac{\beta b}{\alpha Kc}\exp(-c) - \frac{b^2}{c^2}\beta L\right) - 2A + \frac{\beta b}{\alpha Kc}$$

$$+ \frac{4b^2}{\pi^2}\left(1 - \cos\frac{\pi x}{2b}\right)\left(\frac{-2Ac^2}{b^2} + \frac{\beta c}{\alpha Kb} + \frac{2Ac^2}{b^2}\cosh(c) - \frac{\beta c}{\alpha Kb}\exp(-c) - \beta L\right) - \frac{\beta x}{\alpha K} \tag{4.41}$$

$$f_b(x) = 2AK\left\{\cosh\left(\frac{cx}{b}\right) + \cos\left(\frac{\pi x}{2b}\right)(\cosh(c) - 1) - \cosh(c)\right\} - \frac{\beta b}{\alpha c}\exp\left(\frac{-cx}{b}\right)$$

$$+ \frac{\beta}{\alpha}\left\{\frac{c}{\alpha Kb} - \frac{b}{c}\exp(-c) - L\right\}\cos\left(\frac{\pi x}{2b}\right) - \frac{\beta}{\alpha}(x + a) + \frac{\beta b}{\alpha c}\exp(-c) + \frac{\beta L}{\alpha} \tag{4.42}$$

$$2A = \frac{\dfrac{b}{c}\left[\left\{\dfrac{\sigma_{sc}}{E_s} + (\alpha_c - \alpha_s)\Delta T + \varepsilon_{sh}\right\} - \dfrac{\beta}{\alpha K}\left\{1 + c - \dfrac{2c}{\pi}\right\}\exp(-c) - \beta\left(bL + \dfrac{2c}{\pi\alpha K} - \dfrac{2bL}{\pi} - \dfrac{1}{\alpha K}\right)\right]}{\sinh(c) - c\cosh(c) - \dfrac{2c}{\pi} + \dfrac{2c}{\pi}\cosh(c)} \tag{4.43}$$
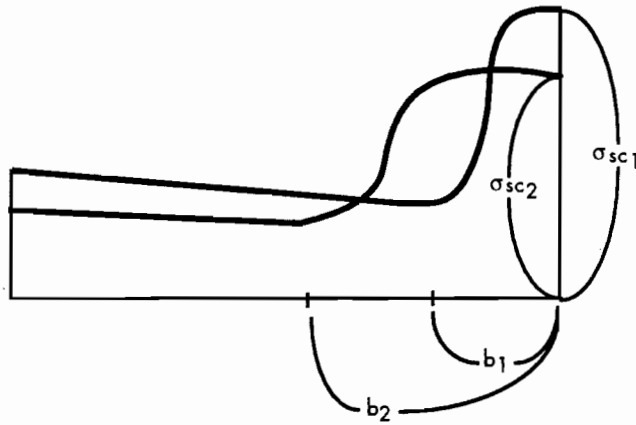
(a) Steel stress at a crack and bond development length from steel boundary condition
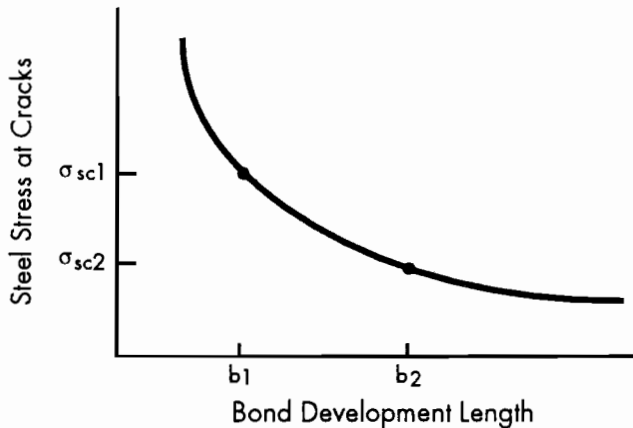
(b) Relationship between steel stress at a crack and bond development length

Figure 4.13. Steel stresses at cracks and bond development length relationship from the steel boundary condition

shorter the bond development length, in order to satisfy the steel boundary condition, which is, intuitively, not correct. One more relationship is needed to get correct values of the steel stress at a crack and the bond development length. Somayaji and Shah (Ref 51) proposed a relationship between the transfer load and the bond development length:

$$b = K_p \frac{P_{tran}}{\Sigma_o} \qquad (4.46)$$

where

K_p = a constant to be determined from pull-out tests,

P_{tran} = the transfer load, which is a difference in the steel force at a crack and at the end of the bond development length.

Therefore $P_{tran} = \sigma_{sc} A_s - \sigma_{so} A_s$, where σ_{so} is the steel stress at $x = 0$ (where bond slippage begins), and

Σ_o = the perimeter of the steel bar.

A relationship between the steel stress at a crack and the bond development length is obtained using Eqs 4.13.

From Eq 4.13,

$$\int_{-a}^{0} d\sigma_{sx} = \frac{1}{D\left(p_s + \frac{1}{n}\right)} \int_{-a}^{0} F_i \, dx \Leftrightarrow$$

$$\sigma_{so} - \sigma_{sm} = \frac{1}{D\left(p_s + \frac{1}{n}\right)} \int_{-a}^{0} F_i \, dx$$

and

$$\therefore \sigma_{so} = \sigma_{sm} - \frac{\int_{-a}^{0} F_i \, dx}{D\left(p_s + \frac{1}{n}\right)} \qquad (4.47)$$

where

σ_{sm} = steel stress at the middle of the geometric model ($x = -a$).

Substituting Eq 4.47 into Eq 4.15 gives

$$\sigma_{so} = \frac{1}{C_1} \sigma_{sc} - \frac{C_2}{C_1} + \frac{\int_{-a}^{b} F_i \, dx}{p_s D C_1} - \frac{\int_{-a}^{0} F_i \, dx}{D\left(p_s + \frac{1}{n}\right)} \qquad (4.48)$$

Since the transfer load is $\sigma_{sc} A_s - \sigma_{so} A_s$, from Eq. 4.48 the transfer load is as follows:

$$P_{tran} = \sigma_{sc} A_s \left(1 - \frac{1}{C_1}\right)$$
$$+ A_s \left\{ \frac{C_2}{C_1} - \frac{\int_{-a}^{b} F_i \, dx}{p_s D C_1} + \frac{\int_{-a}^{0} F_i \, dx}{D\left(p_s + \frac{1}{n}\right)} \right\} \qquad (4.49)$$

Values between $1/266$ and $1/,385$ in^2/lb are best fit values for K_p from the tests (Ref 51) and $\Sigma_o = \pi\phi$.

Therefore, from Eq 4.46,

$$b = \frac{\phi}{(4)(266)} \left\{ \sigma_{sc}\left(1 - \frac{1}{C_1}\right) + \left(\frac{C_2}{C_1} - \frac{\int_{-a}^{b} F_i\, dx}{p_s D C_1} + \frac{\int_{-a}^{0} F_i\, dx}{D\left(p_s + \frac{1}{n}\right)}\right) \right\} \qquad (4.50)$$

The last two terms in Eq 4.50 do not contribute to the value of the bond development length. For a slab segment length of 10 feet and a maximum frictional stress of 3 psi at a crack (which are fairly large values) the bond development length owing to the two terms is around 0.04 inch for ordinary design conditions. C_1 and C_2 depend on design variables and environmental conditions. Therefore, bond development length is an increasing function of steel stress at a crack, as shown in Figure 4.14. Equation 4.50 provides another relationship between the steel stress at a crack and the bond development length. Equations 4.45 and 4.50 provide two independent relationships between the steel stress at a crack and the bond development length. Therefore, solving Eqs 4.45 and 4.50 simultaneously gives the values of the steel stress at a crack and the bond development length. Once the steel stress at cracks and bond development length are determined, stresses in the concrete and the steel are easily found from equations developed earlier.
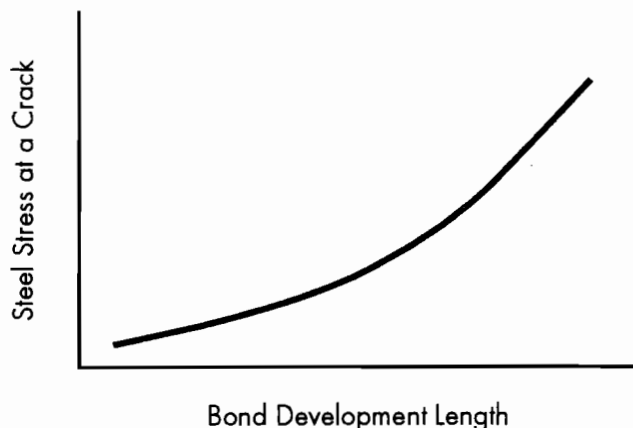
Figure 4.14. Steel stress at a crack and bond development length from Somayaji's assumption (Ref 51)

SUMMARY

In solving the governing equations, several assumptions, in addition to those made at the beginning of the analysis, were made to simplify the computations. The correctness of the solutions is limited by how valid the assumptions are. The assumptions made are reiterated below.

(1) Steel stresses at cracks are the same at every crack.

(2) The bond development length is proportional to the transfer load.

(3) Steel stresses at cracks are constant and is the same as those for uniform cracks.

It is considered that assumption (1) does not yield serious error for the reasons given in this and the previous section. Assumption (2) has not been proved experimentally. However, intuitively, assumption (2) seems reasonable. Assumption (3) had to be made because locations of zero steel displacements could not be determined. The validity of this assumption needs to be investigated.

Stresses and displacements in the concrete and steel are easily determined once the bond stress distribution function is found. Since the bond stress distribution function (BSDF) depends on the steel stress at cracks and the bond development length, they must be determined first. Two relationships are necessary because there are two unknowns. One is the steel boundary condition. The other is a relationship between steel stress at cracks and the bond development length. However, in spite of the simplifying assumptions made above, the equations are too complex to solve directly. An iterative method is used to solve the system of equations. A detailed explanation of how the system of equations is solved is presented in Chapter 5.

The analysis method developed so far is deterministic in that variabilities in the system input or output are not considered. In this study, system output is defined as transverse crack spacing distributions. The variations in the system outputs are caused by the variabilities in the system inputs. There can be many ways to incorporate the variabilities of the inputs into the system model to predict the variations in the system output. If the system is very simple, a closed form solution is possible. However, if the system is very complex, such as the system of equations developed in the previous section, where many variables are related through non-linear equations, a closed form solution may not be possible. A different approach is necessary. In this study, a Monte Carlo method was selected for its simplicity and for its ease of implementation into the computer program.

MONTE CARLO METHOD

This technique mathematically simulates the variability in the performance of a family of similar

objects. To do this, two things are required. First, a mathematical relationship between the system performance and each variable component must be known. Second, the statistical properties of the distribution of each variable in this relationship must be known (Ref 54).

A mathematical relationship between the system performance (stresses in the concrete and steel) and each variable component (design and environmental variables) was obtained in the previous section. Therefore, it is necessary to identify the variabilities in the input variables. Steel variables, such as the amount, bar size, and modulus of elasticity, have very little variation. The depth of longitudinal steel has a significant effect on crack development (Ref 3). The variation of the depth of longitudinal steel was investigated in Reference 3. However, a definite conclusion concerning whether or not the variation was significant could not be made. More study of this subject is necessary. It is believed that there is little variation in subbase friction characteristics. Marshall et al (Ref 55) found that the coefficient of variation of slab thickness was negligible. At a given time, environmental conditions are considered almost identical within one project.

The next variable investigated is concrete material properties. The thermal coefficient of concrete is determined largely by the aggregate type and content, which was discussed in the previous chapter. Marshall et al also found that the coefficient of variation of the density was very small, averaging 1.7 percent, which implies that aggregates are evenly distributed. The variation of thermal coefficient measured with the cores taken from the pavement slabs was negligible (Ref 56). Drying shrinkage may vary from location to location; however, no field data are available on this subject.

It is known that there is a variation in concrete tensile strength from location to location. As discussed in the previous chapter, concrete tensile strength depends largely on the bond characteristics between cement paste and the aggregate surface. The bond strength between cement paste and the aggregate surface, for a given water/cement ratio and aggregate type, depends on local conditions, such as aggregate surface shape, texture, or the existence of voids between cement paste and the aggregate surface. The tensile strength of concrete is governed by the weakest element in it. Therefore, the problem becomes finding the proverbial weakest link in a chain. After the amount of longitudinal reinforcing steel, the concrete tensile strength was found to have the most significant effect on crack spacing. There is a sizable variation in concrete tensile strength and, therefore, the methodology to include this variability in the mechanistic model was developed. Major research work in identifying the concrete tensile strength has been conducted in the pavement area, while, in the structural engineering field, there has been much concrete compressive strength research because, in structural engineering, concrete tensile strength is considered negligible, whereas compressive strength is of concern. Another reason is that the testing of compressive strength is easy to run, while tensile strength is not as easy to measure.

The variation in the concrete tensile strength was measured in a study by Marshall (Ref 55), and there were differences between projects. The coefficient of variation within given projects was very consistent at about 20 percent. The distribution of concrete flexural strengths along the pavement length is shown in Figure 4.15. The data were obtained on US290 in Houston (Ref 68). The shape is sufficiently close to the normal distribution. There is a close relationship between flexural strengths and tensile strengths. Therefore, it is assumed that the concrete tensile strength has normal distribution along the pavement length.
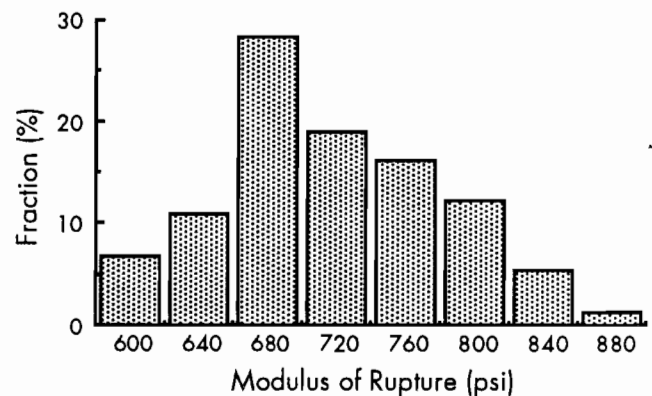
Figure 4.15. Modulus of rupture distribution obtained along the pavement length (Ref 68)

Since the statistical properties of the concrete tensile strength are known, the Monte Carlo method can be applied. The application of the Monte Carlo method to the analysis of the pavement sections consists of the following procedures. The pavement section is divided into a certain number, n, of segments. It is assumed that cores were taken at each nodal point and tensile strength tests were conducted. The distribution of the tensile strength is normal. Since mean and standard deviations characterize the normal distribution, if the average strength and standard deviation of the tensile strength are known, it is possible to generate the tensile strength value for each core. This strength conforms to a given average and a standard deviation value. Once the strength values are assigned to each node, an analysis is conducted

to find where the crack will occur. For example, in Figure 4.16, even though the maximum stress occurs at node number 6, the difference between tensile strength and stress is maximum at node number 8.

Therefore, a crack will occur at node number 8 instead of node number 6, where maximum stress occurs. The Monte Carlo method continues this process throughout the length of the pavement.
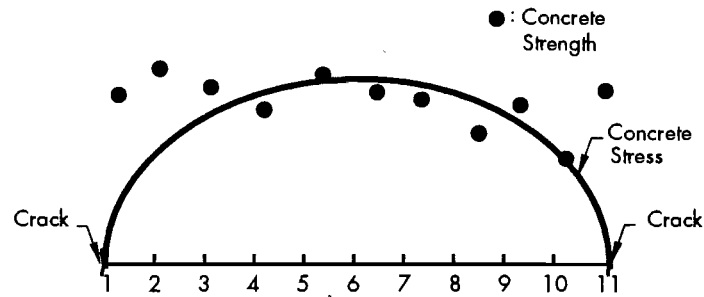
Figure 4.16. Illustration of Monte Carlo method

CHAPTER 5. METHOD OF SOLUTION

The system of equations developed in Chapter 4 is complex because many variables are involved in nonlinear forms. In this study, the iteration process was used to solve these equations. In this chapter, methodologies for solving the system of equations are explained.

STEEL STRESS AND BOND DEVELOPMENT LENGTH

Examining the cracking responses of CRC pavements is equivalent to determining concrete stresses along the pavement. If the rate of concrete stress changes is known, researchers can determine concrete stresses at any point using the boundary condition that sets concrete stresses at zero at crack faces. The rate of concrete stress changes is not constant, but varies along the pavement length. In Chapter 4, the rate of concrete stress changes was obtained. It was different in the fully bonded zone and the bond development zone. In the fully bonded zone, it was a function of subbase friction (Eq 5.1) whereas it was a function of bond stress and subbase friction in the bond development zone (Eq 5.2), as shown below:

$$\frac{d\sigma_{cx}}{dx} = \frac{-F_i}{nD\left(p_s + \frac{1}{n}\right)} \quad \text{(Fully Bonded Zone)} \quad (5.1)$$

$$\frac{d\sigma_{cx}}{dx} = -\frac{4f_b(x)p_s}{\phi} - \frac{F_i}{D} \quad (5.2)$$
(Bond Development Zone)

The two equations illustrate that subbase friction, bond stress, and bond development length are all that is required to determine concrete stress distributions. Determination of subbase friction is discussed in the next section. In Chapter 4, it was shown that bond stress distributions are determined if steel stresses at cracks and bond development lengths are known. In this section, it is explained how steel stresses at cracks and bond development lengths are determined.

Since there are two unknowns, i.e., steel stresses at cracks and bond development lengths, two

independent relationships are required. One relationship is the steel boundary condition. In this study, it is assumed that steel stresses at cracks are constant regardless of slab segment lengths. If the crack spacings are uniform, steel displacements will be zero at cracks and at the middle of slab segments. Therefore, the steel boundary condition is applied between a crack and the middle of a slab segment of mean crack spacing (2L), as follows:

$$\int \sigma_{sx} \, dx = E_s \alpha_s \Delta T L \quad (5.3)$$

The left term in Eq 5.3 is an area under the steel stress distribution curve, that is, over half of a slab segment length. Since the right term in Eq 5.3 is constant for a given slab segment length and environmental condition, bond development length increases monotonically as steel stress at a crack increases, which is shown in Figure 4.14. Remember that there is a relationship between steel stresses at a crack and at the middle of a slab segment (Eq 4.15). The higher the steel stress at a crack, the higher that at the middle of a slab segment.

The other is a relationship between steel stresses at cracks and bond development lengths. In this study, a relationship proposed by Somayaji and Shah (Ref 51) was used:

(See Eq 5.4, top of next page.)

From Eq 5.4, it is shown that bond development length increases along with steel stress at a crack. The last two terms in Eq 5.4 do not contribute to the value of bond development length, as explained in the previous chapter. Therefore, bond development length is a monotonically increasing function of steel stress at a crack.

There are two functions that relate steel stress at a crack to bond development length. Therefore, it is possible to find a correct solution. The process is shown in Figure 5.1. Curve 1 is derived from Eq 5.4, and curve 2 is derived from Eq 4.45. For a given steel stress at a crack, two bond development lengths are derived from two relationships. Correct values of steel stress at a crack and bond development length must satisfy both Eqs 5.3 and 5.4. For a

$$b = \frac{\phi}{(4)(266)} \left[\sigma_{sc} \left(1 - \frac{1}{C_1}\right) + \left\{ \frac{C_2}{C_1} - \frac{\int F_i\,dx}{p_s\,DC_1} + \frac{\int F_i\,dx}{D\left(p_s + \frac{1}{n}\right)} \right\} \right] \tag{5.4}$$

given steel stress at a crack, two values of b are obtained. Let b_1 be a bond development length from Eq 5.4 and let b_2 be taken from the steel boundary condition (Eq 5.3). The steel stress value at a crack which yields the same bond development length needs to be found. Two relationships defining steel stress at a crack and bond development length are monotonically increasing and decreasing functions. Therefore, the correct value of bond development length is always between two bond development lengths derived from Eqs 5.3 and 5.4. The procedures given below are based on the existence of a correct answer between two values for b.

(1) An arbitrary value is assumed for bond development length. Steel stress at a crack is found from Eq 5.4, assuming zero subbase friction.

(2) With the steel stress obtained in Step (1), the bond development length is found which satisfies the steel boundary condition. Two bond development lengths are compared. And if the difference between the two values is within the closure limit, proceed with Step (5). Otherwise,

a larger value is assigned as the upper limit (UL) and a smaller value as the lower limit (LL) for bond development length. An average value of UL and LL is assigned as the new bond development length.

(3) With the new bond development length, steel stress at a crack is computed using Eq 5.4. With that steel stress at a crack, a bond development length is obtained from the steel boundary condition (Eq 5.3). If the difference between b_1 and b_2 is within the closure limit, proceed to Step (5). Otherwise, there are eight situations regarding b_1, b_2, UL, and LL as follows:

(a) when $b_1 > b_2$

    (i) $b_1 > $ UL and $b_2 < $ LL: previous values for UL and LL are preserved.

    (ii) $b_1 > $ UL and $b_2 > $ LL: the previous value for UL is preserved and b_2 is the new LL.

    (iii) $b_1 < $ UL and $b_2 < $ LL: b_1 becomes the new UL and the previous LL is preserved.
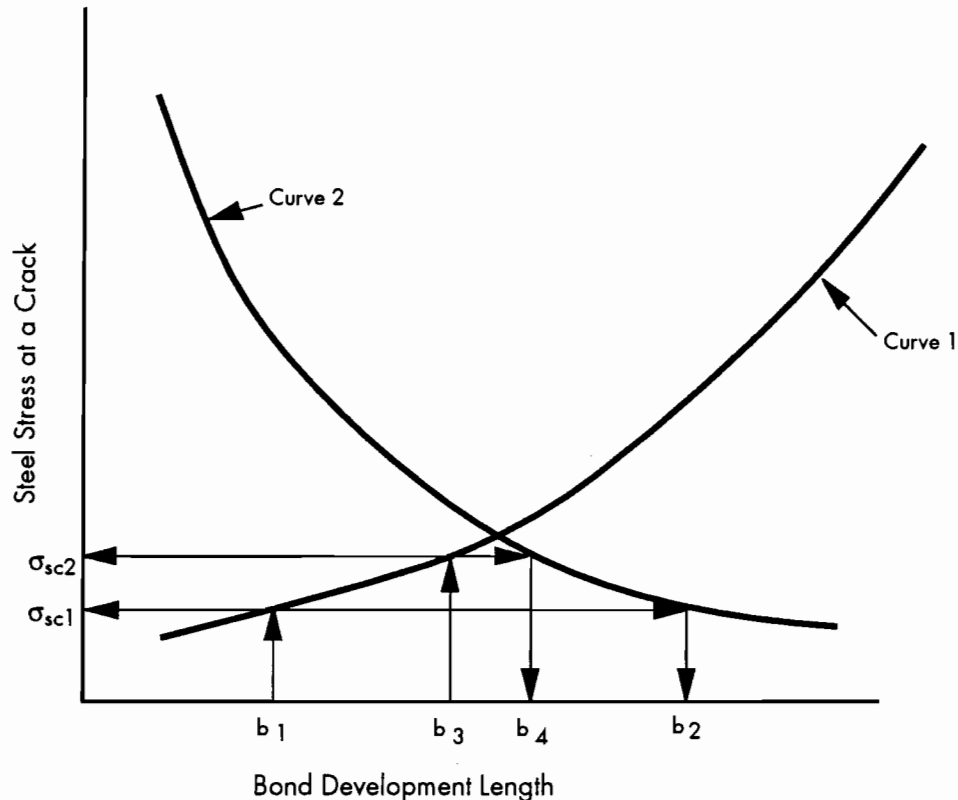
Figure 5.1. Algorithm used to find bond development length and steel stress at a crack

(iv) b_1 < UL and b_2 > LL: b_1 and b_2 become the new values for UL and LL.

(b) when b_1 < b2
  (i) b_1 > LL and b_2 < UL: b_1 and b_2 become new values for LL and UL.
  (ii) b_1 > LL and b_2 > UL: the previous value for UL is preserved and b_1 becomes the new LL.
  (iii) b_1 < LL and b_2 < UL: b_2 becomes the new UL and the previous LL is preserved.
  (iv) b_1 < LL and b_2 > UL: previous values for UL and LL are preserved.

(4) After new values are computed for UL and LL using the above algorithm, an average value of UL and LL is assigned as a bond development length. With the new bond development length, go back to Step (3).

(5) Using the values from Step (3), compute the concrete and steel stresses. Displacements in the concrete and steel are found using stresses and boundary conditions which state that displacements of concrete and steel are zero at the middle of the slab segment. Once, concrete displacements are found, subbase frictions are calculated. If the differences between previous subbase friction values and new values are within the closure limit, they are correct values. Otherwise, with the values of steel stress at a crack, bond development length, and subbase friction, Steps (3) and (4) are taken.

Step (5) is explained in detail in the next section. Once the values for steel stress at a crack and for bond development length are found, the bond stress distribution function (BSDF) is obtained from Eq 4.42. Stresses in the concrete and the steel are found from Eqs 4.10, 4.14, and 4.9, 4.13, respectively, after subbase friction values are determined.

SUBBASE FRICTION

Subbase frictional stress at the interface between the PCC slab and the subbase is related to the relative movement between them, as is the bond stress between the concrete and the steel. Since the subbase is assumed to be stationary, the concrete displacements become the relative movement between the PCC slab and the subbase. The maximum subbase friction stress occurs at around 0.03 inch of concrete displacement. The maximum values for subbase frictional stresses vary, depending on subbase types, as shown in Table 3.6.

Concrete displacements are computed, if concrete stress distributions are known, as follows:

$$u_{cx} = -(\alpha_c \Delta T + \varepsilon_{sh})x + \frac{1}{E_c}\int \sigma_{cx}\,dx \qquad (5.5)$$

Equation 5.5 is solved together with the boundary condition for concrete displacements, which is that the concrete displacements are zero at the middle of a slab segment. Since the displacements in concrete are not known initially, subbase frictional stress cannot be determined. In this study, an iterative method is utilized to determine subbase frictional stress. It is assumed that the distribution of subbase frictional stresses along the slab length can be approximated as a linear function of a distance from the middle of slab segments. The procedures to determine subbase frictional stresses are described below:

(1) Initially, zero subbase friction is assumed.
(2) Steel stress at a crack and bond development length are found, and BSDF is obtained. Stresses and displacements in the concrete and steel are computed.
(3) Subbase frictional stresses are calculated from concrete displacement values and the slab-movement-subbase-frictional-resistance relationship.
(4) The distribution of subbase frictional stresses along the slab segment is illustrated in Figure 3.2(c). This distribution is approximated by a linear function, using regression analysis (Figure 4.12). The slope of the curve is computed and used for Q in Eq 4.40.
(5) With the value for Q, concrete displacements are computed and a new value for Q is computed.
(6) If the difference between the previous and new values for Q was within the closure limit, the correct solutions were obtained. Otherwise, an average of the two values of Q is computed and Steps (2) through (6) are repeated.

SUMMARY

The method of finding steel stress at a crack and bond development length described in this chapter has shown fast convergence in a computer program. Once steel stress at a crack and bond development length are computed, the bond stress distribution function is found. Since the assumption has been made that steel stresses at cracks and bond development lengths are the same for all slab segments, stresses in the concrete and the steel in any slab segments are computed using the equations obtained in Chapter 4. The cracking responses of CRC pavements are then examined.

46

CHAPTER 6. MECHANISTIC DISTRESS PREDICTION MODEL

The unique features of CRC pavements are that transverse cracking is unavoidable and that there is a strong correlation between transverse crack spacing characteristics and pavement performance. Once the correlation is found, the results of the theoretical analysis developed in the previous chapters can be used to estimate CRC pavement life in terms of the frequency of pavement distresses for various environmental and design conditions. In this chapter, major failure modes affecting CRC pavement performance are discussed. Mechanisms of major failures and their relationship with transverse crack spacings are discussed. A method is developed to predict pavement life in terms of the frequency of punchouts and is incorporated into computer program CRCP-5.

PERFORMANCE OF CRC PAVEMENTS

Pavement performance is defined as the serviceability trend of a section of pavement with increasing numbers of axle load applications. Present serviceability of pavement is the ability of a specific section of pavement to serve high-speed, high-volume, and mixed (truck and automobile) traffic in its existing condition (Ref 58). Three variables, i.e., slope variance, cracking, and patching, are included in the measure of present serviceability for rigid pavement developed in the AASHO Road Test. Cracking and patching add little to the accuracy of the present serviceability prediction equations. Therefore, in many instances, the use of roughness measurements alone is sufficient for predicting the serviceability index. In CRC pavements, slope variance or roughness is primarily determined by the sophistication of the pavement surface construction and is not significantly affected by the traffic load applications up to a certain point. After that point, the serviceability index drops rather quickly due to the surface roughness developed by the fatigue failure of concrete. Studies conducted at the Center for Transportation Research found that the serviceability index of a pavement with heavy maintenance does not appear to change with time or traffic. On the other hand, the number of failures (punchouts and patches) increased with traffic applications (Ref 59). This suggests that the present serviceability index (PSI) may not be an adequate indicator of the pavement condition. The

number of failures may be a better indicator of the structural condition of CRC pavements. Chou et al (Ref 59) developed a distress index which consists of the numbers of punchouts and patches per mile and suggested that the distress index be used as a pavement rehabilitation criterion.

MAJOR FAILURE MODES IN CRC PAVEMENTS

It is necessary to define what constitutes pavement failure in order to estimate pavement life. Yoder et al (Ref 60) made a distinction between two different types of failure. Structural failure is a breakdown of one or more of the pavement components. Functional failure is such that the pavement will not carry out its intended function without causing discomfort to passengers or high stress in the vehicle passing over it, due to its roughness. In CRC pavements, structural failures lead to functional failures. Therefore, the major concern in this study is structural failures.

A study by McCullough et al (Ref 6) found that the punchout is a major failure manifestation in CRC pavements. The punchout is a structural failure in which a small segment of pavement is loosened from the main body and displaced downward under traffic. The punchout usually is bounded by two closely spaced transverse cracks, a longitudinal crack, and the pavement edge and, sometimes, by the branches of a Y-crack and the pavement edge. Punchouts are invariably associated either with short transverse crack spacings (1 to 2 feet) or Y-cracks (Ref 2). Since transverse cracks are unavoidable in CRC pavements, it is necessary to prevent longitudinal cracks, closely spaced transverse cracks, and Y-cracks in order to prevent punchouts.

There are two types of mechanisms in longitudinal cracking. One is warping due to temperature variations through the pavement depth. The other is cracking due to the wheel loads. Longitudinal cracking due to warping has been observed at early age in CRC pavements. Warping stress increases with pavement width up to a certain distance. Figure 6.1 shows the warping stresses of 8-inch-thick slabs for various slab lengths. A warping stress of as high as 400 psi develops for a 24-foot slab. For a 12-foot slab, which is a lane width and a

Figure 6.1. Warping stresses for 8-inch-thick slab for 20°F temperature differentials between top and bottom

practically minimum longitudinal joint spacing, warping stress is substantially lower than for 24 feet. Use of warping joints at 12-foot intervals became a common practice, and longitudinal cracking due to warping was significantly reduced.

Many factors affect longitudinal cracking due to wheel loads. These factors include transverse crack spacing, magnitude of wheel load, and structural continuity at transverse cracks. The fact that punchouts are invariably associated with narrow transverse cracks strongly indicates that transverse crack spacing is an important factor. CRC pavement slabs, subjected to wheel loads, behave differently, depending on transverse crack spacings. Figure 6.2 presents the relationship between wheel load
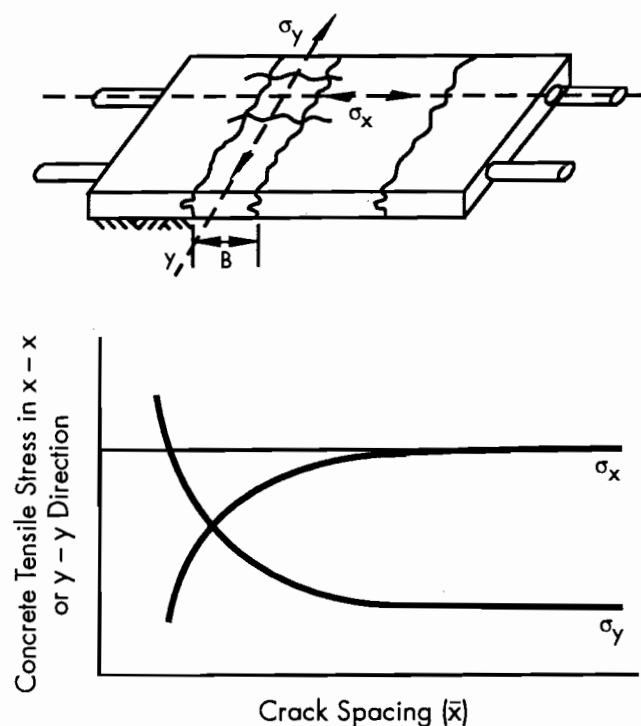
Figure 6.2. Variations in wheel load stresses as affected by transverse crack spacings

stresses and transverse crack spacings. Slabs with small transverse crack spacings act as beams in the transverse direction, and the wheel load stress for the transverse direction becomes dominant. For slabs with larger transverse crack spacings, wheel load stress in the longitudinal direction is greater than that in the transverse direction. The structural continuity at the transverse cracks affects the wheel load stress. The definition of "structural continuity at the transverse cracks" was discussed in Chapter 2. If the crack width is negligible and perfect aggregate interlock is provided, wheel load stress in the transverse direction will be kept low. On the other hand, if the aggregate interlock is lost and the transverse crack spacing is very small, wheel load stress in the transverse direction will be considerable. Once the aggregate interlock is lost, deflection due to wheel load will increase, which in turn aggravates the loss of aggregate interlock and eventually will lead to longitudinal cracking.

Transverse cracks usually do not cross the pavement in a straight line, but tend to meander. In terms of the causes, there are two kinds of transverse cracks: those developed during the early ages due to environmental conditions, and those developed from the combined effect of environmental and wheel loads. Distribution of concrete stresses due to environmental loads was shown in Figure 3.2(d). There is not much variation in concrete stresses away from cracks. The environmental loading rate is very slow and, therefore, the weakest points in the concrete are connected to form transverse cracks. Concrete is more heterogeneous in the early ages than during later ages because, in the early ages, the aggregate remains very strong while the cement paste is comparatively weak. Therefore, transverse cracks developed in the early ages because of environmental loadings tend to meander more. By the time the pavement is open to traffic, concrete gains a relatively large portion of its ultimate strength and becomes more homogeneous, compared with the concrete of early ages. The loading rate of the external wheel load is considerably fast compared to that of environmental loads. Transverse cracks occur in a cross section which contains the weakest elements, instead of connecting the weakest points. The effect is that transverse cracks developed because of the combination of environmental and wheel loads tend to have straight lines. In a condition survey, it was observed that there was a correlation between the shape of transverse cracks and crack widths. Y-cracks usually had bigger crack widths, whereas straight transverse cracks had small crack widths. It is important to prevent very early cracking, by using improved curing compounds or placing concrete when there is not a large temperature difference between day and night.

In CRC pavements with 12-foot longitudinal warping joints, longitudinal cracks due to warping rarely occur. Y-cracks can be prevented by exercising proper construction techniques. Fatigue cracking because of wheel load applications is a primary cause of longitudinal cracking. Therefore, in properly constructed CRC pavements, close transverse cracks connected with longitudinal fatigue cracks caused by wheel load applications are the major mode of punchouts. As shown in Figure 6.3, the number of punchouts increases with traffic load applications, which implies that the longitudinal fatigue cracks due to repeated loadings are the major cause of punchouts. Theoretically, no punchouts will occur if
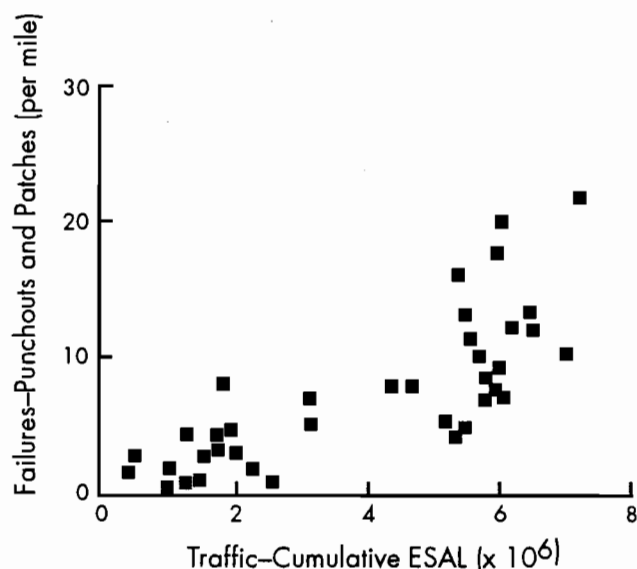
Figure 6.3. Number of failures with age (Ref 59)

no wheel load is applied, even when the transverse cracks are very narrow. On the other hand, if concrete does not have a fatigue endurance limit, all the concrete slabs will result in punchouts when the wheel load continues to be applied until the fatigue life of the pavement is reached. It is necessary to estimate wheel load stress in order to evaluate the possibility of punchouts. For a given slab thickness and wheel load, wheel load stress varies, depending on the transverse crack spacings.

TRANSVERSE CRACK SPACING AND WHEEL LOAD STRESS

Accurate evaluation of the flexural strength of concrete and of wheel load stress is needed in order to predict longitudinal cracking due to fatigue. There are several factors affecting wheel load stress. In this research, a factorial experiment was set up to include the effects of various levels of the factors.

Factorial Experiment

Factors affecting wheel load stress include (1) slab thickness, (2) transverse crack spacing, (3) wheel load, (4) subgrade modulus of reaction, and (5) structural continuity at transverse cracks. Three slab thicknesses (8, 12, and 15 inches) and six transverse crack spacings (1, 2, 4, 6, 8, and 12 feet) were selected. The preliminary investigation of the effect of various wheel loads on fatigue life indicated that the use of the equivalency factor developed at the AASHO Road Test resulted in a unique answer regardless of wheel loads. Therefore, one level of wheel load, i.e., 9,000 lb, was selected. Initial runs of a computer program with 200 and 500 psi/inch for subgrade modulus of reaction indicated that there was very little difference in wheel load stress for those two subgrade modulus values. Therefore, one level of subgrade modulus value, i.e., 200 psi/inch, was selected. Structural continuity at transverse cracks is believed to play an important role in wheel load stress. However, a computer program capable of incorporating various conditions at transverse cracks is not available at this time. Therefore, this investigation has a limitation in that respect, and more study is needed in this area.

Stress Evaluation

Computer program ILLISLAB, developed at the University of Illinois, was selected for this study. Stress values obtained from the computer program for various conditions are presented in Appendix C and are shown in Figure 6.4. At a crack spacing of 6 feet, stresses in both the longitudinal and transverse directions are very close. For crack spacings of less than 6 feet, stress in transverse directions is larger than that in longitudinal directions. A regression equation was obtained for the values in Appendix C, as follows:
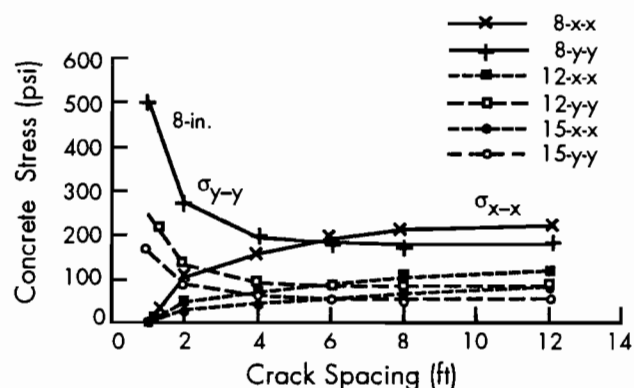
Figure 6.4. Wheel load stresses for various crack spacings and slab thicknesses

$$\sigma = e^{9.8474} \, D^{-1.8143} \, X^{-0.4477} \qquad (6.1)$$

where

σ = wheel load stress in transverse direction, psi;

e = base of natural log;

D = slab thickness, inches; and

X = crack spacing, feet.

Since the effects of aggregate interlock and longitudinal reinforcement are ignored, stress values obtained in this study are believed to be higher than the actual values. In order to include the effect of aggregate interlock and longitudinal reinforcement, a stress reduction factor considering various conditions of transverse cracks needs to be developed.

FATIGUE FAILURE OF CONCRETE

When a material fails under repeated loads, when each load applied to the material is smaller than a single static load which would cause failure, it is said to have failed in fatigue. Tests have shown that fatigue specimens had fewer broken aggregate particles than specimens which fail in a static test (Ref 61). Thus, failure at the bond interface is probably dominant in fatigue; in mortar, fatigue failure is believed to take place at the interface of the fine aggregate particles (Ref 24). There are different fatigue failures depending on the loading type: fatigue failure in compression, in flexure, or in tension. If CRC pavement slabs fail, it is because of fatigue in flexure, and this study concerns the fatigue behavior in flexure.

Literature Review

In the early 1920's, Clemmer (Ref 62) conducted a research study to identify fatigue characteristics of concrete pavement. Beams were loaded at a stress level of 50 percent of the modulus of rupture. All 15 beams survived 1,130,876 cycles of load applications. The load was then increased to 61 percent of the modulus of rupture and seven specimens failed at from 17,000 to 200,000 cycles. A number of specimens remained intact after a total of 1,540,000 cycles and the load was increased to 70 percent of the modulus of rupture. The remainder failed at 1,100 to 91,000 additional cycles of load applications. With these procedures, Clemmer found that beams with previous stress histories could resist a greater number of applications of load at an increased stress intensity as long as the first stages of loading were below some critical value. This finding is explained by the increase in strength due to a densification of concrete caused by the initial low-stress level cycling, in a manner similar to improvement in strength under moderate sustained loading (Ref 24).

Murdock and Kesler (Ref 63) found that fatigue life varied, depending on the range of applied stresses, as shown in Figure 6.5. R is a measure of
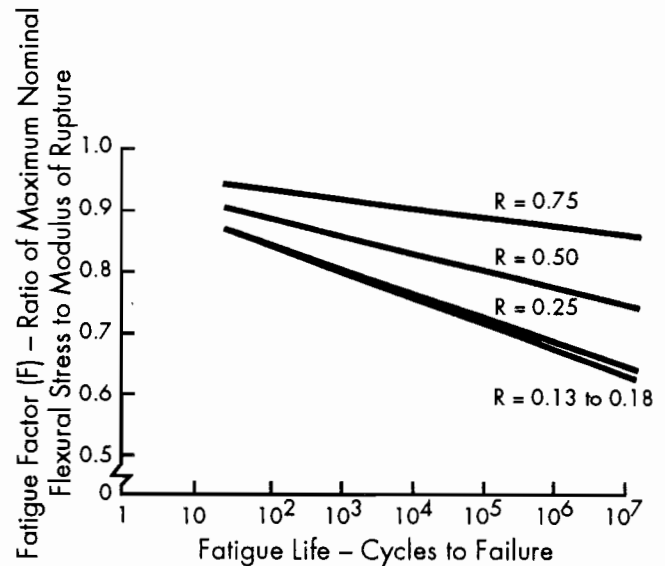
Figure 6.5. **Effect of the range of stress on the behavior of plain concrete under fatigue loading (Ref 63)**

the range of applied stresses, which is a ratio of flexural stress at minimum load to the flexural stress at maximum load. In none of the test series did the data indicate the existence of an endurance limit, although many of the specimens sustained more than ten million repetitions of stress without failure. The researchers also noticed that the repeated loads which plain concrete might sustain for a finite number of repetitions without failure was a critical percentage of the static ultimate flexural strength. Furthermore, this percentage is a function of the range of stress to which the concrete is subjected.

Hudson and Scrivner (Ref 64) derived a relationship between rigid pavement performance and stress in the AASHO Road Test. Critical stresses were computed for various slab thicknesses and load positions. The critical stresses were correlated with the pavement serviceability index and the number of load applications. A regression analysis was made and the following equation resulted:

$$W_{2.5} = \frac{10^{16.30}}{\sigma_1^{4.22}} \qquad (6.2)$$

where

$W_{2.5}$ = the predicted number of applications to a serviceability of 2.5, and

σ_1 = the critical compressive edge stress.

Hilsdorf and Kesler (Ref 65) investigated fatigue strength of concrete under repeated loads when the minimum and the maximum loads varied during the test or when the repeated load cycles were interrupted by rest periods. A total of 185 plain concrete specimens were used. In the phase one study, the effect of a rest period on the fatigue strength was investigated. Periodic rest periods increased the fatigue strength subjected to repeated flexural loads. This increase became more pronounced as the length of the rest periods increased to 5 minutes. In phase 2, two studies determining the effect of variable loads were made. In Program 1, n_1 cycles of repeated loads were applied at a stress level S_1. After the n_1 cycles, the stress level was increased to S_2 and the test continued until the specimen failed, after an additional n_2 cycles. Program 2 was a reversal of Program 1 insofar as the higher stress level was applied first, and after the n_1 cycles, the load was decreased from S_1 to S_2. The researchers found that the fatigue strength and the life of concrete subjected to repeated loads of varying magnitude were influenced by the sequence in which these loads were applied. The fatigue life of a specimen in Program 1 was larger than that of a specimen in Program 2. In other words, a specimen with a higher pre-applied stress level had a longer fatigue life compared to the fatigue life of a specimen in which the lower stress level was applied first. The researchers also evaluated the adequacy of Miner's hypothesis using the plain concrete specimens. Miner's hypothesis gives unsafe values of the fatigue strength of concrete under high loads; however, it was too conservative for low loads.

Vesic et al (Ref 66) studied the fatigue behavior of rigid pavement using the AASHO Road Test data. They found that the tensile stresses in pavement slabs represented the best indicators of pavement performance. A study of the relationship between maximum stress in the slab and the number of load applications to a PSI of 2.5 revealed that the relationship was consistent regardless of the slab thickness, or axle type (single or tandem). They state:

This most significant finding confirms the soundness of a rational, mechanistic approach to the design of rigid pavements. It demonstrates beyond a doubt that failure in pavement performance is not a phenomenon of chance, as some statistical approaches tend to suggest, but a phenomenon that has a definite mechanical cause (Ref 66).

A regression equation correlating flexural stress and the number of 18K equivalent load applications was derived as follows:

$$N = 225,000 \left(\frac{f}{\sigma} \right)^{4.00} \qquad (6.3)$$

where

N = number of 18K equivalent single axle load applications,

f = flexural strength, and

σ = flexural stress.

Equations 6.2 and 6.3 represent the relationship between the number of load applications up to a PSI of 2.5 and wheel load stress. Therefore, these equations do not necessarily correlate the number of applications to fatigue cracking. The results of laboratory fatigue tests cannot be applied to CRC pavements because any point in a CRC pavement slab experiences reversals in wheel load stresses as a vehicle passes. In laboratory tests, stress reversals do not occur, and, therefore, laboratory tests overestimate fatigue life of pavement concrete. In predicting longitudinal fatigue cracking, a relationship is needed between the number of applications and fatigue cracking. Further research is needed to refine fatigue characteristics in CRC pavements.

Variability in Fatigue Life of Concrete

As in the other concrete properties, there is a variability in fatigue strength of concrete. In 1958, McCall (Ref 67) developed a probability model for fatigue strength. However, the number of specimens used, 9, limits the validity of the model. Hudson and Scrivner (Ref 64) found that the standard deviation of log $W_{2.5}$ in Eq 6.2 was 0.042. The mean value of log $W_{2.5}$ is 6.18 for a stress value of 250 psi. Therefore, the coefficient of variation of fatigue life was 0.7 percent, which is very low. However, it is believed that the variability will be larger than that from Eq 6.2. However, little information is available on this subject. More research is needed.

PREDICTION OF PUNCHOUTS

It was shown that wheel load stresses varied, depending on crack spacings. Therefore, fatigue life for slabs with different crack spacings varies. As discussed earlier, punchout develops when narrow transverse cracks are connected by longitudinal cracks. As a result, the prediction of punchouts is equivalent to the prediction of longitudinal cracks. Since the relationship of transverse crack spacing with wheel load stress in the transverse direction and the fatigue equation are assumed, it is possible to develop a method for predicting punchouts. Figure 6.6 illustrates the methodology for estimating the number of punchouts. The procedure is described below.

(1) Divide crack spacings into groups, such as 0-1 feet, 1-2 feet, and so on.
(2) Select a crack spacing range and compute the number of cracks in that range in a mile.
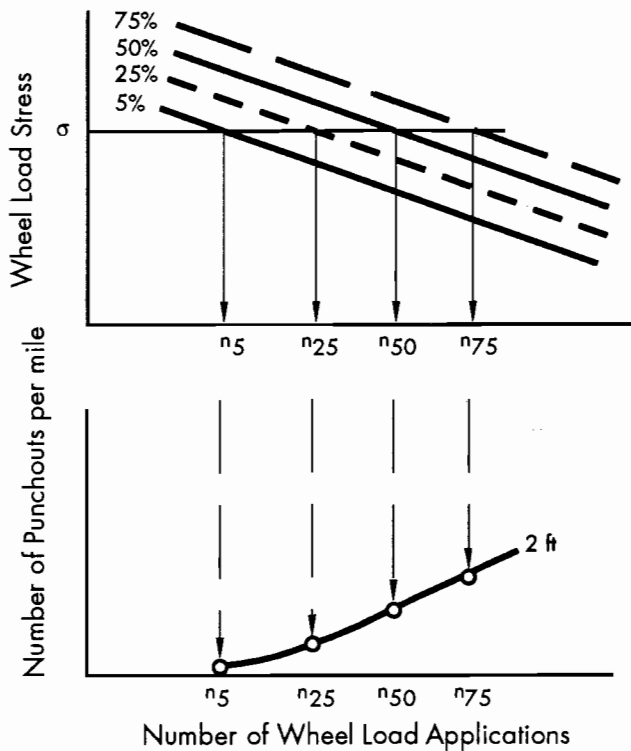
Figure 6.6. Algorithm to compute number of punchouts

(3) Compute the wheel load stress in transverse directions using Eq 6.1.

(4) For the wheel load stress value from (3), calculate the number of applications corresponding to various probabilities of fatigue failure.

(5) Compute the number of punchouts for various numbers of applications by multiplying the number of cracks in a mile by the corresponding probability of failure.

(6) Select the next crack spacing range and compute the number of cracks in that range in a mile and repeat Steps (3) through (5).

If Steps (2) through (6) are completed for the maximum crack spacing range, add the number of punchouts obtained for various crack spacing ranges.

Incorporation of Fatigue Effect into Computer Program CRCP-5

The methodology developed above to predict the number of punchouts requires the calculation of the number of cracks in each crack spacing group and the probability of fatigue failure for various crack spacings. These calculations are most efficiently achieved by the computer program. The above procedures were incorporated into computer program CRCP-5. The flow diagram for this part is shown in Figure 6.7.
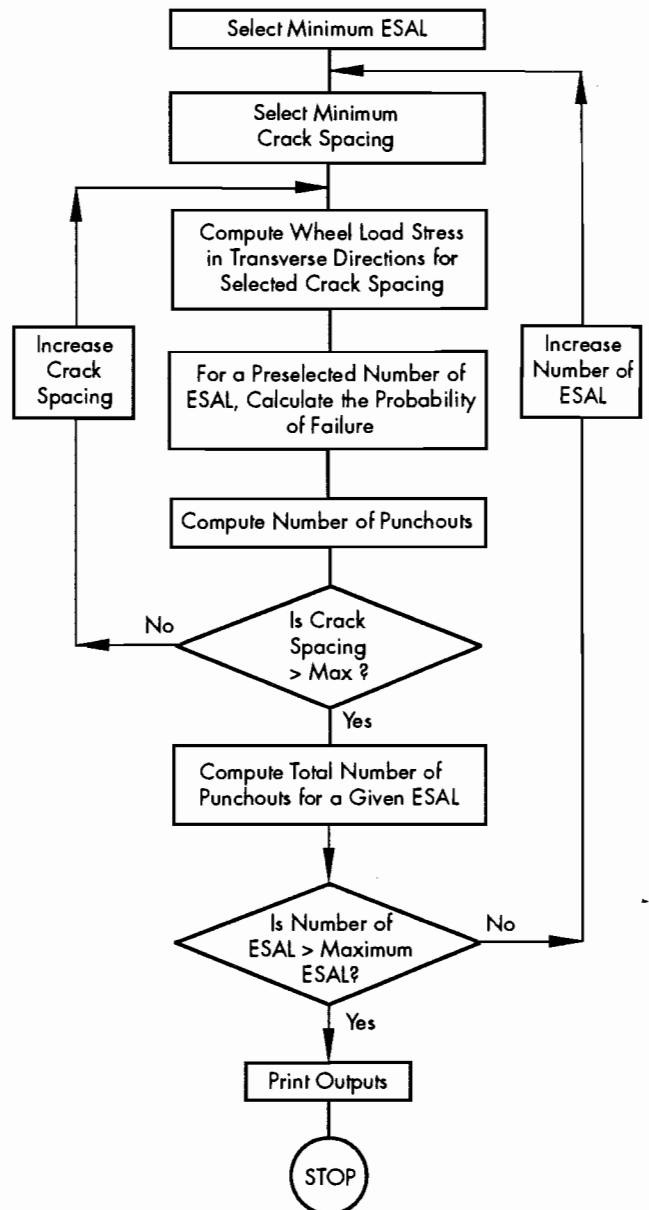
Figure 6.7. Flow diagram for predicting punchouts

SUMMARY

A major distress in CRC pavements is punchouts. Punchouts occur when very narrow transverse cracks are connected by longitudinal cracks. Therefore, longitudinal fatigue cracking due to wheel load applications plays an important role. The fatigue life of concrete largely depends on the stress-strength ratio. Transverse crack spacing has a significant effect on wheel load stress. Therefore, different numbers of fatigue failures, or punchouts, will result for various crack spacings.

A methodology was developed to predict distresses in terms of punchouts in CRC pavements.

The methodology was incorporated into computer program CRCP-5. Further research is necessary to identify fatigue characteristics of CRC pavements. The findings from further research can be used to calibrate and to refine the equations used in the program.

CHAPTER 7. DESCRIPTION OF COMPUTER PROGRAM CRCP-5

The mechanistic analysis, the Monte Carlo method, and the mechanistic distress prediction model described in the previous chapter were incorporated into a computer program. In this chapter, a brief history of the previous versions of the program is presented, followed by the working system of the computer program. Input format is introduced, and the output is explained.

BRIEF HISTORY OF COMPUTER PROGRAM CRCP

Computer program CRCP was developed as a result of NCHRP Research Project 1-15 (Ref 3). The program analyzes the complex CRC pavement system and predicts the structural responses, such as mean crack spacing, crack width, concrete and steel stresses, and displacements of the concrete and steel at any nodal point. The effect of the wheel loads was not included in program CRCP-1. CRCP-1 was modified to include the effect of the wheel loads, and it resulted in CRCP-2 (Ref 57). As improved information on material properties, such as age–drying shrinkage and age–tensile strength, became available, the CRCP-2 computer program was revised to include information on material properties and was called CRCP-3. The methodology to determine the crack spacing was investigated, and the findings were incorporated into the CRCP-3 program. Thus CRCP-4 was developed. The inclusion of material variabilities and of the mechanistic distress prediction model resulted in the modification of CRCP-4.

DESCRIPTION OF CRCP-5

CRCP-5 is written in FORTRAN 77 and stored in the CDC mainframe computer. It can be transferred to an IBM mainframe or to personal computers without any difficulty. In the CDC mainframe at The University of Texas at Austin compilation time takes around 40 seconds with the FTN5 compiler when using optimization option 3. The optimization option in the FTN5 compiler is used to optimize the logic sequence in the computer program, and it minimizes the CPU time. Actual running time ranges from 30 to 45 seconds, depending on the number of cracks to be developed. A full listing of the program is contained in Appendix D.

Basically, CRCP-5 consists of two parts. One part analyzes the structural responses of the pavement system and predicts transverse crack spacing distributions. The other part estimates pavement life in terms of distress manifestations. In the first part, the Monte Carlo method is applied to include material variabilities in the mechanistic analysis. The fatigue behavior of concrete and the relationship between wheel load stress and crack spacings are utilized in the second part to develop a mechanistic distress prediction model.

Because of its design, the Monte Carlo method requires a considerable amount of computation time. During the development of the program, an effort was made to improve the efficiency of the program.

Working Systems of CRCP-5

In the first part of the program, concrete stresses along the analysis length are evaluated. These stresses are compared with concrete tensile strengths at each node to determine whether or not a crack will occur and, if so, where the crack will occur. A methodology to evaluate concrete stresses is described in Chapters 4 and 5. A flowchart diagram of CRCP-5 is shown in Figure 7.1. Each important task is conducted in a different subroutine so that any modification can be accomplished without too much effort. The main program controls the general flow of problem solving sequences. First, the main program reads and echo-prints input values so that a user can detect any possible input errors (Task 1). The input format is explained in the next section.

In the Monte Carlo analysis, statistical distributions of variables need to be known. Since concrete tensile strength is assumed to be normally distributed along the pavement, normal random numbers are generated using IMSL (International Mathematics Science Library). A pavement length of 250 feet is selected as an analysis length. This analysis length is divided into 3,000 nodes, and, therefore, each nodal element length is 1 inch. A total of 3,001 random numbers are generated and one number is assigned to each node. This task is conducted in Subroutine RANNOR.

Most of the concrete properties and environmental conditions vary with age. Accordingly, CRC

Flow Diagram

BEGIN

1 — READ and ECHOPRINT Input Data

2 — READ SEED and Generate Random Numbers

3 — Increment Time and Calculate Temperature Drop and Shrinkage and Tensile Strength

4 — Is Time Greater than Specified Number of Days? — Yes → **12** Is Number of Runs Greater than NPROB? — No (loops back to 2)

4 — No ↓

5 — Solve CRCP Model for Steel Stress at a Crack, Bond Development Length, BSDF with Zero Subbase Friction

6 — Compute Displacements and Corresponding Frictional Forces

7 — With Computed Frictional Forces, Solve CRCP Model for Steel Stress at a Crack, Bond Development Length, BSDF, Stresses, Displacements, Corresponding Frictional Forces

8 — Test Tolerance on Frictional Forces — No (loops back) / Yes ↓

9 — Compute D_i – Stress-Strength of Concrete at Node i, $i = 1.3001$

10 — Min(D_i) < 0? — No (loops back) / Yes ↓

11 — Cracking Occurs at i Change Model Geometry

12 — Is Number of Runs Greater than NPROB? — Yes ↓

13 — Compute Crack Spacing Distribution

14 — Analyze CRCP with Mean Crack Spacing for Stresses and Displacements

15 — PRINT Output

Figure 7.1 Flow diagram of computer program CRCP-5

pavement behavior changes with age. Therefore, the analysis must take this into account. In this study, a time incremental approach used in the previous models is adopted. The analysis begins from day one through the end of the analysis period. In this study,

the analysis period is defined as the length of time between the pouring of the concrete and the occurrence of the minimum temperature of the first winter. An analysis is made each day for the first 28 days. For a given time, time dependent concrete

properties and the temperature difference from a reference point, i.e., curing temperature, are computed (Task 3). Concrete tensile strengths are assigned to each node, using mean strength and normal random numbers. All of these tasks are accomplished within subroutine TDV.

CRC pavement age is incremented and compared to the specified analysis period (Task 4). If the CRC pavement age equals the analysis period, then it is determined whether the number of simulations is equal to the number of simulations specified (Task 12). If the number of simulations completed equals the number specified, then crack spacing distributions are computed (Task 13). Otherwise, the analysis is continued.

A methodology to solve the system of equations, developed in Chapter 4, is described in Chapter 5. For given conditions, steel stresses at cracks and bond development length are computed using a geometric model whose length is equal to the mean crack spacing, assuming zero subbase friction (Task 5). After steel stresses at cracks and bond development length are determined, stresses and displacements of concrete and steel at each node are computed. Subbase frictional stresses are evaluated with concrete displacements (Task 6). The slope of subbase frictional stresses along the pavement length is determined by regression analysis (Figure 4.12) (Task 8). Tasks 6 and 8 are conducted in Subroutine FRIC. The slope of subbase frictional stresses along the pavement length is compared with the previous slope. If the difference is within a closure limit, the next task (Task 9) is conducted. Otherwise, an average value of the two slopes is computed, and Task 7 is repeated until a closure limit on the slope of subbase frictional stresses along the pavement length is reached. Tasks 5 and 7 are performed in Subroutine STRESS.

Once steel stress at a crack and bond development length are determined, concrete stress at each node is computed from Eqs 4.10 and 4.14. The difference between concrete stress and strength at each node is determined (Task 9). The slope of subbase frictional stresses along the pavement length obtained in Task 6 is used in Eqs 4.10 and 4.14. It is determined whether or not the minimum value of the difference between concrete stress and strength is less than zero (Task 10). Tasks 9 and 10 are conducted in Subroutine CRACK. If the difference is less than zero, it is assumed that a crack develops where the minimum value occurs. In this case, new mean crack spacing is computed (Task 11), and steps from Task 5 on are repeated. Otherwise, time is increased, and steps from Task 3 on are repeated. Task 11 is accomplished in subroutine SPACING.

Since the Monte Carlo method simulates pavement behavior in the computer, and since the sequence of tensile strength values along the pavement is not known, it is necessary to perform the analysis as many times as possible. The variable NPROB is the number of simulations specified by a user. Whenever an analysis is completed at the end of the analysis period, the number of simulations performed is compared to NPROB. If the number of runs is less than NPROB, another analysis is begun with new concrete strength distributions. If the number of runs is equal to NPROB, crack spacing distributions are computed (Task 13). The tasks described so far are done in the first part of the program.

Working Systems of CRCP-5, Part 2

In the second part, a mechanistic analysis is performed to estimate the frequency of punchouts. For this analysis, a relationship between transverse crack spacings and wheel load stresses in transverse directions needs to be known. A methodology to predict the frequency of punchouts is discussed in the previous chapter.

Wheel load stresses in transverse directions are computed for each crack spacing range, using Eq 6.1 (Task 14). For given 18K ESALs, probabilities of failure for each crack spacing range are determined (Task 15). The number of punchouts per mile is calculated by adding the product of the probability of failure for each crack spacing range and the number of slab segments with that crack spacing range (Task 16). The number of 18K ESAL is increased and is compared with the maximum 18K ESAL that a user specifies. If it is greater than the maximum 18K ESAL, the program prints the output and the analysis stops. Otherwise, Tasks 16 through 18 are repeated. The second part of the program is performed in subroutine PUNCH.

INPUT GUIDE FOR CRCP-5

Detailed information on the input format is given in Appendix E. In this section, a brief description of the input variables is presented. Seven categories of input variables are needed for the computer program. They are (1) steel related variables, such as percent longitudinal steel, bar diameter, thermal coefficient, and modulus of elasticity; (2) concrete related variables, such as slab thickness, tensile strength and its variability, drying shrinkage, thermal coefficient, and modulus of elasticity; (3) environmental conditions, such as curing temperature, minimum temperature during the 28 days after the setting of the concrete, and minimum temperature in the first winter; (4) wheel load stress information, such as the magnitude of the wheel load, tire pressure, modulus of subgrade reaction, and wheel load radius; (5) subbase friction characteristics; (6) seed values for the generation of random numbers; and (7) fatigue characteristics of concrete.

DESCRIPTION OF CRCP-5 OUTPUT

With the given input values, CRCP-5 determines crack spacing distribution at any time and predicts the pavement life in terms of the frequency of punchouts. The output consists of four parts. In the first part, the echo prints of all input values are provided. Wheel load stress is also presented here.

Detailed information on CRC pavement behavior, including environmental changes for a given time period, appears in the second part. Temperature drop, drying shrinkage, mean crack spacing, mean crack width, and stresses in the concrete and steel are presented on each day up to a specified period. The coefficient of variation of crack spacings is also presented.

In the third part, information on CRC pavement behavior at the end of the analysis period is presented. It includes mean crack spacing, mean crack width, steel stress at a crack, and bond development length for slabs with mean crack spacing. Cumulative crack spacing distribution is also presented in both tabular and graphical form.

Half of the mean crack spacing at the end of the analysis period is divided by 100 nodes, and an analysis is made to get the information on frictional resistances, displacements, and stresses in the concrete and the steel at each nodal point. This information is presented in this part.

The results of the analysis made that estimated the frequency of punchouts, and, therefore, the pavement life, are presented in the fourth part. The numbers of punchouts for various 18-kip ESAL applications are presented. These results are also graphically presented in the fourth part. A sample output of CRCP-5 is contained in Appendix F.

CHAPTER 8. EXAMPLE PROBLEMS

In this chapter, the effects of major variables on structural responses and the frequency of distresses are examined. For this purpose, CRCP-5 is run with a wide range of input values. In this chapter, structural responses for various levels of input values are examined, with bond stress and displacement distributions, and results from the mechanistic distress prediction model are presented.

STRUCTURAL RESPONSES

In this part of the chapter, the predictions from the mechanistic analysis for structural responses are examined. Major input variables are selected and three levels of values—low, medium, and high—are selected for each major input variable. For the other variables, values which represent average design and environmental conditions are used. Input data used in this chapter are presented in Appendix G.

Steel Variables

In this section, the effect of steel variables on the CRCP-5 predictions is presented. Three structural responses, i.e., crack spacing, crack width, and steel stress at a crack, are important variables that will be considered in the design. These three variables are related to each other. In order to investigate the effect of each variable, a slab segment with 5-foot spacing is analyzed and detailed information on structural variables is discussed.

Percent Longitudinal Steel. Three levels—0.4, 0.6, and 0.7 percent—were selected. Figure 8.1 presents the results. Two types of coarse aggregates are considered. As the percent of longitudinal steel increases, mean crack spacing decreases. A larger quantity of steel provides a greater restraint on concrete volume changes and results in higher concrete stresses and smaller crack spacings. Concrete containing siliceous river gravel has smaller crack spacings. As discussed in Chapter 3, the thermal coefficient depends largely on the coarse aggregate used. Concrete with siliceous river gravel has a higher thermal coefficient than limestone aggregate. For the same temperature changes, concrete containing siliceous river gravel experiences larger volume changes and results in smaller crack spacing. The difference
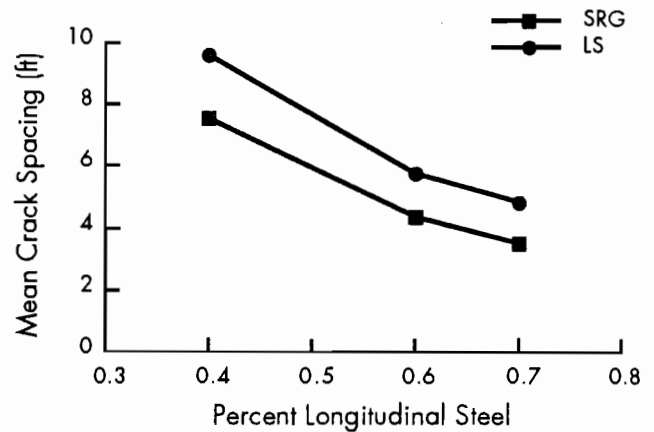
Figure 8.1. Mean crack spacing vs. percent longitudinal steel for pavements containing SRG and LS coarse aggregates

in mean crack spacings between two coarse aggregate types is due to thermal coefficients.

The variations in mean crack spacings for the first 28 days for various percents of longitudinal steel are presented in Figure 8.2. Before the pavement is open to traffic, all the cracks are induced by volume change mechanisms. In this study, the wheel load
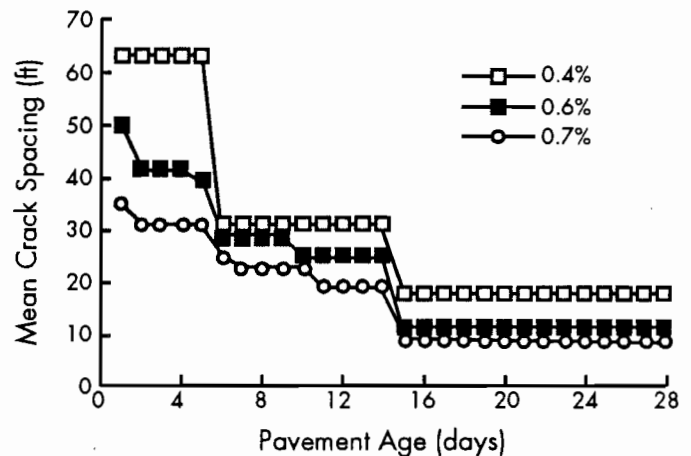
Figure 8.2. Changes in mean crack spacings with age for various longitudinal steel percentages

58

was applied on the 14th day. In Figure 8.2, there was an abrupt decrease in crack spacings when the wheel load was applied. In reality, cracks will develop gradually, because the application of wheel loads does not cause cracks to develop all the way through the pavement depth. Initially, cracks will be induced at the bottom first and spread up through the top because of the combination of volume change mechanisms and further wheel load applications. At the end of the analysis period, the mean crack spacings for 0.4, 0.6, and 0.7 percent sections were 7.6, 4.4, and 3.5 feet, respectively. The reduction in mean crack spacings between 28 days and the end of the analysis period is due to additional wheel load applications, larger temperature drops, and further drying shrinkage of the concrete.

In Figure 8.3, the effects of longitudinal steel on concrete volume change stresses are presented. For a 5-foot slab segment, a difference of as large as 100 psi is developed between sections with 0.4 and 0.6 percent steel. A new crack will develop if the stress is larger than the strength in order to relieve stresses. The differences between sections with various percent steel shown in Figure 8.2 are due to the differences in volume change stresses, as shown in Figure 8.3.

Figure 8.4. Effect of bar size on mean crack spacing for SRG and LS aggregate

area. The larger steel surface area increases stress transfer from the steel to the concrete, thereby restraining concrete volume changes more effectively. Using smaller bars leads to narrower crack spacings. The effect of bar size on concrete volume change stresses is shown in Figure 8.5. For the same 5-foot crack spacing, there is a 50 psi difference when #5 and #7 bars are used. Concrete stress changes are large in the bond development zone. Note that the bond development length increases with bar size. Since the steel surface area per unit volume of concrete is smaller for larger size bars, more bond development length is required to transfer the forces in the steel to the concrete by means of bond slip.

Figure 8.3. Volume change stress distributions of concrete as affected by percent longitudinal steel

Bar Size. The amount of steel is not the only factor affecting the degree of restraint on concrete volume changes. Restraint on concrete volume changes depends in part on bar size. Figure 8.4 shows the effect of bar size on mean crack spacings. There is no interaction between bar size and aggregate type. For the same percent longitudinal steel, using smaller bars provides a larger steel surface

Figure 8.5. Effect of bar size on concrete stress distributions

Concrete Variables

The significance of concrete properties on cracking was discussed in Chapter 3. Concrete represents

most of the volume of the PCC layer in CRC pavements. Concrete properties influence CRC pavement behavior. Concrete strength is controlled by changing the mix design or other variables. The effect of temperature variation on cracking was shown in Chapter 3 (Figure 3.18). It indicates the significance of the thermal coefficient of concrete. Since the thermal coefficient of concrete largely depends on the coarse aggregate type used and cannot be changed significantly by mix designs, different crack spacings result from different aggregate types used, provided other conditions are the same. Drying shrinkage affects cracking, especially during early ages. The effects of the modulus of elasticity on the development of cracks are not significant.

Tensile Strength. The effect of concrete strengths on the development of crack spacings is shown in Figure 8.6. Three levels of strengths were considered.
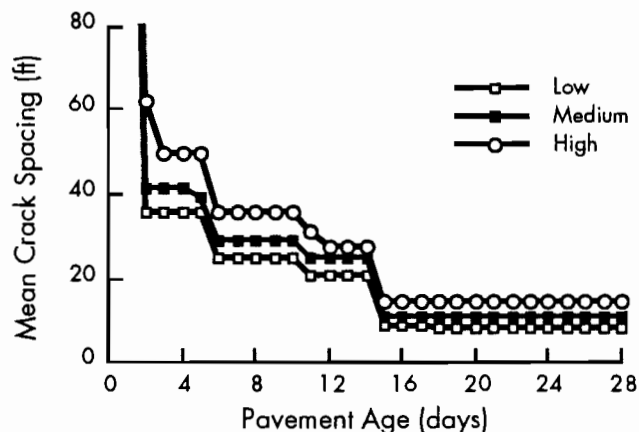
Figure 8.6. Variations in mean crack spacings with age as affected by concrete tensile strength

High values were 1.1 times the medium values. Low values were 0.9 times the medium values. Larger mean crack spacings result when high strength concrete is tested. At the end of the analysis period, mean crack spacings of 3.41, 4.39, and 5.21 feet were obtained for low, medium, and high strength concrete, respectively. There is a relationship between concrete tensile strength and water cement ratio. Drying shrinkage and tensile strength are not independent. However, in this study, all other variables are kept constant in order to investigate the effect of one factor at a time. If the relationship between tensile strength and drying shrinkage is considered, the difference in crack spacings is larger.

Thermal Coefficient. As discussed in Chapter 3, the thermal coefficient of concrete depends primarily on the coarse aggregate type used. Drying shrinkage is also affected by coarse aggregate type. In this

study, two coarse aggregate types, limestone (LS) and siliceous river gravel (SRG), are considered. Project 422 and other studies (Refs 24, 29, and 49) found that thermal coefficient values for LS and SRG are 4×10^{-6} and 6×10^{-6} inch/inch/°F, respectively. Figure 8.7 shows how mean crack spacings change with age for SRG and LS aggregate concretes. The

Figure 8.7. Changes in mean crack spacings with ages as affected by aggregate types

effect of the thermal coefficient is vividly shown. A low thermal coefficient of concrete containing LS aggregate results in larger crack spacings. Cumulative crack spacings for both aggregates are presented in Figure 8.8. Figure 8.9 presents concrete stress distributions for concretes with three thermal
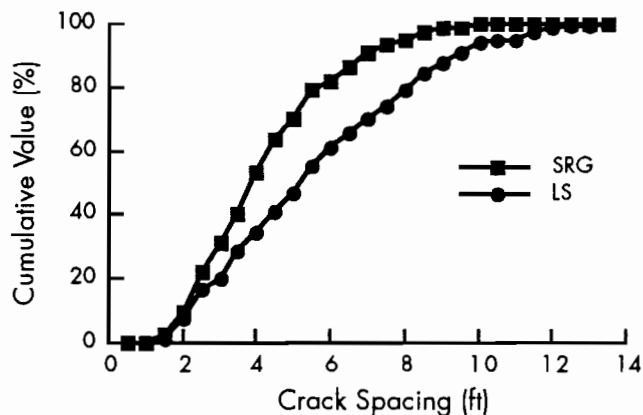
Figure 8.8. Cumulative crack spacing distributions for pavements containings SRG and LS coarse aggregates

coefficient values. For 5-foot crack spacing with 20 degrees of temperature drop and 0.6 percent longitudinal steel, there was a 50 psi difference between concretes with thermal coefficients of 4 and 8×10^{-6} inch/inch/°F. The difference is larger if the value of the temperature drop becomes larger.
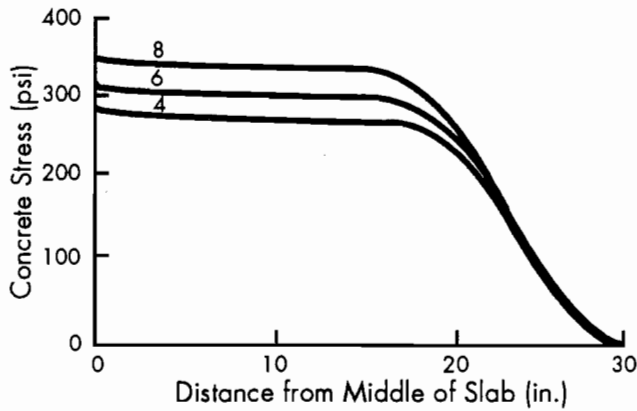
Figure 8.9. Volume change stress distributions of concrete as affected by thermal coefficient of concrete

Material Variability

Material variability, especially that of tensile strength, has a large influence on cracking development. The lower the variability, the more uniform the distributions. Figure 8.10 presents cumulative crack spacing distributions for three levels of variabilities. Under the same conditions, larger variability
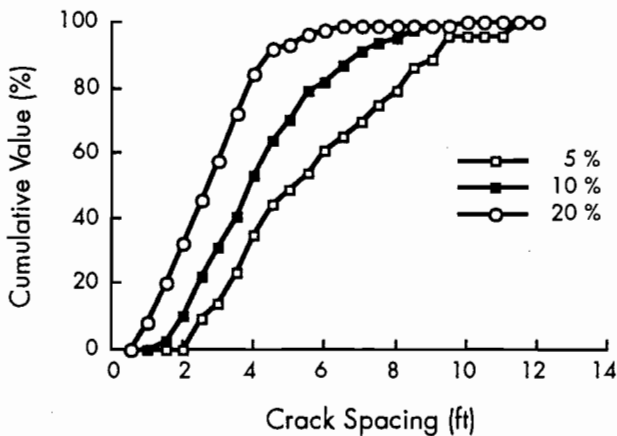
Figure 8.10. Cumulative crack spacing distributions for different variables in concrete tensile strength

leads to narrower crack spacings. Desirable crack spacing ranges are between 3.5 and 8 feet. When the tensile strength has a 20 percent coefficient of variation, only 20 percent of the slab segments are in a desirable range. On the other hand, more than 50 percent of the slab segments are within the desirable range, if a 5 percent coefficient of variation is maintained in concrete tensile strength.

Investigation of Bond Stress and Displacement Distributions

In order to examine the distributions of bond stresses and displacements from CRCP-5, a slab segment of 5 feet was selected and analyzed for three temperature drops—20, 40, and 60 degrees.

Bond Stress Distribution. Figure 8.11 illustrates the bond stress distributions. Maximum bond stresses remain almost the same for three temperature drops.
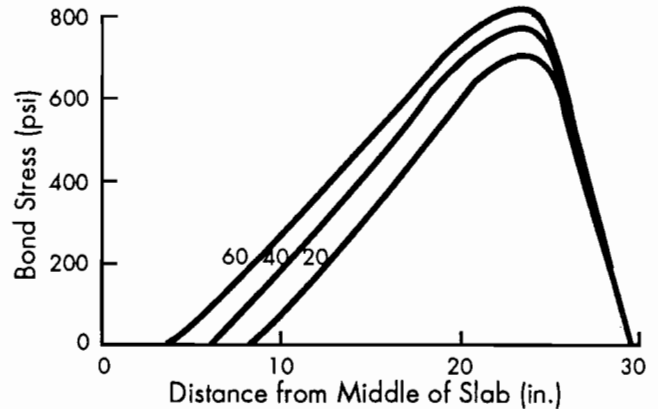
Figure 8.11. Bond stress distributions for various temperature drops

As temperature drops become larger, bond development length increases. There is little difference in bond stresses for three temperature drops between cracks and the locations of maximum bond stress. However, bond stress increases between the middle of the slab and the location of maximum bond stress during drops in temperature. This illustrates that as the temperature continues to fall, bond stresses progress toward the middle of the slab.

Distribution of Displacements. Figure 8.12 presents displacements of concrete and steel. In this example, the assumption was that the steel displacements were zero at cracks. Concrete displacements are practically linear, with distance from the middle of the slab. Steel displacements increase with distance from the middle of the slab, with the greatest steel displacements occurring between the middle of the slab and a crack.
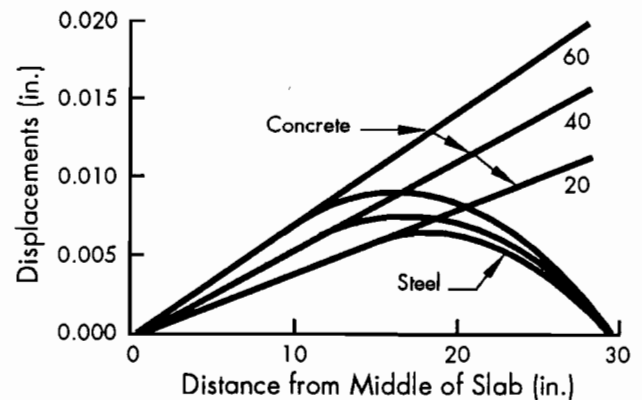
Figure 8.12. Distributions of concrete and steel displacements

DISTRESS PREDICTIONS

CRCP-5 is the first model of the CRCP series that attempts to evaluate the frequency of distresses using mechanistic analysis. For an accurate evaluation, values of several variables must be known. These values include fatigue behavior of CRC pavement, wheel load stresses affected by the conditions of cracks, and the modulus of rupture of concrete. As discussed in Chapter 6, fatigue behavior of rigid pavements is not well known yet. In order to get accurate predictions, more information is needed about fatigue behavior of rigid pavement and about the relationship between wheel load stress and the conditions of cracks.

In this section, the results from the second part of CRCP-5, which is a distress prediction model, are discussed. The background and methodology were described in Chapter 6. Punchouts are invariably associated with very small crack spacings. Therefore, crack spacing distributions as well as mean crack spacings affect the frequency of punchouts. Figure 8.13 presents the frequency of punchouts for various load applications. Two coarse aggregates are
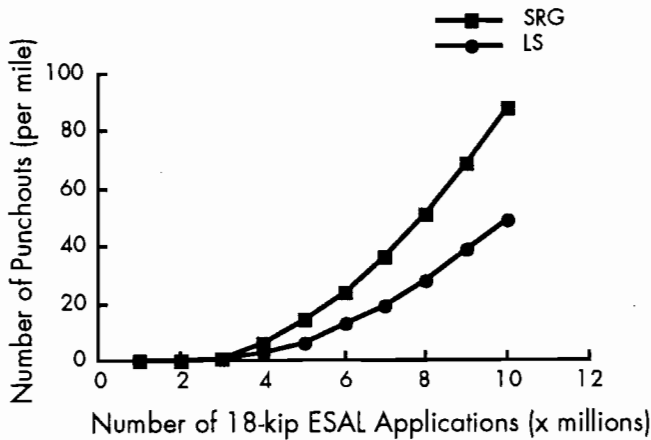
Figure 8.13. Relationship between frequency of distress and wheel load applications for concrete containing SRG and LS as coarse aggregates

considered. In Figure 8.8, 30 percent of the slab segments in the SRG section have spacings of less than · 3 feet. In the limestone section, 20 percent have crack spacings of 3 feet or less. This difference in crack spacing distributions has an effect on the development of punchouts. As expected, SRG concrete pavement experiences more punchouts than LS concrete pavement. Variability in concrete properties also has an effect on the frequency of punchouts. Crack spacing distributions resulting from different material variabilities are shown in Figure 8.10. The difference in crack spacing distributions resulted in large variations in the frequency of punchouts, as

shown in Figure 8.14. If 14 punchouts per mile are considered as a terminal condition of CRC pavements, there is a large difference in the life of pavements, depending on the variability in concrete strength.
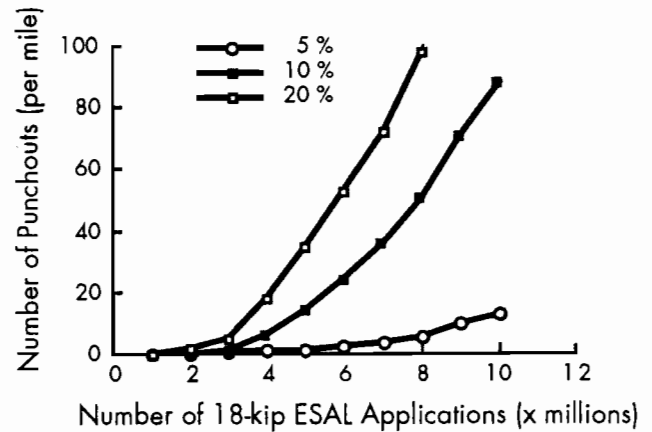
Figure 8.14. Frequency of distress vs wheel load applications affected by variables in concrete tensile strength

One way to get equal life for pavements sections with different coarse aggregates is to change steel design. For example, if #7 bar is used for a SRG sec-- tion instead of #6 bar, larger crack spacings will result and will lead to crack spacing distribution and pavement life similar to those of LS sections, as shown in Figure 8.15. However, the effect of a larger crack width which will result from a larger crack spacing and the thermal coefficient of SRG concrete on wheel load stresses must be identified. Once the relationship is identified, design strategies can be developed to provide equal pavement lives for pavement sections containing various coarse aggregates.
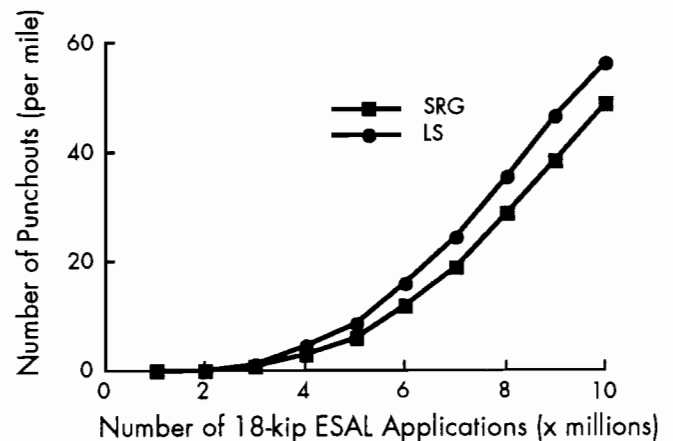
Figure 8.15. Change in the frequency of distress by modifying steel design

SUMMARY

Several example problems were presented in order to demonstrate the capabilities of CRCP-5. In spite of several simplifying assumptions made, the results from the first part of CRCP-5 seem to be reasonable. The verification of this part could be made using data from the rigid pavement data base at the Center for Transportation Research. It was shown that the second part of CRCP-5, to estimate the frequency of punchouts, could be used to develop design strategies in order to provide equal performances with pavements of different material properties and environmental conditions. However, further research is necessary to fully identify the fatigue behavior of CRC pavements and the relationship between wheel load stress and other variables.

CHAPTER 9. FUTURE VERIFICATION

The computer program developed in this study can predict crack spacing distributions and estimate pavement life. In order for this program to be useful, further study is needed to verify the program. In this chapter, several suggestions are made regarding future verification of the program.

CRACK SPACING DISTRIBUTION

The first part of computer program CRCP-5 analyzes CRC pavement systems and predicts crack spacing distributions. In this study, the variation of concrete tensile strength is considered as the most significant variable influencing crack spacing distributions. In the field study, concrete strength variation along the pavement length needs to be measured. In this process, it is important to separate the total variation from the variation due to testing, sampling, and error, so that pure variation can be determined. Once the variation and other input values are found, predictions are made from CRCP-5. Predicted mean crack spacing, crack spacing distribution, and standard deviation of crack spacings are to be compared to the actual values. A survey on a sufficient length of pavement is necessary in order to minimize unnecessary variations resulting from localized conditions, such as lapping or joints.

For a given temperature drop and drying shrinkage, concrete stress distributions are known from CRCP-5. It is recommended that the relationship between concrete tensile strengths and the location of cracking be investigated.

In addition to the crack spacings, it is necessary to evaluate the accuracy of crack width predictions. The relationship of crack widths to crack spacings can be determined. The information on these areas will show whether or not the assumption of linear elasticity in material properties is valid.

PUNCHOUT VS. TRAFFIC

The second part of CRCP-5 estimates pavement life using the crack spacing distributions obtained in the first part of the program. An accurate evaluation of fatigue characteristics of pavement concrete is essential. As mentioned in the previous chapter, a true fatigue equation for CRC pavement has not been developed. A fatigue equation is needed to estimate

pavement life. The Rigid Pavement Data Base developed in Project 472 at the Center for Transportation Research provides excellent information. A fatigue model can be developed using the data base. It is known that concrete fatigue life depends on strength stress ratio. The general form of the fatigue equation is

$$N = A\left(\frac{f}{\sigma}\right)^B \qquad (9.1)$$

where N is the fatigue life, A and B are constants to be determined, and the others are the same as before.

In a future study, constants A and B need to be determined. Once a fatigue equation is developed, the methodology developed in this study can be used to estimate pavement life for various design and environmental conditions.

DESIGN EXPERIMENT

In this section, general suggestions on the field study to verify the first part of CRCP-5 are made. The verification must be conducted for various design conditions. In order to get as much information as possible, a design experiment needs to be set up. Variables that will be studied are slab thickness; steel variables, such as percent longitudinal steel and bar size; various concrete properties; and environmental conditions.

For a given project, it is not feasible to change slab thicknesses. Therefore, field studies need to be conducted for different projects to investigate the effect of slab thicknesses. The effect of steel variables can be studied without a great effort. For a given project, percent longitudinal steel is changed by adding more bars or using fewer bars. The effect of bar size is investigated by using different bar sizes. The effect of concrete properties resulting from different coarse aggregate types can be evaluated by using various aggregate types. The study of the effect of environmental conditions is achieved by selecting test sections at different projects.

Figure 9.1 presents a set of test sections for a given project. The effect of slab thickness and environmental conditions cannot be studied. However,
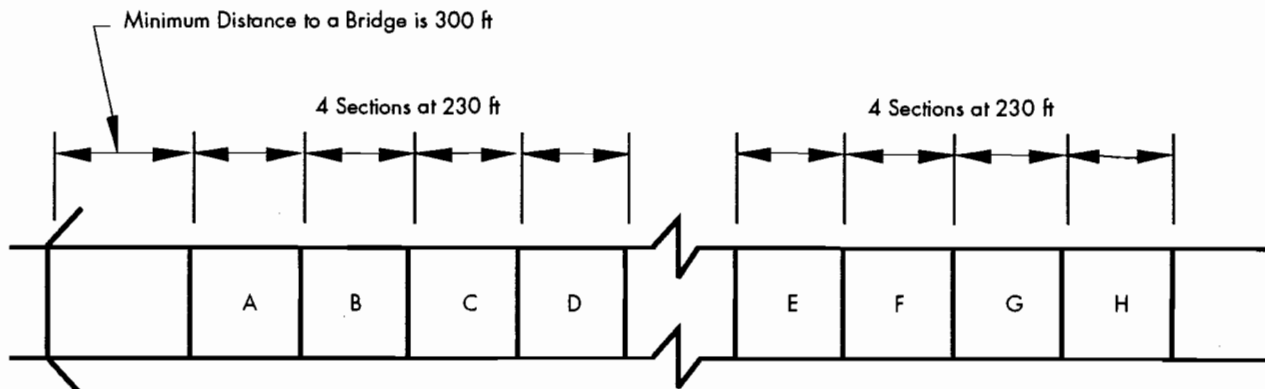
Figure 9.1. Suggested layout of test sections

the rest of the variables are investigated. For a given coarse aggregate type, at least four test sections are recommended. Various values of percent longitudinal steel, for example, high, medium, and low, can be used at each test section. In the fourth section, a different bar size with the same percent steel as one of the three sections is used so that the effect of bar size can be evaluated. Total test sections at a given

project will be four times the number of coarse aggregate types used. Two hundred feet is recommended for the length of each test section in order to minimize the interactions with adjacent sections. At least 30 feet may be necessary for transition. Therefore, a total of 920 feet is necessary with one coarse aggregate type for a given project.

CHAPTER 10. SUMMARY, CONCLUSIONS, AND RECOMMENDATIONS

This chapter presents a summary of the purposes and findings of the study, together with some of the conclusions which can be drawn from it. Concurrently, some of the major limitations are reviewed and recommendations for further study are proposed.

SUMMARY

The aim of this research has been to develop a methodology to include the stochastic nature of material properties in the analysis of CRC pavement systems and to estimate pavement life in terms of frequency of distresses. In the mechanistic anaysis of CRC pavement, it was found that bond stresses at the interface between the concrete and the steel were an important variable. The characteristics of bond stresses are very complex. It is impossible to develop bond stress distributions theoretically for various conditions. The bond stress characteristics are determined from actual tests. Numerous studies found that bond stress is a function of bond slip. However, the relationship between bond stress and bond slip is not unique but varies from location to location. As a result, a unique constitutive equation could not be found. From laboratory tests, it was found that bond stress distribution has a unique shape. Maximum bond stress occurred at almost the same location for various steel forces at cracks. The non-existence of a unique constitutive equation for bond and for a unique shape for bond stress distribution led to the assumption of a bond stress distribution function. Boundary conditions were used to determine the function. Once the function is determined, the system of equations is solved with ease.

After a review of presently available techniques for the mechanistic analysis of stochastic systems, a simulation approach was selected as a tool to include material variabilities in the analysis. The Monte Carlo method was adopted for simulation of CRC pavement behavior. Among the variables in the material properties, variability of concrete tensile strength was considered in the Monte Carlo simulation. The application of the Monte Carlo method to the mechanistic analysis resulted in the modification of the existing theoretical model. The newly developed model can estimate transverse crack spacing

distributions for various design and environmental conditions.

The second purpose of this research has been to develop a mechanistic distress prediction model. Currently, several models are available for distress predictions. These models were developed by analyzing field data with regression analysis. In this study, an effort was made to identify the relationship between distresses and variables having a bearing on them. One of the major distress types in CRC pavement is punchouts. The prerequisite of punchouts is the existence of very close transverse cracks. When crack spacings are very narrow, large wheel load stress develops in transverse directions. This large stress causes fatigue cracks to develop in longitudinal directions. It is possible to estimate the frequency of longitudinal fatigue cracking. In this study, a scheme to estimate the number of punchouts for various numbers of wheel loads was developed.

RESULTS AND CONCLUSIONS

The primary result is a model that simulates the observed pavement behavior. This model can be used to design CRC pavements or to meet various design and environmental conditions. The secondary conclusions are stated below.

(1) An accurate evaluation of bond stress is essential in analyzing early CRC pavement behavior. The bond stress model used in this study is believed to realistically represent bond behavior in CRC pavements.

(2) Steel stresses at cracks are practically constant regardless of crack spacings. It is believed that steel failures are caused by the shearing action of wheel loads. It is important to keep cracks tight to reduce chances of steel shearing failures.

(3) The thermal coefficient of concrete has a significant effect on structural responses of CRC pavements. Using different coarse aggregate types can lead to different crack spacing distributions and, therefore, variations in pavement life. Computer program CRCP-5 can be used to evaluate the effect of coarse aggregate types on pavement behavior.

66

(4) The Monte Carlo method was used to simulate pavement behavior. From a limited number of test problems, it was found that the method provides reasonable answers.

(5) The distress prediction model developed in this study can be used to estimate pavement life in terms of frequency of distresses. This model enables us to evaluate the effect of each variable on the pavement life. Therefore, this model can be used as a design program. An economic analysis of the CRC pavement system can be performed with this model.

LIMITATIONS OF THIS STUDY

In the development of the model, several assumptions had to be made to simplify computations. The accuracy of the results depends on the validity of the assumptions, which must be carefully examined. The assumptions which may limit the validity of the model in this study are discussed below.

(1) Steel stress at a crack is constant regardless of crack spacings. This assumption is valid only when concrete slab movements are symmetrical with respect to the middle of the slab segment. When the crack spacings are uniform, slab movements will be symmetrical with respect to the middle of the slab. It is not known whether the same holds for slabs with non-uniform crack spacing distributions.

(2) For slab segments with non-uniform crack spacing distributions, a steel boundary condition can be applied to a slab segment with mean crack spacing. This assumption had to be made because the location of zero steel displacements could not be determined. If the crack spacings are uniformly distributed, this assumption is correct. However, for non-uniform crack spacing distributions, the validity of this assumption needs to be investigated.

(3) Warping effects are neglected. When temperature differentials between the tops and bottoms of the slabs are large, concrete tries to warp. Since there is a restraint on the warping from concrete's own weight and longitudinal steel bars, warping stresses will develop. It is believed that neglecting the warping effect may seriously limit the validity of the analysis.

(4) The shape of the bond stress distribution function (BSDF) was assumed. Since there was no unique constitutive equation for bond stress and bond slip, BSDF was assumed and the system of equations was solved. Even though the shape of BSDF used in this study is very close to that found in the actual test, the relationship between variables affecting BSDF, such as bar diameter and modulus of elasticity of concrete, and BSDF needs to be identified and incorporated in BSDF.

(5) The fatigue equation developed at the AASHO Road Test is used for estimating longitudinal fatigue cracking. Strictly speaking, the fatigue equation developed at the AASHO Road Test is not a fatigue equation. The number of wheel load applications was measured until the PSI of the pavement section became 2.5. Since more than one crack develops when the PSI reaches 2.5, it is believed that such equations over-predict the fatigue life.

RECOMMENDATIONS FOR FURTHER RESEARCH

In Chapter 2, needed research in CRC pavement design was discussed. In this section, the research to improve and to refine CRCP-5 is discussed. It is imperative to make assumptions as realistically as possible. Therefore, this section is closely related to the above section.

(1) Slab movements need to be measured for slabs with non-uniform crack spacing distributions. The findings will verify or will reject assumption (1) in the previous section.

(2) True fatigue characteristics of CRC pavements need to be known. This can be achieved using existing field data from the rigid pavement data base at the Center for Transportation Research.

(3) Wheel load stresses which are affected by various loading positions in CRC pavements need to be identified.

(4) The relationship between structural continuity at the cracks and wheel load stresses must be found. Maximum allowable crack widths to keep structural continuity can be found for different aggregate types or for various slab thicknesses.

(5) The warping effect needs to be included in the model. It will require the knowledge of bond stress characteristics in two dimensions. As of now, no information is available on this subject.

REFERENCES

1. "Failure and Repair of Continuously Reinforced Concrete Pavement," Report No. 60, Highway Research Board, July 1979.

2. "The AASHTO Guide for the Design of Pavement Structures," American Association of State Highway and Transportation Officials, Washington D. C., 1986.

3. McCullough, B. Frank, A. A. Ayyash, W. R. Hudson, and J. P. Randall, "Design of Continuously Reinforced Concrete Pavements for Highways," NCHRP 1-15, Center for Highway Research, The University of Texas at Austin, August 1975.

4. Vetter, C. P., "Stresses in Reinforced Concrete Due to Volume Changes," *Transactions*, Vol 98, Proceedings of the American Society of Civil Engineers, 1933.

5. "AASHO Interim Guide for Design of Pavement Structures," American Association of State Highway Officials, Washington D. C., 1972.

6. McCullough, B. Frank, J. C. M. Ma, and C. S. Noble, "Limiting Criteria for the Design of CRCP," Research Report No. 177-17, Center for Highway Research, The University of Texas at Austin, August 1979.

7. McCulough, B. Frank, and W. B. Ledbetter, "LTS Design of Continuously Reinforced Concrete Pavement," *Journal of the Highway Division*, Vol 86, No. HW 4, Proceedings of the American Society of Civil Engineers, December 1960.

8. "Design and Construction – Continuously Reinforced Concrete Pavement," Continuously Reinforced Pavement Group, Chicago, Illinois 1968.

9. Crawford, R. A., and D. W. Anderson, "Continuously Reinforced Concrete Pavement Performance – Five Year Report," South Dakota Department of Highways, Physi. Res. Sec., 1968.

10. "Continuously Reinforced Concrete Pavement," National Cooperative Highway Research Program No. 16, Highway Research Board, 1973.

11. "Design Specification of CRCP (B)-85," Texas State Department of Highways and Public Transportations, 1985.

12. Lepper, Henry A., Jr, and J. B. Kim, "Tests of Reinforced Splices for Continuously Reinforced Concrete Pavements," Highway Research Record No. 50, Highway Research Board, 1964.

13. McCullough, B. Frank, "Evaluation of Terminal Anchorage Installations on Rigid Pavements," Highway Research Record No. 362, Highway Research Board, 1971.

14. McCullough, B. Frank, "Design Manual for Continuously Reinforced Concrete Pavement," United States Steel Corporation, Spring 1970.

15. "Joint-Related Distress in PCC Pavement – Cause, Prevention, and Rehabilitatin," National Cooperative Highway Research Program No. 56, Highway Research Board, 1979.

16. Lee, A., "Maryland's Two Continuously Reinforced Concrete Pavements – A Progress Report," Highway Research Record No. 5, Highway Research Board, 1963

17. Chou, Chia-Pei, B. Frank McCullough, W. R. Hudson, and C. S. Saraf, "Development of a Long-Term Monitoring System for Texas CRC Pavement Network," Research Report 472-2, Center for Transportation Research, The University of Texas at Austin, December 1988.

18. "Proposed Design Standard CRCP-(B) 87," Texas State Department of Highways and Public Transportations, 1987.

19. Teller, L. W., and E. J. Sutherland, "A Study of Structural Action of Several Types of Transverse and Longitudinal Joint Design," Public Roads Vol 17, No. 7, September, 1936.

20. Ricci, Eduardo A., A. H. Meyer, W. R. Hudson, and K. H. Stokoe, II, "The Falling Weight Deflectometer for Nondestructive Evaluation

of Rigid Pavements," Research Report 387-3F, Center for Transportation Research, The University of Texas at Austin, November 1985.

21. Haas, Ralph, and W. R. Hudson, *Pavement Management Systems*, Robert E. Krieger Publishing Company, 1986.

22. M. P. Nielsen, *Limit Analysis and Concrete Plasticity*, Prentice Hall, Inc., 1984.

23. Roy, D. M., and G. R. Gouda, "Porocity – Strength Relation in Cementitious Materials with Very High Strengths," Journal of American Ceramic Society No. 10, 1973.

24. Neville, A. M., *Properties of Concrete*, Third Edition, Pitman, 1981.

25. Jones, R., and M. F. Kaplan, "The Effect of Coarse Aggregate on the Mode of Fracture of Concrete in Compression and Flexure," Magazine of Concrete Research, Vol 9, No. 26, August 1957.

26. Erntroy, H. C., and B. W. Shacklock, "Design of High-Strength Concrete Mixes," Proceedings of a Symposium on Mix Design and Quality Control of Concrete, May 1954.

27. Browne, R. D., "Thermal Movement of Concrete," Current Practice Sheet, No. 3PC/06/01, Cement and Concrete Association, Waxham Springs, Concrete, November 1972.

28. Powers, T. C., and T. L. Brownard, "Studies of the Physical Properties of Hardened Portland Cement Paste," Proceedings of the ACI, Vol 43, Oct-Dec 1946, Jan-Apr 1947.

29. Orchard, D. F., *Concrete Technology,* Vol 1, Properties of Materials, 4th Edition, Applied Science Publishers Ltd, 1979.

30. Troxell, G. E., J. M. Raphael, and T. E. Davis, "Long-Term Creep and Shrinkage Tests of Plain and Reinforced Concrete Concrete," Proceedings, American Society of Testing Materials, 1958.

31. Carlson, R. W., "Drying Shrinkage of Concrete as Affected by Many Factors," a paper presented at the 41st Annual Meeting of the ASTM, June-July 1938.

32. Abou-Ayyash, Adnan, "Mechanistic Behavior of Continuously Reinforced Concrete Pavement," Ph.D. Dissertation, The University of Texas at Austin, May 1974.

33. McCullough, B. Frank, M. C. Won, and K. Hankins, "Long-Term Performance Study of Rigid Pavements," 4th International Conference for Design and Rehabilitation of Rigid

Pavements, Purdue University, West Lafayette, Indiana, April 1989.

34. Wesevich, J. W., B. Frank McCullough, and N. H. Burns, "Stabilized Subbase Friction Study for Concrete Pavements," Research Report 459-1, Center for Transportation Research, The University of Texas at Austin, April, 1987.

35. Westergaard, H. M, "Computation of Stresses in Concrete Roads," Proceedings, Highway Research Board, Fifth Annual Meeting, December 1925.

36. Gutierrez de Velasco, Manuel, and B. Frank McCullough, "Summary Report for 1978 CRCP Condition Survey in Texas," Research Report 177-20, Center for Transportation Research, The University of Texas at Austin, January 1981.

37. Eligehausen, Rolf, E. P. Popov, V. B. Vitelmo, "Local Bond Stress-Slip Relationships of Deformed Bars Under Generalized Excitations," Report No. UCB/EERC-83/23, Earthquake Engineering Research Center, University of California, Berkeley, October 1983.

38. Wimsatt, Andrew W., B. Frank McCullough, and N. H. Burns, "Methods of Analyzing and Factors Influencing Frictional Effects of Subbases," Research Report 459-2F, Center for Transportation Research, The University of Texas at Austin, November 1987.

39. Lutz, Leroy A., and P. Gergely, "Mechanics of Bond and Slip of Deformed Bars in Concrete," ACI No. V, 1967, 64-52.

40. Watstein, David, and N. A. Seese, "Effect of Type of Bar on Width of Cracks in Reinforced Concrete Subjected to Tension," Proceedings, ACI Journal, Vol 16 No.4, February 1945.

41. Watstein, David, and R. G. Mathey, "Width of Cracks in Concrete at the Surface of Reinforcing Evaluated by Means of Tensile Bond Specimens," Proceedings, ACI Journal, Vol 56, July 1957.

42. Clark, Arthur P. , "Bond of Concrete Reinforcing Bars," Proceedings, ACI Journal, Title No. 46-11, November 1949.

43. Nilson, Arthur H., "Internal Measurement of Bond Slip," Proceedings, ACI Journal, Title No. 69-41, July 1972.

44. Mains, R. M., "Measurement of the Distribution of Tensile and Bond Stresses Along Reinforcing Bars," Proceedings, ACI Journal, Title No. 48-17, November 1951.

45. Tassios, T. P., and P. J. Yamopoulos, "Analytical Studies on Reinforced Concrete Members Under Cyclic Loading Based on Bond Stress-Slip Relationships," Proceedings, ACI Journal Vol 78 No. 3, May-June 1981.

46. Mylrea, T. D., "Bond and Anchorage," Proceedings, ACI Journal, Vol. 44, March 1948.

47. Perry, Ervin S., and J. N. Thompson, "Bond Stress Distribution on Reinforcing Steel in Beams and Pullout Specimens," Proceedings, ACI Journal, Title No. 63-44, August 1966.

48. Chapman, Ralph A., and S. P. Shah, "Early-Age Bond Strength in Reinforced Concrete," ACI Material Journal, Title No. 84-M44, November-December 1987.

49. "Concrete Manual," Seventh Edition, United States Department of the Interior, Bureau of Reclamation, Denver, Colorado, 1966.

50. Shelby, M. D., and B. Frank McCullough, "Experience in Texas with Continuously Reinforced Concrete Pavement," Bulletin 274, Highway Research Board, January 1960.

51. Somayaji, S., and S. P. Shah, "Bond Stress Versus Slip Relationship and Cracking Response of Tension Members," Proceedings, ACI Journal, Title No. 78-20. May-June 1981.

52. Jiang, D. H., S. P. Shah, and A. T. Andonian, "Study of the Transfer of Tensile Forces by Bond," Proceedings, ACI Journal, Title No. 81-24, May-June 1984.

53. Shunsheng Yang, and Jiakui Chen, "Bond Slip and Crack Width Calculations of Tension Members," Title No. 85-S39, ACI Structural Journal, July-August 1988.

54. Hart, Gary C., *Uncertainty Analysis, Loads, and Safety in Structural Engineering*, Prentice-Hall, 1982.

55. Marshall, Bryant P., and T. W. Kennedy, "Tensile and Elastic Characteristics of Pavement Materials," Research Report 183-1, Center for Highway Research, The University of Texas at Austin, June 1977.

56. Nam, Young K., and M. Won, "Gulf Freeway Project," Technical Memorandum 422-5, Center for Transportation Research, The University of Texas at Austin, March 1987.

57. Ma, James, and B. Frank McCullough, "CRCP-2, An Improved Program for the Analysis of Continuously Reinforced Concrete Pavements," Research Report No. 177-9, Center for Highway Research, The University of Texas at Austin, August 1979.

58. "The AASHO Road Test," Report 5, Pavement Research, Highway Research Board, Special Report 61E, 1962.

59. Chou, Chia-Pei, and B. Frank McCullough, "Development of a Distress Index and Rehabilitation Criteria for Continuously Reinforced Concrete Pavements Using Discriminant Analysis," Transportation Research Record 1117, Transportation Research Board, 1987.

60. Yoder, E. J., and M. W. Witczak, *Principles of Pavement Design*, Second Edition, John Wiley & Sons, Inc., 1975.

61. Assimacopoulos, B. M., R. F. Warner, and C. E. Ekberg, "High Speed Fatigue Tests on Small Specimens of Plain Concrete," Journal of Prestressed Concrete Institute, Vol 4, August 1961.

62. Clemmer, H. E., "Fatigue of Concrete," Proceedings, American Society of Testing Materials, Vol 22, Part II, 1922.

63. Murdock, J. W., and C. E. Kesler, "Effect of Range of Stress on Fatigue Strength of Plain Concrete Beams," ACI Journal, Proceedings Vol 55, No. 2, August 1959.

64. Hudson, W. R., and F. H. Scrivner, "AASHO Road Test Principal Relationships—Performance with Stress, Rigid Pavements," The AASHO Road Test, Proceedings of a Conference Held May 16-18, 1962 St. Louis, Mo. Highway Research Board, Special Report 73.

65. Hildorf, Hubert K., and C. E. Kesler, "Fatigue Strength of Concrete Under Varying Flexural Stresses," Proceedings, ACI Journal, Vol 63, October 1966.

66. Vesic, Aleksandar S., and S. K. Saxena, "Analysis of Structural Behavior of AASHO Road Test Rigid Pavements," National Cooperative Highway Research Program, No. 97, Highway Research Board, 1970.

67. McCall, John T., "Probability of Fatigue Failure of Plain Concrete," Proceedings, ACI Journal, Vol 55, August 1958.

68. Hankins, K., and M. Won, "Condition Survey on U.S. 290," Technical Memorandom 422-25, Center for Transportation Research, The University of Texas at Austin, March, 1988.

APPENDIX A. SOLUTION OF EQUATION 4.39

$$w''(x) - \alpha K w(x) = \alpha(Cx^2 + D) + \alpha E \cos\left(\frac{\pi x}{2b}\right) + \frac{F_i}{DE_c} \tag{A.1}$$

$$F_i = \Theta(x + a), \text{ and } \beta = \frac{\Theta}{DE_c} \quad \text{(see Fig 4.12)}$$

Then, Eq A.1 becomes:

$$w''(x) - \alpha K w(x) = \alpha(Cx^2 + D) + \alpha E \cos\left(\frac{\pi x}{2b}\right) + \beta(x + a) \tag{A.2}$$

This is a second-order non-homogeneous differential equation. Using the method of variation of parameters,

$$u' = \frac{w_2 r}{W} \qquad v' = \frac{w_1 r}{W}$$

$$W_p(x) = -w_1 \int \frac{w_2 r}{W} dx + w_2 \int \frac{w_1 r}{W} dx$$

where

$$W = \text{Wronskian of } w_1 \text{ and } w_2,$$
$$= w_1 w_2' - w_1' w_2,$$
$$r = \alpha(Cx^2 + D) + \alpha E \cos\left(\frac{\pi x}{2b}\right) + \beta(x + a)$$

where w_1, w_2 = solutions of the homogenous equation (A.2); w_1 and w_2 become:

$$w_1 = \exp(x\sqrt{aK}) \qquad w_2 = e(-x\sqrt{aK})$$

$$\therefore W = -2\sqrt{\alpha K}$$

$$-uw_1 = -\frac{C}{2K}\left(x^2 + \frac{2x}{\sqrt{\alpha K}} + \frac{2}{\alpha K}\right) - \frac{D}{2K} + \frac{\alpha E}{2\sqrt{\alpha K}} \frac{\frac{\pi^2}{4b^2}}{\alpha K + \frac{\pi^2}{4b^2}}\left(\frac{2b}{\pi}\sin\frac{\pi x}{2b} - \frac{4b^2\sqrt{\alpha K}}{\pi^2}\cos\frac{\pi x}{2b}\right) \tag{A.3}$$

$$-\frac{\beta x}{2\alpha K} - \frac{\beta}{2\alpha K\sqrt{\alpha K}} - \frac{\beta a}{2\alpha K}$$

$$vw_2 = -\frac{c}{2K}\left(x^2 - \frac{2x}{\sqrt{\alpha K}} + \frac{2}{\alpha K}\right) - \frac{D}{2K} - \frac{\alpha E}{2\sqrt{\alpha K}} \frac{\frac{\pi^2}{4b^2}}{\alpha K + \frac{\pi^2}{4b^2}}\left(\frac{2b}{\pi}\sin\frac{\pi x}{2b} + \frac{4b^2\sqrt{\alpha K}}{\pi^2}\cos\frac{\pi x}{2b}\right) \tag{A.4}$$

$$-\frac{\beta x}{2\alpha K} + \frac{\beta}{2\alpha K\sqrt{\alpha K}} - \frac{\beta\alpha}{2\alpha K}$$

$$\int W_{P(x)}\,dx = -\frac{C}{K}x^2 - \frac{2C}{\alpha K^2} - \frac{D}{K} - \frac{\alpha E}{\alpha K + \frac{\pi^2}{4b^2}}\cos\frac{\pi x}{2b} - \frac{\beta x}{\alpha K} - \frac{\beta\alpha}{\alpha K} \tag{A.5}$$

Therefore, the general solution is

$$W(x) = A\exp(x\sqrt{\alpha K}) + B\exp(-x\sqrt{\alpha K}) - \frac{C}{K}x^2 - \frac{2C}{\alpha K^2} - \frac{D}{K} - \frac{\alpha E}{\alpha K + \frac{\pi^2}{4b^2}}\cos\frac{\pi x}{2b} - \frac{\beta(x+a)}{\alpha K} \tag{A.6}$$

Check:

$$w''(x) = A\alpha K\exp(x\sqrt{\alpha K}) + B\alpha K\exp(-x\sqrt{\alpha K}) - \frac{2C}{K} + \left(\frac{\pi}{2b}\right)^2\frac{\alpha E}{\alpha K + \frac{\pi^2}{4b^2}}\cos\frac{\pi x}{2b}$$

$$w''(x) - \alpha Kw(x) = \alpha Cx^2 + \alpha D + \frac{\alpha E}{\alpha K + \frac{\pi^2}{4b^2}}\left\{\left(\frac{\pi}{2b}\right)^2 + \alpha K\right\}\cos\frac{\pi x}{2b} + \beta(x+a)$$

$\therefore$ O.K.

$$\text{Let } c = b\sqrt{\alpha K}$$

Then

$$W(x) = A\exp\left(\frac{cx}{b}\right) + B\exp\left(-\frac{cx}{b}\right) - \frac{1}{K}\left[Cx^2 + \frac{2C}{\alpha K} + D\right] - \frac{\alpha E}{\alpha K + \frac{\pi^2}{4b^2}}\cos\left(\frac{\pi x}{2b}\right) - \frac{\beta(x+a)}{\alpha K} \tag{A.7} = (4.40)$$

APPENDIX B. DERIVATION OF COEFFICIENTS OF EQUATION 4.39

In Appendix A;

$$W(x) = A \exp\left(\frac{cx}{b}\right) + B \exp\left(-\frac{cx}{b}\right) - \frac{1}{K}\left[Cx^2 + \frac{2C}{\alpha K} + D\right] - \frac{\alpha E}{\alpha K + \frac{\pi^2}{4b^2}} \cos\left(\frac{\pi x}{2b}\right) - \frac{\beta(x+a)}{\alpha K}$$

(B.1)

Constants A, B, C, D, and E are found from boundary conditions. These boundary conditions are given below.

Since $u_{cx} = u_{sx}$ in the fully bonded zone, the boundary conditions at the end of the fully bonded zone $(x = 0)$ are

(1) $w(x) = 0$ (no slip),

(2) $w'(x) = 0$ (compatibility),

(3) $w''(x) = 0$ (no bond stress),

At a crack $(x = b)$

(4) $w'(x) = \frac{\sigma_{sc}}{E_s} + \left\{(\alpha_c - \alpha_s)\Delta T + \varepsilon_{sh}\right\}$ (no concrete stress), and

(5) $w''(x) = \frac{F_i}{E_c D}$ (no bond stress).

$$w(x=0) = 0 \Leftrightarrow A + B - \frac{2C}{\alpha K^2} - \frac{D}{K} - \frac{\alpha E}{\alpha K + \left(\frac{\pi}{2b}\right)^2} - \frac{\beta a}{\alpha K} = 0$$

(B.2)

$$w'(x=0) = 0 \Leftrightarrow \frac{c}{b}A - \frac{c}{b}B - \frac{\beta}{\alpha K} = 0$$

(B.3)

$$w''(x=0) = 0 \Leftrightarrow \frac{c_2}{b^2}A + \frac{c^2}{b^2}B - \frac{2c}{K} + \left(\frac{\pi}{2b}\right)^2 \frac{\alpha E}{\alpha K + \left(\frac{\pi}{2b}\right)^2} = 0$$

(B.4)

$$w'(x=b) = \frac{\sigma_{sc}}{E_s} + \left\{(\alpha_c - \alpha_s)\Delta T + \varepsilon_{sh}\right\} \Leftrightarrow \frac{c}{b}Ae^c - \frac{c}{b}Be^{-c} - \frac{2Cb}{K} + \frac{\pi}{2b}\frac{\alpha E}{\alpha K + \left(\frac{\pi}{2b}\right)^2} - \frac{\beta}{\alpha K}$$

(B.5)

$$= \frac{\sigma_{sc}}{E_s} + \left\{(\alpha_c - \alpha_s)\Delta T + \varepsilon_{sh}\right\}$$

$$w''(x=b) = \frac{c^2}{b^2}Ae^c + \frac{c^2}{b^2}Be^{-c} - \frac{2C}{K} = \frac{F_i b}{E_c D} = \beta(b+a)$$

(B.6)

73

From (B.3)

$$B = A - \frac{\beta b}{\alpha K c} \tag{B.7}$$

From (B.6)

$$C = \frac{K}{2}\left\{\frac{c^2}{b^2}Ae^c + \frac{c^2}{b^2}\left(A - \frac{\beta b}{\alpha K c}\right)e^{-c}\right\} - \frac{\beta(b+a)K}{2}$$

$$= \frac{Kc^2}{2b^2}\left\{2A\cosh(c) - \frac{\beta b}{\alpha K c}e^{-c} - \frac{b^2}{c^2}\beta(b+a)\right\} \tag{B.8}$$

From (B.4)

$$E = \left(-\frac{c^2}{b^2}A - \frac{c^2}{b^2}B + \frac{2C}{K}\right)\frac{\alpha K + \left(\frac{\pi}{2b}\right)^2}{\alpha}\left(\frac{2b}{\pi}\right)^2$$

$$= \left[-2A\frac{c^2}{b^2} + \frac{c^2}{b^2}\frac{\beta b}{\alpha K c} + \frac{c^2}{b^2}\left\{2A\cosh(c) - \frac{\beta b}{\alpha K c}e^{-c} - \frac{b^2}{c^2}\beta(b+a)\right\}\right]\frac{\alpha K + \left(\frac{\pi}{2b}\right)^2}{\alpha}\left(\frac{2b}{\pi}\right)^2 \tag{B.9}$$

From (B.2)

$$D = (A+B)K - \frac{2C}{\alpha K} - \frac{\alpha K}{\alpha K + \left(\frac{\pi}{2b}\right)^2}\left[-2A\frac{c^2}{b^2} + \frac{\beta c}{\alpha b K} + \frac{c2}{b^2}\left\{2A\cosh(c) - \frac{\beta b}{\alpha K c}e^{-c} - \frac{b^2}{c^2}\beta(b+a)\right\}\right]\bullet$$

$$\frac{\alpha K + \left(\frac{\pi}{2b}\right)^2}{\alpha}\left(\frac{2b}{\pi}\right)^2 - \frac{\beta a}{\alpha}$$

$$\therefore D = 2AK - \frac{\beta b}{\alpha c} - K\left(\frac{2b}{\pi}\right)^2\left\{-2A\frac{c^2}{b^2} + \frac{\beta c}{\alpha b K} + \frac{c^2}{b^2}\left(2A\cosh(c) - \frac{\beta b}{\alpha K c}e^{-c} - \frac{b^2}{c^2}\beta(b+a)\right)\right\}$$

$$- \frac{2}{\alpha K}\frac{Kc^2}{2b^2}\left\{2A\cosh(c) - \frac{\beta b}{\alpha K c}e^{-c} - \frac{b^2}{c^2}\beta(b+a)\right\} - \frac{\beta a}{\alpha} \tag{B.10}$$

From (B.5)

$$\frac{c}{b}Ae^c - \frac{c}{b}\left(A - \frac{\beta b}{\alpha K c}\right)e^{-c} - \frac{2b}{K}\frac{Kc^2}{2b^2}\left\{2A\cosh(c) - \frac{\beta b}{\alpha K c}e^{-c} - \frac{b^2}{c^2}\beta(b+a)\right\}$$

$$+ \frac{\pi}{2b}\left(\frac{\alpha}{\alpha K + \left(\frac{\pi}{2b}\right)^2}\right)\left(\frac{aK + \left(\frac{\pi}{2b}\right)^2}{\alpha}\right)\left(\frac{2b}{\pi}\right)^2\left[-2A\frac{c2}{b^2} + \frac{\beta c}{\alpha b K} + \frac{c^2}{b^2}\left(2A\cosh(c) - \frac{\beta b}{\alpha K c}e^{-c} - \frac{b^2}{c^2}\beta(b+a)\right)\right] - \frac{\beta}{\alpha K} =$$

$$\frac{c}{b}2A\sinh(c)+\frac{\beta}{\alpha K}e^{-c}-\frac{c^2}{b}2A\cosh(c)+\frac{\beta c}{\alpha K}e^{-c}+\beta b(b+a)-2A\left(\frac{2c^2}{\pi b}\right)+\frac{2\beta c}{\alpha K\pi}$$

$$+\frac{2c^2}{\pi b}\left[2A\cosh(c)-\frac{\beta b}{\alpha Kc}e^{-c}-\frac{b^2}{c^2}\beta(b+a)\right]-\frac{\beta}{\alpha K}$$

$$=\frac{\sigma_{sc}}{E_s}+\left\{(\alpha_c-\alpha_s)\Delta T+\varepsilon_{sh}\right\}$$

$$\Leftrightarrow 2A\left\{\frac{c}{b}\sinh(c)-\frac{c^2}{b}\cosh(c)-\frac{2c^2}{\pi b}+\frac{2c^2}{\pi b}\cosh(c)\right\}$$

$$=\frac{\sigma_{sc}}{E_s}+\left\{(\alpha_c-\alpha_s)\Delta T+\varepsilon_{sh}\right\}-\frac{\beta}{\alpha K}e^{-c}-\frac{\beta c}{\alpha K}e^{-c}$$

$$-\beta b(b+a)-\frac{2bc}{\alpha K\pi}+\frac{2c^2 b\beta}{\pi b\alpha Kc}e^{-c}+\frac{2c^2}{\pi b}\left(\frac{b^2}{c^2}\right)\beta(b+a)+\frac{\beta}{\alpha K}$$

$$\therefore 2A=\frac{\dfrac{b}{c}\left[\dfrac{\sigma_{sc}}{E_s}+\left\{(\alpha_c-\alpha_s)\Delta T+\varepsilon_{sh}\right\}-\left(\dfrac{\beta}{\alpha K}+\dfrac{\beta c}{\alpha K}-\dfrac{2\beta c}{\pi\alpha K}\right)e^{-c}-\beta\left(bL+\dfrac{2c}{\pi\alpha K}-\dfrac{2bL}{\pi}-\dfrac{1}{\alpha K}\right)\right]}{\left(\sinh(c)-c\cosh(c)-\dfrac{2c}{\pi}+\dfrac{2c}{\pi}\cosh(c)\right)}$$

APPENDIX C. WHEEL LOAD STRESSES VS TRANSVERSE CRACK SPACINGS

Slab Thickness (in.)						
Stress Direction	8		12		15	
Crack Spacing (ft)	$\sigma_{x\text{-}x}$	$\sigma_{y\text{-}y}$	$\sigma_{x\text{-}x}$	$\sigma_{y\text{-}y}$	$\sigma_{x\text{-}x}$	$\sigma_{y\text{-}y}$
1.0	0.0	502.4	0.0	243.5	0.0	243.5
2.0	103.2	273.1	46.2	132.9	29.8	88.4
4.0	157.6	194.2	70.5	92.0	45.4	60.5
6.0	191.7	182.8	87.2	84.9	56.3	55.4
8.0	212.8	180.8	100.9	83.5	65.8	54.3
12.0	218.8	179.2	116.3	83.6	79.8	54.4

Figure C.1. Wheel load stresses in transverse and longitudinal directions.

APPENDIX D. LISTING OF CRCP-5

```
      PROGRAM CRCP5 (INPUT,OUTPUT,TTY,TAPE5=INPUT,TAPE6=OUTPUT,
      1TAPE9=TTY)
C     ------- -----
C
C
C
C
C
C                            C R C P - 5
C                            - - - -   -
C
C            CONTINUOUSLY REINFORCED CONCRETE PAVEMENT
C
C            VERSION 5.2 (LAST REVISION: JANUARY 1990)
C
C      REVISED ON NOVEMBER 1988 BY MOONCHEOL WON UNDER PROJECT 422
C      -------------   -------------      -----------
C
C           CRCP-5 IS A REVISION OF CRCP-4.  THE BOND STRESS DISTRIBUTION USED
C      IN CRCP-4 WAS MODIFIED SO THAT MORE REALISTIC BOND STRESS MODEL IS USED.
C      THE EFFECT OF MATERIAL VARIABILITIES IS INCLUDED.  A MONTE CARLO METHOD
C      IS USED.  MECHANISTIC DISTRESS PREDICTION MODEL IS DEVELOPED AND
C      INCORPORATED INTO CRCP-5.  FOR MORE INFORMATION ON CRCP-5, REFER TO
C      CTR REPORT 422-4 MECHANISTIC ANALYSIS OF CONTINUOUSLY REINFORCED
C      CONCRETE PAVEMENT CONSIDERING MATERIAL CHARACTERISTICS, VARIABILITY, AND
C      FATIGUE BY MOONCHEOL WON AND B.F. MCCULLOUGH.
C
C
C
C      A NOTE ON CRCP-1, CRCP-2, CRCP-3, AND CRCP-4:
C      - ---- -- ---- -  ---- -  ---- -  --- ---- -
C
C      CRCP-1 - VERSION 1.0, DECEMBER 1973, ADNAN ABOU-AYYASH.
C               COMPUTER SOLUTION FOR THE ANALYSIS OF CONTINUOUSLY
C               REINFORCED CONCRETE PAVEMENT (CRCP) CONSIDERING THE EFFECT
C               OF TEMPERATURE VARIATION AND DRYING SHRINKAGE.  WRITTEN BY
C               ADNAN ABOU-AYYASH UNDER RESEARCH PROJECT 1-15 (REP
C               1-15).
C
C      CRCP-2 - VERSION 2.1, MARCH 1977, JAMES MA.
C               AN EXTENSION AND REVISION OF THE CRCP-1 COMPUTER PROGRAM.
C               THE INCLUSION OF EXTERNAL LOAD AND THE MODIFICATIONS OF THE
C               MATHEMATICAL MODELS AS WELL AS THE COMPUTER PROGRAM CRCP-1
C               RESULTED IN A REVISED PROGRAM DESIGNATED CRCP-2.  WRITTEN BY
C               JAMES MA UNDER RESEARCH PROJECT 177-9 (REPORT CFHR 177-9).
C
C      CRCP-3 - VERSION 3.0, MARCH 1985, UNKNOWN REVISOR.
C               IT USES A MORE RECENT FORMULA FROM THE U.S. BUREAU OF
C               RECLAMATION FOR THE AGE-TENSILE RELATIONSHIP.  ALSO MINOR
C               ERRORS IN CRCP-2 SUCH AS BAD FORMAT STATEMENTS WERE
C               CORRECTED AND SOME MODIFICATIONS WERE INCLUDED SO THAT
C               NECESSARY INPUT DATA IS ECHOED.  THESE LAST CHANGES WERE
C               DONE BY JEANNETTE M. GARCIA, CTR PROGRAMMER.
C
C
C      CRCP-4 - VERSION 4.0, DECEMBER 1985, MOONCHEOL WON.
```

```
C            ALGORITHM TO DETERMINE CRACK SPACINGS FOR VARIOUS AGES WERE
C            INVESTIGATED AND THE FINDINGS WERE INCORPORATED INTO CRCP-3.
C
C     ************************************************************************
C
C
C
C     PROGRAM OPERATION
C     ------- ---------
C
C         THIS PROGRAM WAS CREATED AND USED ON THE CDC DUAL CYBER 170/750
C
C     THIS PROGRAM CALLS INTERNATIONAL MATHEMATICS AND SCIENCE LIBRARY,
C     THEREFORE, IMSL SHOULD BE LOADED WHEN EXECUTED.
C
C     THE FOLLOWING SEQUENCE OF COMMANDS IS NECESSARY IN ORDER TO
C     COMPILE THE FORTRAN PROGRAM, LOAD IMSL, AND GENERATE AN ABSOLUTE
C     BINARY FILE ON THE UNIVERSITY OF TEXAS' COMPUTER SYSTEM (CDC DUAL
C     CYBER 170/750)
C
C       RFL,100000/           - INCREASE FIELD LENGTH FOR COMPILATION
C       FTN5, I=SCRCP5, OPT=3 - COMPILE FORTRAN SOURCE WITH FTN COMPILER
C       LDSET,LIB=IMSLIBF/ - LOAD IMSL LIBRARY
C       LGO DATAFILE          - EXECUTE WITH DATAFILE
C
C
      COMMON/BLOCK1/IC(1000),JL,SSS(3001)
      COMMON/BLOCK2/CSTH(3001),DS(3001),CV,STCRACK,CRWTH
      COMMON/BLOCK3/BAR,PS,AC,AS,TSH,SH,DT(360),FR
      COMMON/BLOCK4/ES,IT,XI,YI,D,TENSON(28),CS(3001),F(3001)
      COMMON/BLOCK5/AHAT,BT,COLDTM,TENSTR,UNWT
      DIMENSION Z(1000),CPX(3001),ICOUN(250),DUMMY(30),ZZ(1000)
      DIMENSION AN1(40),NPROB(2),AN2(18),PERCEN(8),ICR(50,50)
      DIMENSION AGEU(30),FEXP(10),YEXP(10),DUMMZ(7),ITEMP(500)
      DIMENSION AGE(8),FUNCT(500,1),XIND(100),RAN(4),TF(500,1)
      DIMENSION SPAC(5,50,90),AVE(50),SD(50),BOND(101)
      DIMENSION UC(3001),US(3001),DSH(50),TS(50)
      REAL K
      DOUBLE PRECISION SEED
      DATA AGE/0.,1.0,3.0,5.0,7.0,14.0,21.0,28.0/
      DATA PERCEN/0.0,15.0,38.0,53.0,63.0,82.0,94.0,100./
      READ(5,1) (AN1(I),I=1,40)
      WRITE(6,2)
      WRITE(6,3) (AN1(N),N=1,40)
      READ(5,4) NR,NPROB,AN2
      WRITE(6,5)  NPROB,AN2
C
C     INPUT STEEL PROPERTIES
C
      READ(5,*) PS,BAR,FY,ES,AS
      WRITE(6,6)
      WRITE(6,7)
      WRITE(6,6)
      WRITE(6,8)
      WRITE(6,9)  PS,BAR,FY,ES,AS
```

```
      PS=PS/100.
C
C       INPUT CONCRETE PROPERTIES
C
      READ (5,*) D,AC,TSH,CV,ECON,FPC,STRNMU,NSTRN,IFY
      WRITE(6,6)
      WRITE(6,10)
      WRITE(6,6)
      WRITE(6,11)  D,AC,TSH,FPC,ECON
      WRITE(6,6)
      WRITE(6,12)
      WRITE(6,6)
      WRITE(6,13) CV
C
C       INPUT ENVIROMENTAL FACTORS
C
      READ (5,*) CUTEMP,NTEMP,DTATM,COLDTM
C
C        INPUT MINIMUM DAILY TEMPERATURE
C
      READ (5,*) (DT(I),I=1,NTEMP)
C
C       INPUT EXTERNAL LOAD
C
      READ (5,*) TMLOD,WHLOAD,WHBASE,SOILK,WHLSTR
      READ(5,*) MAXITE,TOL
C
C         MAKE DEFAULT SETTINGS
C
         IF(IFY.LE.0) IFY = 2
         IF(TOL.LE.0.0) TOL = 5.0
         IF (STRNMU.LE.0.0) STRNMU = 1.0
         IF (COLDTM.LT.NTEMP) COLDTM = NTEMP
         IF (TMLOD.GE.NTEMP) TMLOD = NTEMP
C
         IF (NSTRN.LE.0) GO TO 50
C
C       INPUT AGE-TENSILE STRENGTH RELATIONSHIP
C
      READ (5,*)  (AGEU(I),TENSON(I),I=1,NSTRN)
      WRITE(6,14)  (AGEU(I),TENSON(I),I=1,NSTRN)
         GO TO 51
50    CONTINUE
      WRITE(6,15)
      WRITE(6,16)
      DO 52 I=1,8
              DUMDUM=FPC*PERCEN(I)*0.01
              DUMDUM=STRNMU*7.5*SQRT(DUMDUM)
      WRITE(6,17)  AGE(I),DUMDUM
   52 CONTINUE
C
C     INPUT SLAB-BASE FRICTION RELATIONSHIP **(FORCE-DISPLACEMENT**)
C
   51 WRITE(6,18)
      READ (5,*)  (FEXP(I),YEXP(I),I=1,IFY)
```

```
        READ(5,*) FLEX,COEFA,COEFB,COEFVA
            IF (IFY.EQ.2) GO TO 53
                 FR=FEXP(1)/YEXP(1)
            WRITE(6,19)  FEXP(1),YEXP(1)
            GO TO 54
53               FR=SQRT(ABS(1/YEXP(1)))*FEXP(1)
            WRITE(6,20)  FEXP(1),YEXP(1)
54      WRITE(6,21)
        WRITE(6,22)  CUTEMP
        WRITE(6,23)
C
        DO 55 I= 1,NTEMP
        TEMPT=DT(I)
        DT(I)=CUTEMP-DT(I)
        WRITE(6,24) I,TEMPT,DT(I)
55      CONTINUE
        WRITE(6,25)  NTEMP,DTATM,COLDTM
        ICOLD=IFIX(COLDTM)
        DT(ICOLD)=CUTEMP-DTATM
C
C          CALCULATE WHEEL STRESS
C
        UNWT=(ECON/(33.*SQRT(FPC)))**.667
        IF (WHLOAD.LE.0.) GO TO 56
        Q1=1.724*D
        IF (WHBASE.GE.Q1) GO TO 57
        BBB=SQRT(1.6*(WHBASE**2)+(D**2))-(.675*D)
        GO TO 58
57      BBB=WHBASE
58      Q2=ECON*(D**3)
        Q3=11.73*SOILK
        STIF=(Q2/Q3)**.25
        Q4=(.316*WHLOAD)/(D**2)
        Q5=ALOG10(STIF/BBB)
        WHLSTR=Q4*(4*Q5+1.069)
56      CONTINUE
        WRITE(6,26)
        WRITE(6,27)
        WRITE(6,28)
        IF (WHLOAD.LE.0.0) GO TO 59
        WRITE(6,29) WHLOAD,WHBASE,SOILK,ECON,TMLOD,WHLSTR
        GO TO 60
59      WRITE(6,30) WHLSTR,TMLOD
60      WRITE(6,31)
        WRITE(6,32)  MAXITE,TOL
        WRITE(6,6)
        WRITE(6,43)
        WRITE(6,6)
        WRITE(6,44) FLEX,COEFA,COEFB,COEFVA
        TOL=0.01*TOL
        READ(5,*) SEED
        DO 61 IXY=1,NR
        IC(1)=1
        IC(2)=3001
        Z(1)=3000.
```

```
          CALL RANNOR(SEED,CPX)
          MID=0
          JL=1
          JXX=0
          DO 62 JX=1,NTEMP
          JXX=JXX+1
          TIME=FLOAT(JX)
          CALL TDV(TIME,AGEU,NSTRN,SDD,TENSTR,CV)
          DO 63 I=1,3001
            CSTH(I)=CPX(I)*SDD+TENSTR
63        CONTINUE
          DO 64 KL=1,10000
            XMEAN=3000./FLOAT(JL)
C   CALCULATE STRESSES IN THE CONCRETE AND STEEL.
          TIMEE=TIME
          CALL STRESS1(TIMEE,Z,XMEAN,SC,B,ECON,TOL)
C   INVESTIGAGE THE POSSIBILITY OF CRACKING AT EACH NODAL POINT.
          CALL CRACK (MID,TMLOD,WHLSTR,TIMEE)
            IF(MID.EQ.-5)  GOTO 65
            JL=JL+1
          CALL SPACING(Z,CV)
64        CONTINUE
65        CONTINUE
C
          ICR(IXY,JXX)=JL
          DO 66 MX=1,JL
66        SPAC(IXY,JXX,MX)=Z(MX)
C
          DSH(JX)=SH
          TS(JX)=TENSTR
62        CONTINUE
          JXX=JXX+1
C
          TIMEE=COLDTM
            TENSTR=TENSON(NSTRN)*SQRT(1.+0.1972*(ALOG10(COLDTM/28.)))
          SDD=TENSTR*CV/100.
          DO 67 I=1,3001
            CSTH(I)=TENSTR+SDD*CPX(I)
67        CONTINUE
          DO 68 KL=1,10000
          XMEAN=3000./FLOAT(JL)
          CALL STRESS1(TIMEE,Z,XMEAN,SC,B,ECON,TOL)
              CALL CRACK(MID,TMLOD,WHLSTR,TIMEE)
              IF(MID.EQ.-5) GOTO 69
            JL=JL+1
          CALL SPACING(Z,CV)
68        CONTINUE
C
69        CONTINUE
          ICR(IXY,JXX)=JL
          DO 70 I=1,JL
70        SPAC(IXY,JXX,I)=Z(I)
61        CONTINUE
          WRITE(6,33)
          DO 71 I=1,JXX
```

```
         SUM1=0.0
         IM=0
         DO 72 J=1,NR
         IM=IM+ICR(J,I)
         DO 73 KI=1,ICR(J,I)
         SUM1=SUM1+SPAC(J,I,KI)
73       CONTINUE
72       CONTINUE
         AVE(I)=SUM1/FLOAT(IM)
71       CONTINUE
C
         WRITE(9,34)
         WRITE(6,35)
         WRITE(9,35)
         DO 74 I=1,JXX-1
         WRITE(6,36) I,DT(I),DSH(I),TS(I),AVE(I)
         WRITE(9,36) I,DT(I),DSH(I),TS(I),AVE(I)
74       CONTINUE
         HOLD=0.0
         DO 75 I=1,NR
         DO 76 J=1,ICR(I,JXX)
         AP=SPAC(I,JXX,J)/12.
         IF(AP.LT.HOLD) GOTO 76
         HOLD=AP
76       CONTINUE
75       CONTINUE
         MAX=IFIX(HOLD+1.0)
         MMX=2*MAX
         DO 77 MA=1,250
77       ICOUN(MA)=0
         DO 78 I=1,NR
         DO 79 J=1,ICR(I,JXX)
         J1=IFIX(0.5+SPAC(I,JXX,J)/6.)
         ICOUN(J1)=ICOUN(J1)+1
79       CONTINUE
78       CONTINUE
         WRITE(6,37)
         WRITE(9,37)
         DO 80 J=1,MMX
         TEM=0.0
            TF(J,1)=FLOAT(ICOUN(J))/FLOAT(IM)*100.
            DO 81 IP=1,J
81             TEM=TEM+TF(IP,1)
            FUNCT(J,1)=TEM
80       CONTINUE
         DO 82 ITZ=1,MMX
         UP=FLOAT(ITZ)/2.+.25
         DOWN=UP-.5
         WRITE(6,38) DOWN,UP,TF(ITZ,1),FUNCT(ITZ,1)
         WRITE(9,38) DOWN,UP,TF(ITZ,1),FUNCT(ITZ,1)
82       CONTINUE
         DO 83 I=1,MMX
         DUMMY(I)=TF(I,1)
83       CONTINUE
         DO 84 IL=1,MMX
```

```
84      XIND(IL)=FLOAT(IL)/2.
        RAN(2)=FLOAT(MAX)
        RAN(1)=0.0
        RAN(3)=0.0
        RAN(4)=100.
        CALL USPLO(XIND,FUNCT,MMX,MMX,1,1,'CUMULATIVE CRACK SPACING DISTRIBU
       1TION',37,'CRACK SPACING (FEET)',20,'CUMULATIVE FRACTION',19,RAN,
       2'+',1,IE)
        XMEAN=AVE(JXX)
        CALL FINAL(XMEAN,SC,B,UC,US,BOND,FLAG)
        WRITE(6,33)
        AAA=AVE(JXX)/12.
        SSUM=0.0
        DO 85 I=1,JL
85      SSUM=SSUM+(SPAC(NR,JXX,I)/12.)**2
        STD=SQRT(SSUM/FLOAT(JL)-AAA**2)
        WRITE(6,39) AAA,STD,CRWTH,SC,B
        WRITE(9,39) AAA,STD,CRWTH,SC,B
        IF(FLAG.EQ.1.0) THEN
          WRITE(6,42)
        ENDIF
        WRITE(6,40)
        DO 86 I=1,101
        DX=XMEAN/200.*FLOAT(I-1)
        WRITE(6,41) I,DX,UC(I),US(I),BOND(I),F(I),CS(I),SSS(I)
86      CONTINUE
        CALL PUNCH(XMEAN,DUMMY,COEFVA,COEFA,COEFB,FLEX)
C
C
1       FORMAT(20A4/20A4)
2       FORMAT (5H1    ,76X,10HI-----TRIM)
3       FORMAT (1X,20A4)
4       FORMAT(I5,20A3)
5       FORMAT (// 5H PROB /1X,2A3,2X,18A4//)
7       FORMAT (10X,1H*,46X,1H* /
       1    10X,48H*               STEEL PROPERTIES              * /
       2    10X,1H*,46X,1H*)
6       FORMAT (10X,48(1H*))
8       FORMAT (// 15X,39H TYPE OF LONGITUDINAL REINFORCEMENT IS  /
       1           26X,14H DEFORMED BARS)
9       FORMAT (// 15X,24H PERCENT REINFORCEMENT =,1PE10.3 /
       1           15X,24H BAR DIAMETER         =,1PE10.3 /
       2           15X,24H YIELD STRESS         =,1PE10.3 /
       3           15X,24H ELASTIC MODULUS      =,1PE10.3 /
       4           15X,24H THERMAL COEFFICIENT  =,1PE10.3 ///)
10      FORMAT (10X,1H*,46X,1H* /
       1    10X,48H*               CONCRETE PROPERTIES           * /
       2    10X,1H*,46X,1H*)
11      FORMAT (// 15X,22H SLAB THICKNESS      =,1PE10.3 /
       1           15X,22H THERMAL COEFFICIENT =,1PE10.3 /
       2           15X,22H TOTAL SHRINKAGE     =,1PE10.3 /
       3           15X,22H COMPRESSIVE STRENGTH=,1PE10.3 /
       4           15X,22H ELASTIC MODULUS     =,1PE10.3//)
14      FORMAT (/// 15X,40H TENSILE STRENGTH DATA AS INPUT BY USER  //
       1           14X,' AGE        MEAN '/
```

```
     1              14X,'(DAYS)    TENSILE'/
     2              14X,'         STRENGTH'/
     3              (15X,F5.1,4X,F5.1))
  15    FORMAT ( / 14X,22H TENSILE STRENGTH DATA / 15X,21(1H*))
  16    FORMAT ( / 15X,43H NO TENSILE STRENGTH DATA IS INPUT BY USER  /
     1           15X,49H THE FOLLOWING AGE-TENSILE STRENGTH RELATIONSHIP  /
     2,          15X,46H IS USED WHICH IS BASED ON THE RECOMMENDATION  /
     3           15X,37H GIVEN BY U.S. BUREAU OF RECLAMATION  //
     4           15X,15H AGE,  TENSILE  /
     5           14X,17H (DAYS) STRENGTH  /)
  17    FORMAT (13X, 2(2X,F5.1))
  12    FORMAT (10X,1H*,46X,1H* /
     1       10X,48H*            VARIATION OF CONCRETE           * /
     2       10X,48H*             TENSILE STRENGTH               * /
     3       10X,1H*,46X,1H*)
  13    FORMAT(//15X,' COEFFICIENT OF VARIATION = ',F4.1,' PERCENT')
  18    FORMAT ( / 10X,48(1H*) / 10X,1H*,46X,1H* /
     1       10X,1H*,5X,35H SLAB-BASE FRICTION CHARACTERISTICS,6X,1H* /
     2       10X,1H*,14X,17H F-Y RELATIONSHIP,15X,1H* / 10X,1H*,46X,1H* /
     3       10X,48(1H*) //)
  19    FORMAT (15X,41HTYPE OF FRICTION CURVE IS A STRAIGHT LINE //
     1     15X,24H MAXIMUM FRICTION FORCE=,F10.4 /
     2     15X,24H MOVEMENT AT SLIDING   =,F10.4)
  20    FORMAT (15X,36HTYPE OF FRICTION CURVE IS A PARABOLA //
     1     15X,24H MAXIMUM FRICTION FORCE=,F10.4 /
     2     15X,24H MOVEMENT AT SLIDING   =,F10.4)
  22    FORMAT (   14X,20H CURING TEMPERATURE=,F5.1 //)
  21    FORMAT (/// 10X,30(1H*) /
     1       10X,1H*,28X,1H* /
     2       10X,30H*        TEMPERATURE DATA      * / 10X,1H*,28X,1H* /
     3       10X,30(1H*) //)
  23    FORMAT (20X,7HMINIMUM,6X,7HDROP IN /
     1       10X,3HDAY,5X,11HTEMPERATURE,2X,11HTEMPERATURE /)
  24    FORMAT (9X,(1X,I3,8X,F5.1,8X,F5.1))
  25    FORMAT (/ 12X,36H DAYS BEFORE CONCRETE GAINS            /
     .             12X,37H FULL STRENGTH                      =,I5,5H DAYS
     .         / 12X,36H MINIMUM TEMPERATURE EXPECTED AFTER   /
     .           12X,37H CONCRETE GAINS FULL STRENGTH        =,F5.1,
     .           22H DEGREES FAHRENHEIT    / 13X,11HDAYS BEFORE,25H REACH
     .ING MIN. TEMP.    =,F5.1,1X,4HDAYS)
  26    FORMAT (1H1 // 10X,48(1H*))
  28    FORMAT (10X,48(1H*))
  27    FORMAT (10X,1H*,46X,1H* /
     1       10X,48H*              EXTERNAL LOAD               * /
     2       10X,1H*,46X,1H*)
  29    FORMAT (// 15X,25H WHEEL LOAD (LBS)       =,1PE10.3 /
     .             15X,25H WHEEL BASE RADIUS (IN) =,1PE10.3 /
     .             15X,25H SUBGRADE MODULUS (PCI) =,1PE10.3 /
     .             15X,25H CONCRETE MODULUS (PSI) =,1PE10.3 /
     .             15X,25H LOAD APPLIED AT        =,1PE10.3,7H TH DAY /
     .             15X,25H CALC.LOAD STRESS (PSI) =,1PE10.3 ///)
  30  . FORMAT (// 15X,25H WHEEL LOAD STRESS (PSI)=,1PE10.3 /
     .         15X,25H LOAD APPLIED AT        =,1X,F4.1,7H TH DAY ///)
  31    FORMAT (// 10X,48(1H*) / 10X,1H*,46X,1H* / 10X,1H*,6X,
     1           33H ITERATION AND TOLERANCE CONTROL ,7X,1H* /
```

```
      2         10X,1H*,46X,1H* / 10X,48(1H*) ///)
32    FORMAT (10X,40H MAXIMUM ALLOWABLE NUMBER OF ITERATIONS=,I5    //
      1         10X,28H RELATIVE CLOSURE TOLERANCE=,F5.1, 8H PERCENT//)
33    FORMAT('1')
34    FORMAT(//)
35    FORMAT('TIME        TEMP        DRYING        TENSILE     MEAN CRACK
      1 '/'(DAYS)      DROP      SHRINKAGE      STRENGTH      SPACING'//)
36    FORMAT(I5,5X,F5.1,5X,E11.4,5X,F8.1,5X,F8.1)
37    FORMAT(1H1/'CRACK SPACING (FT)   FRACTION (%)   CUMULATIVE VALUE',
      1' (%)'/)
38    FORMAT(2X,F5.2,' - - ',F5.2,9X,F6.2,13X,F6.2)
39    FORMAT(' AT THE END OF THE ANALYSIS PERIOD'//
      1' MEAN CRACK SPACING                   = ',F6.2,' FEET'/
      2' STANDARD DEVIATION OF CRACK SPACING = ',F6.2,' FEET'/
      3' CRACK WIDTH                          = ',F6.4,' INCHES'/
      4' STEEL STRESS AT A CRACK              = ',F6.0,' PSI'/
      5' BOND DEVELOPMENT LENGTH              = ',F6.1,' INCHES'/////)
40    FORMAT(' STATION   DISTANCE    DISPLACEMENTS        BOND   FRICTIO'
      2,         'NAL       STRESSES IN'/
      3         '                      (INCHES)   CONCRETE    STEEL    STRESS    STRESS'
      4,'      CONCRETE   STEEL'//)
41    FORMAT(I6,4X,F7.2,4X,F7.5,3X,F7.5,2X,F8.2,2X,F8.2,2X,F8.2,2X,F8.2)
42    FORMAT(//'CLOSURE LIMIT CONDITION HAS NOT BEEN SATISFIED.'/
      1'CAUTION IS NEEDED WHEN INTERPRETING THE RESULTS'//)
43    FORMAT(10X,'*',46X,'*',/
      1   10X,'*         CONCRETE FATIGUE CHARACTERISTICS        *',/
      2      10X,'*',46X,'*')
44    FORMAT(//15X,'FLEXURAL STRENGTH OF CONCRETE = ',F5.1,' PSI',
      1/,       15X,'COEFFICIENT A IN FATIGUE EQN. = ',F8.1,
      2/,       15X,'COEFFICIENT B IN FATIGUE EQN. = ',F5.1,
      3/,       15X,'C.O.V. OF CONCRETE FATIGUE    = ',F5.1,' %')
      STOP
      END
C
C

      SUBROUTINE CRACK(MID,TMLOD,WHLSTR,TIMEE)
      COMMON/BLOCK1/IC(1000),JL,SSS(3001)
      COMMON/BLOCK2/CSTH(3001),DS(3001),CV,STCRACK,CRWTH
      COMMON/BLOCK3/BAR,PS,AC,AS,TSH,SH,DT(360),FR
      COMMON/BLOCK4/ES,IT,XI,YI,D,TENSON(28),CS(3001),F(3001)
      IF(TIMEE.LE.TMLOD) GOTO 1
      DO 2 I=1,3001
      CS(I)=CS(I)+WHLSTR
2     CONTINUE
1     CONTINUE
      DO 3 I=1,3001
        DS(I)=CSTH(I)-CS(I)
3     CONTINUE
      HOLD=10000.0
      DO 4 I=1,3001
      IF(DS(I).LE.HOLD) THEN
      HOLD=DS(I)
      IMIN=I
      ENDIF
4     CONTINUE
```

```
              IF(HOLD.GT.0.0) GOTO 5
              DO 6 KM=1,JL+1
              IF(IC(KM).EQ.IMIN) GOTO 5
    6         CONTINUE
              IF(IC(JL+1).EQ.IMIN) GOTO 5
              IC(JL+2)=IMIN
              JM=JL+2
              DO.7 I=1,JL+1
              I1=I+1
              DO 8 J=I1,JM
              IF(IC(I).LE.IC(J)) GOTO 8
              HOLD=IC(I)
              IC(I)=IC(J)
              IC(J)=HOLD
    8         CONTINUE
    7         CONTINUE
              MID=5
              RETURN
    5         MID=-5
              RETURN
              END
C
C
C
              SUBROUTINE RANNOR(SEED,CPX)
              DIMENSION CPX(3001)
              DOUBLE PRECISION SEED
              DO 1 I=1,3001
                 CPX(I)=GGNQF(SEED)
    1         CONTINUE
              RETURN
              END
C
C
C
              SUBROUTINE TDV(TIME,AGEU,NSTRN,SDD,TENSTR,CV)
              COMMON/BLOCK3/BAR,PS,AC,AS,TSH,SH,DT(360),FR
              COMMON/BLOCK4/ES,IT,XI,YI,D,TENSON(28),CS(3001),F(3001)
              DIMENSION AGEU(30)
              DO 1 I=1,NSTRN
                    J=I
                 IF (TIME.LE.AGEU(I)) GO TO 2
    1         CONTINUE
    2         CONTINUE
C
C         COMPUTE SLOPE BY LINEAR INTERPOLATION
                  SLOPE=(TENSON(J)-TENSON(J-1))/(AGEU(J)-AGEU(J-1))
                  TENSTR=TENSON(J-1)+SLOPE*(TIME-AGEU(J-1))
              SDD=TENSTR*CV/100.
C
              XM=26.*EXP(.36*D)
              SH=TSH*TIME/(XM+TIME)
              RETURN
              END
C
```

```
C
      SUBROUTINE STRESS1(TIMEE,Z,XMEAN,SC,B,ECC,TOL)
************************************************************************
*     THE ALGORITHM TO DETERMINE BOND DEVELOPMENT LENGTH WAS EXAMINED AND    *
*     MORE EFFICIENT METHODOLOGY WAS DEVELOPED AND INCORPORATED INTO THE     *
*     CRCP-5 PROGRAM.                                                        *
************************************************************************
      COMMON/BLOCK1/IC(1000),JL,SSS(3001)
      COMMON/BLOCK2/CSTH(3001),DS(3001),CV,STCRACK,CRWTH
      COMMON/BLOCK3/BAR,PS,AC,AS,TSH,SH,DT(360),FR
      COMMON/BLOCK4/ES,IT,XI,YI,D,TENSON(28),CS(3001),F(3001)
      COMMON/BLOCK5/AHAT,BT,COLDTM,TENSTR,UNWT
      DIMENSION UC(3001),US(3001),Z(1000)
      DIMENSION CCSS(3001),XZP(3001)
      REAL K,N,L
      PARAMETER (PI=3.14159, K=30000.)
      A1(C)=C*(SINH(C)-C*COSH(C)+2.*C*(COSH(C)-1.)/PI)
      A2A(C)=SC*B/(ES*A1(C))+((AC-AS)*DZ+SH)*B/A1(C)-BT*B*(1.+C-
     12.*C/PI)*EXP(-C)/(ALPHA*K*A1(C))-BT*B*(B*L+2.*C/(PI*ALPHA
     2*K)-2.*B**2/PI-1./(ALPHA*K))/A1(C)
      SS(B)=(4.*320.*B/BAR-(C2-C3)/C1-AHAT*(L-B)**2/(2.*D*(PS+1./N)))/
     1(1.-1./C1)
      QQ(C)=A2A(C)*K*((B/C)**2*(COSH(C)-1.)-B**2*COSH(C)/2.+4.*B**2*
     1(COSH(C)-1.)/PI**2)-BT*B**3*(EXP(-C)-1.)/(ALPHA*C**3)-BT*B**3
     2/(ALPHA*C**2)+BT*4.*B**2*(C/(ALPHA*K*B)-B*EXP(-C)/C-L)/(ALPHA*
     3PI**2)-BT*(B**3/6.+A*B**2/2.)/ALPHA+BT*B**2*L*EXP(-C)/(2.*ALPHA
     4*C)+BT*L*B**2/(ALPHA*2.)
      FBX(W)=A2A(C)*K*(COSH(C*W/B)-COSH(C)+(COSH(C)-1.)*COS(PI*W/
     1(2.*B)))-BT*B*EXP(-C*W/B)/(ALPHA*C)+(BT*C/(ALPHA*K*B)-BT*B*
     2EXP(-C)/C-BT*L)/ALPHA*COS(PI*W/(2.*B))-BT*(W+A)/ALPHA
     3+BT*B*EXP(-C)/(ALPHA*C)+BT*L/ALPHA
      XINT(W)=A2A(C)*K*(B*SINH(C*W/B)/C+2.*B*SIN(PI*W/(2.*B))*
     1(COSH(C)-1.)/PI-COSH(C)*W)+BT*B**2*(EXP(-C*W/B)-1.)/(ALPHA*C
     2**2)+BT*(C/(ALPHA*K*B)-B*EXP(-C)/C-L)*2.*B*SIN(PI*W/(2.*B))/
     3(ALPHA*PI)-BT*(W**2/2.+A*W)/ALPHA+BT*B*EXP(-C)*W/(ALPHA*C)+
     4BT*L*W/ALPHA
      SS2(C)=C1/L*(AS*DZ*ES*L+(C2-C3)*L/C1+(AHAT*A**3/4.+AHAT*A**2*B/2.)
     1/(D*(PS+1./N))-4.*QQ(C)/BAR)
      DO 1 I=1,3001
1     CS(I)=0.0
      IT=IFIX(TIMEE)
      DZ=DT(IT)
      EC=ECC*(35.*TIMEE)/(35.*TIMEE+40.)
      C2=EC*(SH+(AC-AS)*DZ)/PS
      N=ES/EC
      ALPHA=4.*(1.+N*PS)/(BAR*ES)
      R=SQRT(ALPHA*K)
      C1=1.+1./(N*PS)
      AHAT=0.0
      BT=0.0
      XL=XMEAN
      L=XL/2.
      LN=L
      DX=L/FLOAT(LN)
      DO 2 JI=1,LN+1
```

```
2       XZP(JI)=FLOAT(JI-1)*DX
3       CONTINUE
        C3=AHAT*L**2/(2.*PS*D)
        DIF1=-1.0
        DO 4 I=1,LN+1
        XZ=FLOAT(I)*DX
        B=XZ
        C=B*R
        A=L-B
        SC=SS(XZ)
        TIM1=SC
        FSX=C
        TIM2=SS2(FSX)
        DIF2=TIM1-TIM2
        DIF=DIF1*DIF2
        IF(DIF.LT.0.0) GOTO 5
        TEM=B
        TSC=SC
        DIF1=DIF2
4       CONTINUE
5       CONTINUE
        NFBZ=(L-TEM)/DX
        SM=(TSC-C2+C3)/C1
        SC=TSC
        DO 6 I=1,NFBZ+1
        XX=-A+DX*FLOAT(I-1)
        SSS(I)=SM-(AHAT/2.*(XX**2+A**2)+AHAT*A*XX)/(D*(PS+1./N))
        CS(I)=SSS(I)/N+EC*((AC-AS)*DZ+SH)
6       CONTINUE
        DO 7 J=NFBZ+2,LN+1
        TXP=FLOAT(J-NFBZ)*DX
        RR=B
        SSS(J)=SC-4./BAR*(XINT(RR)-XINT(TXP))
        CS(J)=4.*PS*(XINT(RR)-XINT(TXP))/BAR+AHAT*(A*(B-TXP)+(B**2-TXP**2)
       1/2.)/D
7       CONTINUE
        UC(1)=0.0
        F(1)=0.0
        SUMC=0.0
        SUMS=0.0
        DO 8 I=2,LN+1
        SUMC=SUMC+(CS(I-1)+CS(I))/2.
        SUMS=SUMS+(SSS(I-1)+SSS(I))/2.
        UC(I)=-(AC*DZ+SH)*XZP(I)+SUMC*DX/EC
8       F(I)=UC(I)*FR
        CRWTH=-2.*UC(LN+1)
        CALL FRIC(AHAT,UC,DX,LN,AHAT2,F)
        BT=AHAT/(EC*D)
        SIG=(AHAT-AHAT2)/AHAT2
        IF(ABS(SIG).LT.TOL) GOTO 9
        AHAT=AHAT2
        GOTO 3
9       CONTINUE
        XBB=2.*B
        DO 10 I=1,JL
```

```
      IF(Z(I).LT.XBB) GOTO 11
10    CONTINUE
      DO 12 I=2,JL+1
      HCS=Z(I-1)/2.
      L=HCS
      A=L-B
      C=B*R
      ITEM=IFIX(HCS)
      MID=IC(I)-ITEM
      IBBS=IC(I)-IFIX(B)
      ISTA=IC(I-1)
      IEND=IC(I)
      SM=(SC-C2+C3)/C1
      DO 13 J1=MID,IBBS
      SSS(J1)=SM-AHAT*FLOAT(J1-MID)**2/(2.*D*(PS+1./N))
      CS(J1)=SSS(J1)/N+EC*((AC-AS)*DZ+SH)
13    CONTINUE
      DO 14 J2=IBBS,IEND
      XD=FLOAT(J2-IBBS)
      SSS(J2)=SSS(IBBS)+4.*XINT(XD)/BAR
      CS(J2)=CS(IBBS)-4.*XINT(XD)*PS/BAR-AHAT*(FLOAT(J2-MID)**2-
     1FLOAT(IBBS-MID)**2)/(2.*D)
14    CONTINUE
      DO 15 J3=ISTA,MID-1
      SSS(J3)=SSS(ISTA+IEND-J3)
      CS(J3)=CS(ISTA+IEND-J3)
15    CONTINUE
12    CONTINUE
      RETURN
11    CONTINUE
      DO 16 I=1,JL
      IF(Z(I).GT.XBB) GOTO 17
      B=Z(I)/2.
      C=B*R
      L=B
      A=0.0
      ITEM=IFIX(B)
      MID=IC(I+1)-ITEM
      ISTA=IC(I)
      IEND=IC(I+1)
      DO 18 JJ=ISTA,IEND
      CS(JJ)=0.0
      SSS(JJ)=0.0
18    CONTINUE
      GOTO 16
17    CONTINUE
      B=XBB/2.
      C=B*R
      HCS=Z(I)/2.
      L=HCS
      A=L-B
      ITEM=IFIX(HCS)
      MID=IC(I+1)-ITEM
      IBBS=IC(I+1)-IFIX(B)
      ISTA=IC(I)
```

```
        IEND=IC(I+1)
        C3=AHAT*HCS**2/(2.*PS*D)
        SM=(SC-C2+C3)/C1
        DO 19 J1=MID,IBBS
        SSS(J1)=SM-AHAT*FLOAT(J1-MID)**2/(2.*D*(PS+1./N))
        CS(J1)=SSS(J1)/N+EC*((AC-AS)*DZ+SH)
19      CONTINUE
        DO 20 J2=IBBS,IEND
        XD=FLOAT(J2-IBBS)
        SSS(J2)=SSS(IBBS)+4.*XINT(XD)/BAR
        CS(J2)=CS(IBBS)-4.*XINT(XD)*PS/BAR-AHAT*(FLOAT(J2-MID)**2-
       1FLOAT(IBBS-MID)**2)/(2.*D)
20      CONTINUE
        DO 21 J3=ISTA,MID-1
        SSS(J3)=SSS(ISTA+IEND-J3)
        CS(J3)=CS(ISTA+IEND-J3)
21      CONTINUE
16      CONTINUE
        SUM=0.0
        DO 22 KM=1,LN
          SUM=SUM+(SSS(KM)+SSS(KM+1))*DX/2.
22      CONTINUE
        RETURN
        END
C
C
C
C
C
        SUBROUTINE SPACING (Z,CV)
        COMMON/BLOCK1/IC(1000),JL,SSS(3001)
        DIMENSION Z(1000)
        IF(CV.GT.0.0) THEN
        DO 1 K=1,JL
          A1=FLOAT(IC(K+1))
          A2=FLOAT(IC(K))
          ZZT=A1-A2
        Z(K)=ZZT
1       CONTINUE
        RETURN
        ELSE
        DO 2 M=1,JL
        Z(M)=3000./FLOAT(JL)
2       CONTINUE
        ENDIF
        RETURN
        END
C
C
        SUBROUTINE FRIC (AHAT,UC,DX,LN,AHAT2,F)
        DIMENSION UC(3001),F(3001)
        COMMON/BLOCK3/BAR,PS,AC,AS,TSH,SH,DT(360),FR
        SUMF1=0.0
        SUMF2=0.0
        DO 1 I=1,LN+1
```

```
          F(I)=FR*UC(I)
         TEMF=FLOAT(I-1)*DX
         SUMF1=SUMF1+TEMF*F(I)
         SUMF2=SUMF2+TEMF*TEMF
1        CONTINUE
         IF(AHAT.NE.0.0) GOTO 2
         AHAT2=SUMF1/SUMF2
         RETURN
2        AHAT=SUMF1/SUMF2
         IF(AHAT.LT.0.0) AHAT=0.0
         AHAT2=(AHAT+AHAT2)/2.
         RETURN
         END
C
C
         SUBROUTINE FINAL(XMEAN,SC,B,UC,US,BOND,FLAG)
         COMMON/BLOCK1/IC(1000),JL,SSS(3001)
         COMMON/BLOCK2/CSTH(3001),DS(3001),CV,STCRACK,CRWTH
         COMMON/BLOCK3/BAR,PS,AC,AS,TSH,SH,DT(360),FR
         COMMON/BLOCK5/AHAT,BT,COLDTM,TENSTR,UNWT
         COMMON/BLOCK4/ES,IT,XI,YI,D,TENSON(28),CS(3001),F(3001)
         DIMENSION UC(3001),US(3001),Z(1000)
         DIMENSION CCSS(3001),XZP(3001),BOND(101)
         REAL K,N,L
         PARAMETER (PI=3.14159, K=30000.)
         A1(C)=C*(SINH(C)-C*COSH(C)+2.*C*(COSH(C)-1.)/PI)
         A2A(C)=SC*B/(ES*A1(C))+((AC-AS)*DZ+SH)*B/A1(C)-BT*B*(1.+C-
        12.*C/PI)*EXP(-C)/(ALPHA*K*A1(C))-BT*B*(B*L+2.*C/(PI*ALPHA
        2*K)-2.*B**2/PI-1./(ALPHA*K))/A1(C)
         SS(B)=(4.*385.*B/BAR-(C2-C3)/C1-AHAT*(L-B)**2/(2.*D*(PS+1./N)))/
        1(1.-1./C1)
         QQ(C)=A2A(C)*K*((B/C)**2*(COSH(C)-1.)-B**2*COSH(C)/2.+4.*B**2*
        1(COSH(C)-1.)/PI**2)-BT*B**3*(EXP(-C)-1.)/(ALPHA*C**3)-BT*B**3
        2/(ALPHA*C**2)+BT*4.*B**2*(C/(ALPHA*K*B)-B*EXP(-C)/C-L)/(ALPHA*
        3PI**2)-BT*(B**3/6.+A*B**2/2.)/ALPHA+BT*B**2*L*EXP(-C)/(2.*ALPHA
        4*C)+BT*L*B**2/(ALPHA*2.)
         FBX(W)=A2A(C)*K*(COSH(C*W/B)-COSH(C)+(COSH(C)-1.)*COS(PI*W/
        1(2.*B)))-BT*B*EXP(-C*W/B)/(ALPHA*C)+(BT*C/(ALPHA*K*B)-BT*B*
        2EXP(-C)/C-BT*(A+B))/ALPHA*COS(PI*W/(2.*B))-BT*(W+A)/ALPHA
        3+BT*B*EXP(-C)/(ALPHA*C)+BT*(A+B)/ALPHA
         XINT(W)=A2A(C)*K*(B*SINH(C*W/B)/C+2.*B*SIN(PI*W/(2.*B))*
        1(COSH(C)-1.)/PI-COSH(C)*W)+BT*B**2*(EXP(-C*W/B)-1.)/(ALPHA*C
        2**2)+BT*(C/(ALPHA*K*B)-B*EXP(-C)/C-L)*2.*B*SIN(PI*W/(2.*B))/
        3(ALPHA*PI)-BT*(W**2/2.+A*W)/ALPHA+BT*B*EXP(-C)*W/(ALPHA*C)+
        4BT*L*W/ALPHA
         SS2(C)=C1/L*(AS*DZ*ES*L+(C2-C3)*L/C1+(AHAT*A**3/4.+AHAT*A**2*B/2.)
        1/(D*(PS+1./N)))-4.*QQ(C)/BAR
         FLAG=0.0
         IT=IFIX(COLDTM)
         DZ=DT(IT)
         COMP=TENSTR/7.5
         EC=33.*UNWT**1.5*COMP
         C2=EC*(SH+(AC-AS)*DZ)/PS
         N=ES/EC
         ALPHA=4.*(1.+N*PS)/(BAR*ES)
```

```
          R=SQRT(ALPHA*K)
          C=B*R
          C1=1.+1./(N*PS)
          L=XMEAN/2.
          C3=AHAT*L**2/(2.*PS*D)
          DX=L/100.
          DO 1 JI=1,101
1         XZP(JI)=FLOAT(JI-1)*DX
          DIF1=-1.0
          DO 2 I=1,101
          XZ=FLOAT(I)*DX
          B=XZ
          C=B*R
          A=L-B
          SC=SS(XZ)
          TIM1=SC
          FSX=C
          TIM2=SS2(FSX)
          DIF2=TIM1-TIM2
          DIF=DIF1*DIF2
          IF(DIF.LT.0.0) GOTO 3
          DIF1=DIF2
2         CONTINUE
3         CONTINUE
          TI=(L-B)/DX
          NFBZ=IFIX(TI+0.5)
          SM=(SC-C2+C3)/C1
          DO 4 JM=1,NFBZ
          XX=-A+DX*FLOAT(JM-1)
          SSS(JM)=SM-(AHAT/2.*(XX**2+A**2)+AHAT*A*XX)/(D*(PS+1./N))
          CS(JM)=SSS(JM)/N+EC*((AC-AS)*DZ+SH)
          BOND(JM)=-AHAT*BAR*DX*FLOAT(JM-1)/(4.*D*(PS+1./N))
4         CONTINUE
          DO 5 I=NFBZ+1,101
          TXP=FLOAT(I-NFBZ-1)*DX
          RR=B
          SSS(I)=SC-4./BAR*(XINT(RR)-XINT(TXP))
          CS(I)=4.*PS*(XINT(RR)-XINT(TXP))/BAR+AHAT*(A*(B-TXP)+(B**2-
         1TXP**2)/2.)/D
          BOND(I)=FBX(TXP)
5         CONTINUE
          UC(1)=0.0
          US(1)=0.0
          F(1)=0.0
          SUMC=0.0
          SUMS=0.0
          DO 6 I=2,101
          SUMC=SUMC+(CS(I-1)+CS(I))/2.
          SUMS=SUMS+(SSS(I-1)+SSS(I))/2.
          UC(I)=-(AC*DZ+SH)*XZP(I)+SUMC*DX/EC
          F(I)=UC(I)*FR
6         US(I)=-AS*DZ*XZP(I)+SUMS*DX/ES
          IF(ABS(US(101)).GT..001.OR.BOND(101).GT.10.0) FLAG=1.0
          CRWTH=-2.*UC(101)
          RETURN
```

```
             END
C
C
C
C
C
      SUBROUTINE PUNCH(XMEAN,DUMMY,COEFVA,COEFA,COEFB,FLEX)
      COMMON/BLOCK4/ES,IT,XI,YI,D,TENSON(28),CS(3001),F(3001)
      COMMON/BLOCK6/XNOR(30),TCS(30)
      DIMENSION N(30),NC(30),NN(30),SIGNN(30),DUMMY(30),NP(30),RAN(4)
      REAL N,NP
      IFATIG(X)=COEFA*(FLEX/X)**COEFB
      STR(Y)=EXP(9.84736)*(1./D)**1.8143*(1./Y)**.44766
      DO 1 I=1,10
        N(I)=0
        NP(I)=0
        NC(I)=0
        NN(I)=0
        SIGNN(I)=0.0
1     CONTINUE
      XMEAN=XMEAN/12.
      NOCT=5280./XMEAN
      DO 2 IRD=1,10
      N(IRD)=FLOAT(IRD)*1000000.
      SUM=0.0
      DO 3 J=1,30
      TEMP=DUMMY(J)/100.
      NC(J)=NOCT*TEMP
      SX=TCS(J)
      AB=STR(SX)
      NN(J)=IFATIG(AB)
      SIGNN(J)=FLOAT(NN(J))*COEFVA/100.
      X=(N(IRD)-FLOAT(NN(J)))/SIGNN(J)
      IF(X.LT.-3.) GOTO 3
      IY=IFIX(10*X-.5)
      IF(IY.EQ.0) IY=1
      IF(IY.GT.30) IY=30
      IF(IY.LT.0.0) GOTO 4
      P=XNOR(IY)
      GOTO 5
4     P=1.-XNOR(-IY)
5       PO=P*FLOAT(NC(J))
      SUM=SUM+PO
3     CONTINUE
      NP(IRD)=SUM
      WRITE(9,6) IRD,NP(IRD)
6     FORMAT(I9,5X,F5.1)
2     CONTINUE
      RAN(1)=0.0
      RAN(2)=10000000.0
      RAN(3)=0.0
      RAN(4)=SUM+10.
      CALL USPLO(N,NP,10,10,1,1,'NUMBER OF FAILURES VS TRAFFIC APPLICATI
     1ONS',42,'TRAFFIC APPLICATIONS (18K ESAL)',31,'NUMBER OF FAILURES P
     2ER MILE',27,RAN,'+',1,IE)
```

```
      RETURN
      END
C
C

      BLOCK DATA
      COMMON/BLOCK6/XNOR(30),TCS(30)
      DATA XNOR/.5398,.5793,.6179,.6554,.6915,.7257,.7580,.7881,.8159,
     *.8413,.8643,.8849,.9032,.9192,.9332,.9432,.9554,.9641,.9713,.9772
     *,.9821,.9861,.9893,.9918,.9938,.9953,.9965,.9974,.9981,.9987/
      DATA TCS/.5,1.0,1.5,2.0,2.5,3.0,3.5,4.0,4.5,5.0,5.5,6.0,6.5,
     $7.0,7.5,8.0,8.5,9.0,9.5,10.0,10.5,11.0,11.5,12.0,12.5,13.0,
     $13.5,14.0,14.5,15.0/
      END
```

APPENDIX E. INPUT GUIDE OF CRCP-5

In CRCP-5, except the first three lines, free format is employed. Therefore, it is important to follow the general rules pertaining to the free format usage.

LINES 1 &2:
>   In the first two lines, alphanumeric problem statements are made. The format for these two lines is 20A4.

LINE 3: NPROB and AN2
>   NPROB is a variable for the number of simulations to be executed. The format for this variable is I5. AN2 is an alpha-numeric statement to identify the problem characteristics using format 20A3.

LINE 4: PS,BAR,FY,ES,AS
>   PS = percent longitudinal steel (%)
>   BAR = bar diameter (inches)
>   FY = yield strength of steel (psi)
>   ES = modulus of elasticity of steel (psi)
>   AS = thermal coefficient of steel (in./in./ F)

LINE 5: D,AC,TSH,CV,ECON,FPC,STRNMU,NSTRN,IFY
>   D= slab thickness (in.)
>   AC = thermal coefficient of concrete (in./in./ F)
>   TSH = total drying shrinkage (in./in.)
>   CV = coefficient of variation of concrete strength (%)
>   ECON = modulus of elasticity of concrete (psi)
>   FPC = concrete compressive strength (psi)
>   STRNMU = the ratio of tensile strength to modulus of rupture
>   NSTRN = number of pairs of age-tensile strength relationship
>   IFY = number of pairs of frictional stress-movement at sliding relationship

LINE 6: CUTEMP,NTEMP,DTATM,COLDTM
>   CUTEMP = curing temperature (F)
>   NTEMP = number of days detailed analysis is desired(days)
>   DTATM = minimum temperature in the first winter (F)

COLDTM = number of days before DTATM occurs (days)

LINE 7 & 8: DT(i), i=1,NTEMP
   DT(i) = minimum temperature at day i

LINE 9: TMLOD, WHLOAD, WHBASE, SOILK, WHLSTR
   TMLOD = number of days before the pavement is open to traffic
   WHLOAD = wheel load (lbs)
   WHBASE = wheel load base radius (in.)
   SOILK = subgrade modulus of reaction (psi/in.)
   WHLSTR = wheel load stress (psi)
   If wheel load stress is known and it is desired to use the known value rather than to use Westergaard's equation, put the stress value. Otherwise, put 0.0 for WHLSTR.

LINE 10: MAXITE, TOL
   MAXITE = maximum number of runs for each iteration
   TOL = tolerance limit (%)

LINE 11: AGEU(i), TENSON(i), i=1,NSTRN
   AGEU(i) = age at ith pair (day)
   TENSON(i) = tensile strength at day AGEU(i) (psi)

LINE 12: FEXP(i),YEXP(i),i=1,IFY
   FEXP(i) = subbase frictional stress at movement YEXP(i) (psi)
   YEXP(i) = slab movement at ith pair (psi)

LINE 13: SEED
   SEED = seed value to generate normal random numbers. This value must be double precision.

LINE 14: FLEX, COEFA, COEFB, COEFVA
   FLEX = ultimate flexural strength of concrete (psi)
   COEFA = coefficient A in concrete fatigue equation
   COEFB = coefficient B in concrete fatigue equation
   COEFVA = coefficient of variation in concrete fatigue failures

APPENDIX F. SAMPLE OUTPUT OF CRCP-5

SENSITIVITY ANALYSIS OF CRCP-5. NOVEMBER 1988 BY MOONCHEOL WON
MEDIUM LEVEL

PROB


```
****************************************************
*                                                  *
*                STEEL PROPERTIES                  *
*                                                  *
****************************************************
```

            TYPE OF LONGITUDINAL REINFORCEMENT IS
                      DEFORMED BARS

         PERCENT REINFORCEMENT = 6.000E-01
         BAR DIAMETER   = 7.500E-01
         YIELD STRESS   = 6.000E+04
         ELASTIC MODULUS   = 2.900E+07
         THERMAL COEFFICIENT   = 5.000E-06


```
****************************************************
*                                                  *
*                CONCRETE PROPERTIES               *
*                                                  *
****************************************************
```

         SLAB THICKNESS   = 1.000E+01
         THERMAL COEFFICIENT   = 6.000E-06
         TOTAL SHRINKAGE   = 8.000E-04
         COMPRESSIVE STRENGTH = 4.000E+03
         ELASTIC MODULUS   = 5.000E+06

```
****************************************************
*                                                  *
*              VARIATION OF CONCRETE               *
*                TENSILE STRENGTH                  *
*                                                  *
****************************************************
```

COEFFICIENT OF VARIATION = 10.0 PERCENT

TENSILE STRENGTH DATA AS INPUT BY USER

AGE (DAYS)	MEAN TENSILE STRENGTH
.0	.0
1.0	237.0
3.0	320.0
5.0	347.0
7.0	371.0
14.0	411.0
21.0	426.0
28.0	432.0

```
****************************************************
*                                                  *
*       SLAB-BASE FRICTION CHARACTERISTICS         *
*               F-Y RELATIONSHIP                   *
*                                                  *
****************************************************
```


TYPE OF FRICTION CURVE IS A STRAIGHT LINE

MAXIMUM FRICTION FORCE=   4.0000
MOVEMENT AT SLIDING   =   -.0300

```
*******************************
*                             *
*      TEMPERATURE DATA       *
*                             *
*******************************


        CURING TEMPERATURE=100.0


              MINIMUM      DROP IN
    DAY     TEMPERATURE  TEMPERATURE

     1         85.0         15..0
     2         85.0         15.0
     3         85.0         15.0
     4         85.0         15.0
     5         85.0         15.0
     6         80.0         20.0
     7         80.0         20.0
     8         80.0         20.0
     9         80.0         20.0
    10         80.0         20.0
    11         75.0         25.0
    12         75.0         25.0
    13         75.0         25.0
    14         75.0         25.0
    15         75.0         25.0
    16         75.0         25.0
    17         75.0         25.0
    18         75.0         25.0
    19         75.0         25.0
    20         75.0         25.0
    21         75.0         25.0
    22         75.0         25.0
    23         75.0         25.0
    24         75.0         25.0
    25         75.0         25.0
    26         75.0         25.0
    27         75.0         25.0
    28         75.0         25.0

    DAYS BEFORE CONCRETE GAINS
    FULL STRENGTH                        =   28 DAYS
    MINIMUM TEMPERATURE EXPECTED AFTER
    CONCRETE GAINS FULL STRENGTH         = 20.0 DEGREES FAHRENHEIT
    DAYS BEFORE REACHING MIN. TEMP.      =180.0 DAYS
```

99

```
****************************************************
*                                                  *
*                EXTERNAL LOAD                     *
*                                                  *
****************************************************
```

```
        WHEEL LOAD (LBS)        = 9.000E+03
        WHEEL BASE RADIUS (IN)  = 6.000E+00
        SUBGRADE MODULUS (PCI)  = 4.000E+02
        CONCRETE MODULUS (PSI)  = 5.000E+06
        LOAD APPLIED AT         = 1.400E+01 TH DAY
        CALC.LOAD STRESS (PSI)  = 1.149E+02
```

```
****************************************************
*                                                  *
*        ITERATION AND TOLERANCE CONTROL           *
*                                                  *
****************************************************
```

```
    MAXIMUM ALLOWABLE NUMBER OF ITERATIONS=    60

    RELATIVE CLOSURE TOLERANCE=  5.0 PERCENT
```

```
****************************************************
*                                                  *
*        CONCRETE FATIGUE CHARACTERISTICS          *
*                                                  *
****************************************************
```

```
        FLEXURAL STRENGTH OF CONCRETE = 790.0 PSI
        COEFFICIENT A IN FATIGUE EQN. =  90000.0
        COEFFICIENT B IN FATIGUE EQN. =    4.0
        C.O.V. OF CONCRETE FATIGUE    =   30.0 %
```

TIME (DAYS)	TEMP DROP	DRYING SHRINKAGE	TENSILE STRENGTH	MEAN CRACK SPACING
1	15.0	.8398E-06	237.0	600.0
2	15.0	.1678E-05	278.5	500.0
3	15.0	.2514E-05	320.0	500.0
4	15.0	.3349E-05	333.5	500.0
5	15.0	.4182E-05	347.0	500.0
6	20.0	.5013E-05	359.0	375.0
7	20.0	.5842E-05	371.0	375.0
8	20.0	.6670E-05	376.7	333.3
9	20.0	.7496E-05	382.4	333.3
10	20.0	.8320E-05	388.1	333.3
11	25.0	.9142E-05	393.9	272.7
12	25.0	.9963E-05	399.6	272.7
13	25.0	.1078E-04	405.3	272.7

14	25.0	.1160E-04	411.0	272.7
15	25.0	.1242E-04	413.1	136.4
16	25.0	.1323E-04	415.3	136.4
17	25.0	.1404E-04	417.4	136.4
18	25.0	.1485E-04	419.6	136.4
19	25.0	.1566E-04	421.7	136.4
20	25.0	.1647E-04	423.9	136.4
21	25.0	.1727E-04	426.0	136.4
22	25.0	.1808E-04	426.9	136.4
23	25.0	.1888E-04	427.7	136.4
24	25.0	.1968E-04	428.6	136.4
25	25.0	.2048E-04	429.4	136.4
26	25.0	.2128E-04	430.3	136.4
27	25.0	.2207E-04	431.1	136.4
28	25.0	.2287E-04	432.0	136.4

CRACK SPACING (FT)	FRACTION (%)	CUMULATIVE VALUE (%)
.25 - - .75	.00	.00
.75 - - 1.25	.00	.00
1.25 - - 1.75	4.08	4.08
1.75 - - 2.25	4.08	8.16
2.25 - - 2.75	4.08	12.24
2.75 - - 3.25	10.20	22.45
3.25 - - 3.75	10.20	32.65
3.75 - - 4.25	6.12	38.78
4.25 - - 4.75	10.20	48.98
4.75 - - 5.25	8.16	57.14
5.25 - - 5.75	8.16	65.31
5.75 - - 6.25	6.12	71.43
6.25 - - 6.75	4.08	75.51
6.75 - - 7.25	4.08	79.59
7.25 - - 7.75	6.12	85.71
7.75 - - 8.25	2.04	87.76
8.25 - - 8.75	2.04	89.80
8.75 - - 9.25	2.04	91.84
9.25 - - 9.75	4.08	95.92
9.75 - - 10.25	.00	95.92
10.25 - - 10.75	4.08	100.00
10.75 - - 11.25	.00	100.00

AT THE END OF THE ANALYSIS PERIOD

MEAN CRACK SPACING   =   5.10 FEET
STANDARD DEVIATION OF CRACK SPACING =   2.31 FEET
CRACK WIDTH   =   .0282 INCHES
STEEL STRESS AT A CRACK   = 45842. PSI
BOND DEVELOPMENT LENGTH   =   23.0 INCHES

STATION	DISTANCE (INCHES)	DISPLACEMENTS CONCRETE	STEEL	BOND STRESS	FRICTIONAL STRESS	STRESSES IN CONCRETE	STEEL
1	.00	.00000	.00000	.00	.00	285.73	-1299.76
2	.31	-.00014	-.00014	.00	.02	285.73	-1299.76
3	.61	-.00027	-.00027	.00	.04	285.73	-1299.77
4	.92	-.00041	-.00041	-.01	.05	285.72	-1299.78
5	1.22	-.00054	-.00054	-.01	.07	285.72	-1299.79
6	1.53	-.00068	-.00068	-.01	.09	285.72	-1299.80
7	1.84	-.00082	-.00082	-.01	.11	285.72	-1299.82
8	2.14	-.00095	-.00095	-.01	.13	285.71	-1299.84
9	2.45	-.00109	-.00109	-.02	.15	285.71	-1299.87
10	2.76	-.00123	-.00123	-.02	.16	285.70	-1299.89
11	3.06	-.00136	-.00136	-.02	.18	285.70	-1299.93
12	3.37	-.00150	-.00150	-.02	.20	285.69	-1299.96
13	3.67	-.00163	-.00163	-.02	.22	285.69	-1300.00
14	3.98	-.00177	-.00177	-.03	.24	285.68	-1300.04
15	4.29	-.00191	-.00191	-.03	.25	285.67	-1300.08
16	4.59	-.00204	-.00204	-.03	.27	285.66	-1300.13
17	4.90	-.00218	-.00218	-.03	.29	285.66	-1300.18
18	5.20	-.00231	-.00231	-.03	.31	285.65	-1300.23
19	5.51	-.00245	-.00245	-.04	.33	285.64	-1300.29
20	5.82	-.00259	-.00259	-.04	.34	285.63	-1300.35
21	6.12	-.00272	-.00272	-.04	.36	285.62	-1300.42
22	6.43	-.00286	-.00286	-.04	.38	285.60	-1300.48
23	6.73	-.00300	-.00300	-.04	.40	285.59	-1300.55
24	7.04	-.00313	-.00313	-.05	.42	285.58	-1300.63
25	7.35	-.00327	-.00327	-.05	.44	285.57	-1300.70
26	7.65	-.00340	-.00340	-.05	.45	285.55	-1300.92
27	7.96	-.00354	-.00354	.46	.47	285.54	-1300.73
28	8.27	-.00368	-.00368	2.00	.49	285.51	-1298.86
29	8.57	-.00381	-.00381	4.55	.51	285.46	-1293.64
30	8.88	-.00395	-.00395	8.13	.53	285.39	-1283.43
31	9.18	-.00409	-.00408	12.70	.54	285.27	-1266.56
32	9.49	-.00422	-.00422	18.28	.56	285.10	-1241.40
33	9.80	-.00436	-.00436	24.84	.58	284.87	-1206.33
34	10.10	-.00449	-.00449	32.37	.60	284.57	-1159.76
35	10.41	-.00463	-.00463	40.86	.62	284.20	-1100.10
36	10.71	-.00477	-.00476	50.28	.64	283.73	-1025.83
37	11.02	-.00490	-.00489	60.62	.65	283.17	-935.41
38	11.33	-.00504	-.00502	71.86	.67	282.50	-827.38
39	11.63	-.00518	-.00515	83.96	.69	281.71	-700.31
40	11.94	-.00531	-.00528	96.90	.71	280.81	-552.79
41	12.24	-.00545	-.00541	110.65	.73	279.77	-383.47
42	12.55	-.00559	-.00554	125.18	.74	278.59	-191.07
43	12.86	-.00572	-.00566	140.45	.76	277.27	25.67
44	13.16	-.00586	-.00578	156.44	.78	275.79	267.93
45	13.47	-.00600	-.00590	173.09	.80	274.15	536.85
46	13.78	-.00613	-.00601	190.38	.82	272.34	833.47

47	14.08	-.00627	-.00613	208.25	.84	270.37	1158.81
48	14.39	-.00641	-.00623	226.67	.85	268.21	1513.78
49	14.69	-.00654	-.00634	245.59	.87	265.87	1899.24
50	15.00	-.00668	-.00644	264.95	.89	263.34	2315.95
51	15.31	-.00682	-.00653	284.71	.91	260.62	2764.61
52	15.61	-.00696	-.00662	304.82	.93	257.70	3245.82
53	15.92	-.00709	-.00671	325.21	.95	254.59	3760.09
54	16.22	-.00723	-.00679	345.83	.96	251.27	4307.84
55	16.53	-.00737	-.00686	366.62	.98	247.75	4889.41
56	16.84	-.00751	-.00693	387.51	1.00	244.03	5505.02
57	17.14	-.00765	-.00699	408.45	1.02	240.10	6154.78
58	17.45	-.00779	-.00705	429.37	1.04	235.96	6838.73
59	17.76	-.00793	-.00709	450.20	1.06	231.62	7556.77
60	18.06	-.00807	-.00713	470.86	1.08	227.07	8308.67
61	18.37	-.00821	-.00716	491.29	1.09	222.33	9094.14
62	18.67	-.00835	-.00718·	511.40	1.11	217.38	9912.70
63	18.98	-.00849	-.00720	531.13	1.13	212.24	10763.80
64	19.29	-.00863	-.00720	550.38	1.15	206.91	11646.73
65	19.59	-.00877	-.00720	569.09	1.17	201.39	12560.67
66	19.90	-.00891	-.00718	587.16	1.19	195.69	13504.64
67	20.20	-.00905	-.00716	604.51	1.21	189.81	14477.54
68	20.51	-.00920	-.00712	621.05	1.23	183.77	15478.11
69	20.82	-.00934	-.00707	636.70	1.25	177.57	16504.97
70	21.12	-.00948	-.00702	651.34	1.26	171.22	17556.58
71	21.43	-.00963	-.00695	664.90	1.28	164.73	18631.22
72	21.73	-.00977	-.00687	677.28	1.30	158.12	19727.05
73	22.04	-.00991	-.00678	688.37	1.32	151.38	20842.04
74	22.35	-.01006	-.00667	698.07	1.34	144.55	21974.03
75	22.65	-.01020	-.00656	706.28	1.36	137.63	23120.64
76	22.96	-.01035	-.00643	712.89	1.38	130.63	24279.38
77	23.27	-.01049	-.00629	717.80	1.40	123.58	25447.53
78	23.57	-.01064	-.00614	720.89	1.42	116.49	26622.22
79	23.88	-.01079	-.00597	722.05	1.44	109.38	27800.39
80	24.18	-.01094	-.00580	721.16	1.46	102.26	28978.81
81	24.49	-.01108	-.00561	718.10	1.48	95.16	30154.02
82	24.80	-.01123	-.00540	712.77	1.50	88.11	31322.39
83	25.10	-.01138	-.00519	705.02	1.52	81.11	32480.11
84	25.41	-.01153	-.00496	694.75	1.54	74.21	33623.13
85	25.71	-.01168	-.00472	681.81	1.56	67.42	34747.22
86	26.02	-.01183	-.00447	666.09	1.58	60.76	35847.94
87	26.33	-.01198	-.00421	647.44	1.60	54.28	36920.62
88	26.63	-.01213	-.00394	625.75	1.62	47.99	37960.38
89	26.94	-.01228	-.00366	600.85	1.64	41.93	38962.13
90	27.24	-.01243	-.00336	572.63	1.66	36.13	39920.54
91	27.55	-.01258	-.00306	540.94	1.68	30.62	40830.06
92	27.86	-.01274	-.00275	505.62	1.70	25.44	41684.90
93	28.16	-.01289	-.00242	466.55	1.72	20.62	42479.03
94	28.47	-.01304	-.00209	423.56	1.74	16.20	43206.19
95	28.78	-.01320	-.00176	376.51	1.76	12.23	43859.87
96	29.08	-.01335	-.00141	325.23	1.78	8.73	44433.30
97	29.39	-.01350	-.00106	269.58	1.80	5.76	44919.47
98	29.69	-.01366	-.00071	209.40	1.82	3.36	45311.11
99	30.00	-.01381	-.00035	144.52	1.84	1.56	45600.67
100	30.31	-.01396	.00001	74.77	1.86	.43	45780.35
101	30.61	-.01412	.00037	-.01	1.88	.00	45842.07

104

Crack Spacing

Mean = 5.10 ft
Std. Dev. = 2.31 ft

Crack Width

.0282 in

. Steel Stress

45842 psi

Bond Development
Length

23.0 in.

Crack Spacing Distribution

F
R
E
Q
%

Spacing (ft)
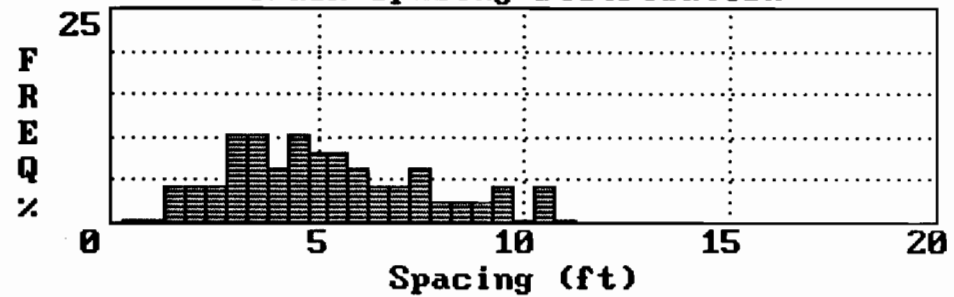
Predicted Failures Per Mile

F
P
M

ESALS (millions)
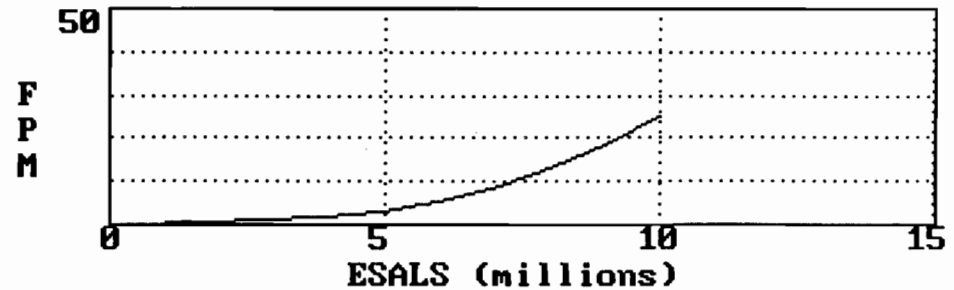
═══ F1 to Toggle Graph, ESC to EXIT ═══

APPENDIX G. INPUT DATA USED IN CHAPTER 8

```
SENSITIVITY ANALYSIS OF CRCP-5.  NOVEMBER 1988 BY MOONCHEOL WON
MEDIUM LEVEL
    1
                .6          .75        60000.  29000000.  .000005
10.0  .000006  .0008  10.  5000000.  4000.  1.0  8  1
   100.       28         20.          180.
  85.  85.  85.  85.  85.  80.  80.  80.  80.  80.  75.  75.  75.  75.  75. 75.
  75.  75.  75.  75.  75.  75.  75.  75.  75.  75.  75.  75.
        14.    9000.   6.0       400.    0.0
60  5.0
0.0 0.0 1. 237. 3. 320. 5. 347. 7. 371.  14.  411.  21.  426.  28.  432.
 4.0         -.03
790. 22000. 4.0 30.0
45826547254255D1


SENSITIVITY ANALYSIS OF CRCP-5.  NOVEMBER 1988 BY MOONCHEOL WON
HIGH PERCENTAGE OF STEEL
    1
                .7          .75        60000.  29000000.  .000005
10.0  .000006  .0008  10.  5000000.  4000.  1.0  8  1
   100.       28         20.          180.
  85.  85.  85.  85.  85.  80.  80.  80.  80.  80.  75.  75.  75.  75.  75. 75.
  75.  75.  75.  75.  75.  75.  75.  75.  75.  75.  75.  75.
        14.    9000.   6.0       400.    0.0
60  5.0
0.0 0.0 1. 237. 3. 320. 5. 347. 7. 371.  14.  411.  21.  426.  28.  432.
 4.0         -.03
790. 22000. 4.0 30.0
45826547254255D1


SENSITIVITY ANALYSIS OF CRCP-5.  NOVEMBER 1988 BY MOONCHEOL WON
LOW PERCENTAGE OF STEEL
    1
                .4          .75        60000.  29000000.  .000005
10.0  .000006  .0008  10.  5000000.  4000.  1.0  8  1
   100.       28         20.          180.
  85.  85.  85.  85.  85.  80.  80.  80.  80.  80.  75.  75.  75.  75.  75. 75.
  75.  75.  75.  75.  75.  75.  75.  75.  75.  75.  75.  75.
        14.    9000.   6.0       400.    0.0
60  5.0
0.0 0.0 1. 237. 3. 320. 5. 347. 7. 371.  14.  411.  21.  426.  28.  432.
 4.0         -.03
790. 22000. 4.0 30.0
45826547254255D1


SENSITIVITY ANALYSIS OF CRCP-5.  NOVEMBER 1988 BY MOONCHEOL WON
LARGER BAR SIZE
    1
                .6          .875       60000.  29000000.  .000005
10.0  .000006  .0008  10.  5000000.  4000.  1.0  8  1
   100.       28         20.          180.
  85.  85.  85.  85.  85.  80.  80.  80.  80.  80.  75.  75.  75.  75.  75. 75.
  75.  75.  75.  75.  75.  75.  75.  75.  75.  75.  75.  75.
        14.    9000.   6.0       400.    0.0
60  5.0
```

```
0.0 0.0 1. 237. 3. 320. 5. 347. 7. 371.  14.  411.  21.  426.  28.  432.
 4.0        -.03
790. 22000. 4.0 30.0
45826547254255D1


SENSITIVITY ANALYSIS OF CRCP-5.  NOVEMBER 1988 BY MOONCHEOL WON
SMALLER BAR SIZE
    1
             .6          .625     60000. 29000000.  .000005
10.0 .000006 .0008 10. 5000000. 4000. 1.0 8  1
  100.      28         20.          180.
  85.  85.  85.  85.  85.  80.  80.  80.  80.  80.  75.  75.  75.  75.  75. 75.
  75.  75.  75.  75.  75.  75.  75.  75.  75.  75.  75.  75.
       14.    9000.  6.0       400.    0.0
60  5.0
0.0 0.0 1. 237. 3. 320. 5. 347. 7. 371.  14.  411.  21.  426.  28.  432.
 4.0        -.03
790. 22000. 4.0 30.0
45826547254255D1


SENSITIVITY ANALYSIS OF CRCP-5.  NOVEMBER 1988 BY MOONCHEOL WON
COARSE AGGREGATE = LS
    1
             .6          .75      60000. 29000000.  .000005
10.0 .000004 .0008 10. 5000000. 4000. 1.0 8  1
  100.      28         20.          180.
  85.  85.  85.  85.  85.  80.  80.  80.  80.  80.  75.  75.  75.  75.  75. 75.
  75.  75.  75.  75.  75.  75.  75.  75.  75.  75.  75.
       14.    9000.  6.0       400.    0.0
60  5.0
0.0 0.0 1. 237. 3. 320. 5. 347. 7. 371.  14.  411.  21.  426.  28.  432.
 4.0        -.03
790. 22000. 4.0 30.0
45826547254255D1


SENSITIVITY ANALYSIS OF CRCP-5.  NOVEMBER 1988 BY MOONCHEOL WON
SMALLER SLAB THICKNESS
    1
             .6          .75      60000. 29000000.  .000005
 8.0 .000006 .0008 10. 5000000. 4000. 1.0 8  1
  100.      28         20.          180.
  85.  85.  85.  85.  85.  80.  80.  80.  80.  80.  75.  75.  75.  75.  75. 75.
  75.  75.  75.  75.  75.  75.  75.  75.  75.  75.  75.
       14.    9000.  6.0       400.    0.0
60  5.0
0.0 0.0 1. 237. 3. 320. 5. 347. 7. 371.  14.  411.  21.  426.  28.  432.
 4.0        -.03
790. 22000. 4.0 30.0
45826547254255D1


SENSITIVITY ANALYSIS OF CRCP-5.  NOVEMBER 1988 BY MOONCHEOL WON
LARGER SLAB THICKNESS
    1
             .6          .75      60000. 29000000.  .000005
13.0 .000006 .0008 10. 5000000. 4000. 1.0 8  1
```

```
     100.      28           20.           180.
   85.  85.  85.  85.  85.  80.  80.  80.  80.  80.  75.  75.  75.  75.  75. 75.
   75.  75.  75.  75.  75.  75.  75.  75.  75.  75.  75.  75.
        14.     9000.    6.0        400.     0.0
60  5.0
0 ᴖ 0.0 1. 237. 3. 320. 5. 347. 7. 371.  14.  411.  21.  426.  28.  432.
  4.0          -.03
790. 22000. 4.0 30.0
45826547254255D1


SENSITIVITY ANALYSIS OF CRCP-5.  NOVEMBER 1988 BY MOONCHEOL WON
LOW VARIABILITY IN CONCRETE TENSILE STRENGTH
    1
              .6          .75        60000.  29000000.   .000005
10.0  .000006  .0008    5.  5000000.  4000.  1.0  8  1
   100.      28           20.           180.
   85.  85.  85.  85.  85.  80.  80.  80.  80.  80.  75.  75.  75.  75.  75. 75.
   75.  75.  75.  75.  75.  75.  75.  75.  75.  75.  75.
        14.     9000.    6.0        400.     0.0
60  5.0
0.0 0.0 1. 237. 3. 320. 5. 347. 7. 371.  14.  411.  21.  426.  28.  432.
  4.0          -.03
790. 22000. 4.0 30.0
45826547254255D1


SENSITIVITY ANALYSIS OF CRCP-5.  NOVEMBER 1988 BY MOONCHEOL WON
HIGH VARIABILITY IN CONCRETE TENSILE STRENGTH
    1
              .6          .75        60000.  29000000.   .000005
10.0  .000006  .0008  15.  5000000.  4000.  1.0  8  1
   100.      28           20.           180.
   85.  85.  85.  85.  85.  80.  80.  80.  80.  80.  75.  75.  75.  75.  75. 75.
   75.  75.  75.  75.  75.  75.  75.  75.  75.  75.  75.
        14.     9000.    6.0        400.     0.0
60  5.0
0.0 0.0 1. 237. 3. 320. 5. 347. 7. 371.  14.  411.  21.  426.  28.  432.
  4.0          -.03
790. 22000. 4.0 30.0
45826547254255D1
```